2007

Antibody targeting of non ionic surfactant vesicles to vascular inflammation

Elizabeth D. Hood
University of South Florida

Antibody Targeting of Non Ionic Surfactant Vesicles to Vascular Inflammation

by

Elizabeth D. Hood

A dissertation submitted in the partial fulfillment
of the requirements for the degree of
Doctor of Philosophy
Department of Chemical Engineering
College of Engineering
University of South Florida

Major Professor: Michael D. VanAuker, Ph.D.
Joel A. Strom, M.D.
Karl Muffly, Ph.D.
Mark Jaroszeski, Ph.D.
Stanley Kranc, Ph.D.

Date of Approval:
November 7, 2007

Keywords: drug delivery, niosomes, vesicles, immunotargeting, atherosclerosis

Dedication

I dedicate this document to my sons, Aaron and Lucas, and to my parents, Alan and Mary, who were always allies to the common enemy in the middle. This work was only possible with the love, support, and patience of my family. Thank you all.

Acknowledgments

I would like to acknowledge the members of my committee for their mentorship and support. Dr. Michael VanAuker and Dr. Strom both challenged and motivated me to present this research as it developed over the years in conferences and symposia which provided me with a wide range of experience and knowledge greater than if I had not ventured out of the lab. Their mentorship gave me the opportunity to present our work at national and international conferences in San Francisco, San Diego, New York City, and New Orleans.

Thanks to Dr Mark Jaroszeski for being an excellent instructor in the classroom and in the laboratory. His experience and guidance with metrology, cell culture and microscopy are very much appreciated.

I want to especially thank Dr Karl Muffly for help with microscopy and cell culture. His endless patience and open door made the research not just possible but enjoyable. I would also like to extend my gratitude to the patience and instruction generously given by Ed Haller, USF Health Pathology Department and manager of the Microscopy Core Facility, for endless hours of assistance and guidance in microscopy and tissue and lipid fixation techniques. Thanks to John Elliot for the Matlab™ image analysis program and TEM images.

Research is impossible without funding; I gratefully acknowledge funding from the University of South Florida New Researchers Award, the Florida Chapter of the Arthritis Foundation for a summer research fellowship, and the Department of Defense US Army Medical Research Acquisition Activity Grant No.W81XWH-05-1-0585, all of which made this work possible.

Note to Reader: The original of this document contains color that is necessary for understanding the data. The original dissertation is on file with the University of South Florida library in Tampa, Florida.

Table of Contents

List of Tables

List of Figures

List of Abbreviations

Alexa Fluor ™ 488	AF
American Heart Association	AHA
Bovine aortic endothelial cell	BAEC
Bovine serum albumin	BSA
Carboxyfluorescein	CF
Carboxyrhodamine	CR
Cellular adhesion molecules	CAMs
Cyanuric chloride	CC
Deionized	DI
Deoxyribonucleic acid	DNA
Dicetyl phosphate	DCP
Diisopropylethylamine	DIPEA
Dulbecco's Modified Eagle Medium	DMEM
Dynamic light scattering	DLS
Endothelial cells	ECs
Extracellular matrix	ECM
Fluorescein isothiocyanate	FITC
Gel exclusion chromatography	GEC
Hank's Balanced Saline	HBS

Hydrophilic-lipophilic balance	HLB
Immunohistochemical	IHC
Institutional Animal Care and Use Committee	IACUC
Intracellular adhesion molecule-1	ICAM-1
Immunoglobulin	IgG
Immunoliposome	IL
Immunoniosome	IN
Interleukin-1 β	IL-1β
Leica Confocal Software	LCS
Molar	M
Monoclonal antibody	mAb
Particle size distribution	PSD
Particle Sizing Systems	PSS
Phosphate buffered saline	PBS
Photomultiplier tube	PMT
Platelet endothelial adhesion molecule-1	PECAM-1
Polyethylene glycol	PEG
Polyethylene oxide	PEO
Polyoxyethylene sorbitan monostearate	Tween 61
Reticuloendothelial system	RES
Scanning electron microscopy	SEM
Sorbitan monostearate	Span 60
Sorbitan monolaurate	Span 40

Sorbitan monopalminate	Span 20
Standard error of the mean	SEM
Synovial lining cells (synoviocytes)	SLs
Tissue factor	TF
Tissue necrosis factor alpha	TNF-α
Transmission electron microscopy	TEM
Ultrasound	US
Ultraviolet	UV
University of South Florida	USF
Vascular adhesion molecule-1	VCAM-1

Antibody Targeting of Non Ionic Surfactant Vesicles to Vascular Inflammation

Elizabeth D. Hood

ABSTRACT

Cardiovascular disease (CVD) and particularly atherosclerosis is a leading cause of morbidity in the developed world. Atherosclerosis and the rupture of vulnerable atherosclerotic plaque cause 70% of deaths from CVD. The progression of atherosclerosis has been identified as a pathological inflammatory process. Targeting atherosclerotic drug therapies to inflammatory markers has emerged as an important and growing research area. The adhesion molecule CD44 has been implicated in the onset and build-up of atherosclerotic lesions throughout the course of development. The research in this dissertation is aimed at targeting anti-inflammatory therapy to activated vascular endothelium with directed with an anti-CD44 antibody, IM7, conjugated to a non ionic surfactant vesicle (niosome) drug carrier. The IM7 conjugated immunoniosome has been shown to bind to endothelial and synovial lining cells *in vitro*.

The preliminary research is involved with the development of the drug delivery vesicle, and the antibody linkage chemistry, along with an analysis of vesicle characteristics and stability. A novel linking chemistry using polyoxyethylene sorbitan monostearate and cyanuric chloride allows antibodies to be conjugated to vesicle surface polymer groups without prior derivatization.

Subsequent research tested the resulting 'immunoniosome's' ability to bind to target antigens with selectivity and specificity. Bovine aortic endothelial cells activated with cytokines provide a model of inflammation. Analysis of binding was done through fluorescent and scanning electron microscopy. *In vivo* uptake of vesicles at sites of inflammation is size dependent. In order to overcome this barrier to uptake, niosome suspensions were thermally extruded to create uniform 200 nm vesicles. Further analysis of the efficacy of the system looked at live cell uptake of the immunoniosomes measured by confocal and transmission electron microscopy. Preparation for *in vivo* murine studies required that the antibody component was modified to counteract the immune response. Finally, the conjugation of antibody fragments to niosomes and the binding and uptake of the vesicles in a live endothelial cell model is evaluated. A viable drug delivery particle showing binding and cellular uptake capabilities in inflammatory cells was produced by this research using a novel surfactant-antibody linker.

1. Prelude

Immunotherapy, the use of antibodies to treat disease, is of great interest in the fields of chronic infectious disease, cancer, cardiovascular, and arthritis research, among others. In 1796, Edward Jenner used a cowpox virus to develop a vaccine against small pox. He discovered that deliberate infection with the virus brought on a mild state of the disease and a subsequent immunity to it[1]. It was Paul Erlich at the beginning of the 20th century who originally discovered antibodies and described the role they play in humoral immunity. He proposed the 'magic bullet' concept of using antibodies to send therapeutic agents to target cells[2]. He also imaged that "a carrier by which to bring therapeutically active groups to the organ in question" would be advantageous[3]. Not until the development of monoclonal antibody (mAb) production could his 'magic bullet' concept be realized. In the 1970s the B cell melanoma was identified as producing a single type of antibody. Georges Jean Franz Köhler and César Milstein invented the process to produce monclonal antibodies in 1975 for which they won a Nobel Prize in Physiology or Medicine in 1984[4]. Gregory Winter developed techniques to humanize monoclonal antibodies for therapeutic uses[5].

In 1965 Dr. Alec Bangham published 'Diffusion Of Univalent Ions Across Lamellae Of Swollen Phospholipids' which is the seminal work of liposome[6], and therefore, vesicular drug delivery. More than forty years later strategic drug delivery using phospholipid or other bilayer model structures continues to be pursued for myriad applications such as vaccinations[7], gene delivery[8],

thrombolysis[9], topical applications[10], tumor targeting [11], vascular targeting[12], transdermal[13], and ophthalmic treatments[10,14] among many others.

The combination of immunotherapy and vesicular drug delivery originated with Paul Erlich at the beginning of the 20th century. Almost eighty years later in 1981, Torchilin and Klibanov reviewed methods for immobilizing proteins on the surfaces of liposomes[15]. Immunotargeting of drugs using an antibody vector bound to a drug carrier has continued to be developed in the fields of cancer and tumor therapy[16-27], and cardiovascular research[28-34]. The use of immunotargeted drug delivery to effect treatment and block progression of damaging inflammatory processes has not been as widely pursued as cancer and tumor targeting, most likely due to the more highly toxic effects that anticancer drugs have on healthy tissues. However, the prevalence of cardiovascular disease and especially atherosclerosis[35], the challenges of restenosis of arteries after angioplasty, the build up of plaques on stent implants, and other effects of inflammatory processes in cardiovascular disease, as well as the questionable systemic side effects produced by cardiovascular drugs[36,37] provide motivation and opportunities for a more succinct therapeutic approach.

Current research into innovative anti-atherosclerotic treatment includes identifying and manipulating the inflammatory mechanisms consistent with the progression of the disease from initial fatty streaks to fibrous plaques to vulnerable complex lesions, uptake mechanisms of macrophage derived foam cells[38], and the identification of the regulatory factors controlling inflammatory response in endothelial cells and uptake of lipoproteins[39,40].

The hypothesis of this research is that an antibody conjugated non ionic surfactant vesicle could be developed and targeted to inflammation with the potential to provide therapeutic benefit by targeting specific inflamed tissues. In order to test this hypothesis the following aims were pursued:

Aim 1. Develop and characterize a targeted drug delivery system using non ionic surfactant vesicles conjugated to monoclonal antibodies specific to an inflammatory target antigen.

Aim 2. Quantify and optimize the immunoniosome-antigen binding in fixed culture aortic endothelial cells with respect to concentrations of both vesicle concentration and antibody density using fluorescence microscopy and computer image analysis.

Aim 3. Observe, describe, and quantify cellular uptake of immunoniosomes in live cells using confocal and electron microscopy.

Aim 4. Once the drug delivery system is sufficiently described, develop a protocol for the *in vivo* evaluation of the adherence and effect of the immuniosomes encapsulating atorvastatin on plaque development in the ApoE knockout mouse model.

The successful completion of these aims would produce a well described drug delivery system ready for *in vivo* testing in an atherosclerotic model.

2. Literature Examination

2.1. Overview

Developing a drug delivery system provokes inquiry into several different disciplines of research. The original idea was to develop a targeting system that would treat atherosclerosis, specifically the vulnerable plaque of atherosclerosis. Investigations into the recent developments and conclusions about atherosclerosis revealed that the disease, like numerous other chronic pathologies such as arthritis, lupus, and chronic obstructive pulmonary disease, is an inflammatory disorder. Systemic implications and common mechanisms in the build up of inflammatory disease are demonstrated by the high incidence of atherosclerosis in rheumatoid arthritis patients without traditional risk factors for the disease[41]. The onset and characteristic phases of atherosclerosis are described, as well as the mechanisms of inflammation and the disease progression. Literature reviews of atherosclerosis lead to investigation of other inflammatory pathologies as a means to identify potential treatment strategies. Furthermore, the mechanisms of disease onset and progression provide targeting strategies; cellular adhesion molecules are mediators of progression of atherosclerosis, among other inflammatory diseases, and are reviewed generally, and the candidate adhesion molecule, CD44 specifically.

Identifying the appropriate drug delivery vehicle provoked research into the large body of work representing drug targeting generally, vesicular drug targeting, and liposomal and niosomal drug delivery specifically. Drug targeting may be directed passively or actively; active targeting is usually mediated with a

vector molecule, and some of the methods and applications of actively targeted drug delivery are reviewed. Finally, a review of targeted imaging and therapy in cardiovascular medicine is reviewed.

2.2. Cardiovascular Disease and Atherosclerosis

2.2.1. Implications of Cardiovascular Disease

The American Heart Association (AHA) lists prevalence among Americans of having one or more types of cardiovascular disease (CVD) at 37.1% for 2004. Over 36% of all deaths of Americans in 2004 were attributed to CVD[35]. Of the different types of CVD, coronary heart disease and its underlying cause, atherosclerosis, is the largest single cause of death[42]. Atherosclerosis is a type of arteriosclerosis, which describes the thickening and hardening of the arteries generally. Atherosclerosis is the build up of lipids, cholesterol, calcium, cellular waste, and fibrin and the proliferation of smooth muscle and inflammatory cells within the sub endothelial space of medium to large arteries[43], specifically including the aorta, carotid, coronary, and peripheral arteries[44]. This evolving accumulation of plaque causes narrowing of the arteries reducing the lumen and the area available for blood flow, and decreases flexibility of vessels to absorb the pressures created by blood flow. Stenosis is defined as “the constriction or narrowing of a passage or orifice”[45].

Atherosclerotic plaques are prone to erosion and/or rupture which produces a release of core lipid and inflammatory contents into the blood stream. As the coagulation factors in the blood contact the inflammatory tissue factor (TF) expressed by the macrophages and the smooth muscle cells, along with other

expressed materials, a blood clot or thrombus forms in the lumen of the blood vessel[42]. A thrombus is the product of the coagulation cascade of the blood; the platelets activated by thrombin form a plug immediately and are further enforced as fibrin fibers are formed by the cascade of coagulation factors[46]. This process is necessary for hemostasis, to reduce blood loss in a damaged blood vessel, for example, however the formation of occlusive thrombi as a result of plaque rupture is the major instigating factor of coronary events[47]. Additionally it has been shown that the plaque's composition is a greater predictor to susceptibility to rupture than size, or degree of stenosis[42]. In fact, many plaques prone to rupture do not appear to be severely stenotic in a coronary angiogram[48-51].

2.2.2. Atherosclerosis Development

Traditionally, atherosclerosis was considered to be a passive lipid processing disorder with plaques gradually evolving over time to eventual occlusion of the blood vessel. In this view the blood vessel itself is considered to be an 'inert tube', not a dynamic structure interacting with blood and extracellular matrix elements and cells, and proteins, which are seen in the normal artery but also actively contribute to the progression of the disease.

Plaques may form as either stable, or unstable, vulnerable. Stable plaques are characterized by a thick fibrous cap, a small core of lipid materials and an unchanged lumen area, whereas vulnerable plaques are characterized by a thin fibrous cap covering a large lipid core containing inflammatory cells.

Atherosclerosis is classified in stages assigning levels of severity to plaques as they develop as seen in Figure 2.1[44]. The initial stage, Phase 1, is

the development of the fatty streak and proliferation of monocytes; the endothelium may be unaffected at this stage and no symptoms are evident[52] as the vasculature compensates by 'remodeling' and maintaining the size of the lumen[53].

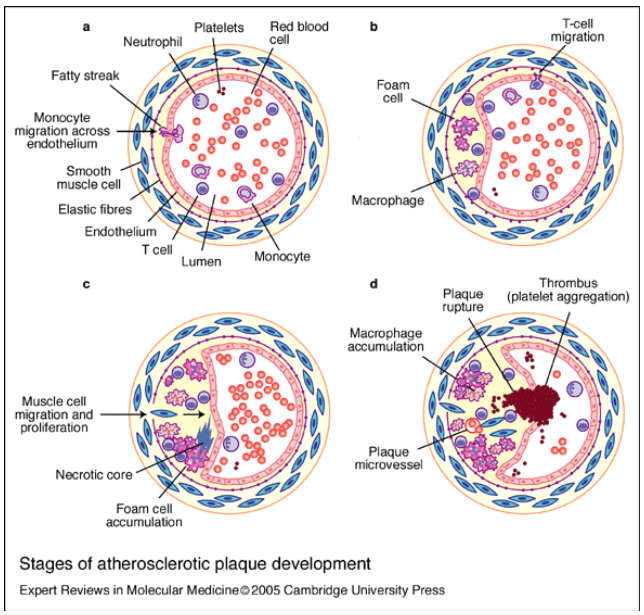

Figure 2.1 The Stages of Atherosclerotic Plaque Development. From [47].

Figure 2.2 shows an outline of the stages describing the disease progression as defined by atherosclerotic lesion development and architecture[47]. At the first stage the small lesions are of three types of increasing complexity; type I consists of lipid-filled foam cells derived from macrophages. Type II lesions contain smooth muscle cells and lipids from the extracellular matrix along with fatty foam cells, and in type III lesions the smooth muscle cells are immersed in connective tissue, fibrils and lipids[54]. Phase 2 is described as advanced, with pre-stenotic lesions with potential to rupture, and progresses into either Phase 3 or 4. Plaques at Phase 2 are either type IV, or type Va; the

former characterized by a large lipid volume and smaller fibrous cap, and the latter having a more extensive cap[47]. Phase 3 lesions are type VI developed from type IV or Va lesions that have ruptured or eroded and form non occlusive thrombi.

Phase 4, as shown in Figure 2.2, is the alternate path from Phase 2, and has severe characteristic symptoms from type VI lesions. Occlusions may be constant or periodic and present clinically as acute coronary syndrome. Because a third of occlusive thrombi come from non stenotic plaque disruption the syndrome may not be obvious until there is severe sudden ischemia or a myocardial infarction (MI)[47]. Finally, in Phase 5 lesions are type Vb or Vc and are either, respectively, calcified or fibrous and may both cause angina (chest pain due to constricted oxygen flow) or ischemia[44].

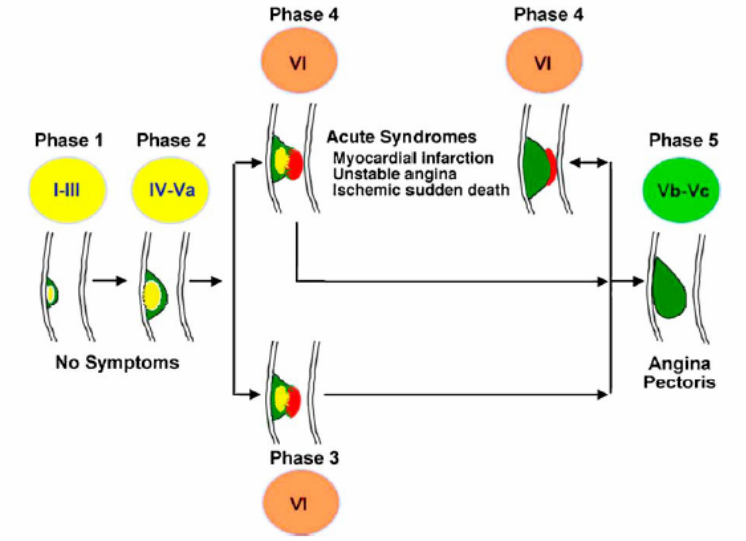

Figure 2.2 The Phases of Atherosclerosis. From [55]

To further complicate an intricate process, the progression of atherosclerotic plaques vulnerable to rupture and thrombus formation and their

triggering events are not homogenous across different areas of the vasculature. Plaque disruption is a critical trigger for acute events in coronary arteries, less so in the carotid, and in the peripheral arteries thrombogenicity (the propensity to form thrombi) is more crucial[42].

2.2.3. Atherosclerosis and Inflammation

Inflammatory processes play a role in vascular disease, rheumatoid and osteoarthritis, chronic obstructive pulmonary disease, and inflammatory bowel disease, lupus, among others. The inflammatory process is characterized by accumulation of inflammatory cells, leukocytes, and macrophages that perpetuate the process and contribute to tissue destruction.

Once understood to be a disorder of lipid accumulation and cholesterol metabolism, atherosclerosis is now described as a "chronic inflammatory disease of the arterial system"[56]; inflammatory factors are implicated in every phase of plaque development. Endothelial cells contacting flowing blood mediate interactions of underlying vessel tissue with blood cells and components. In normally functioning endothelium, which forms a monolayer of cells on a basement membrane that cover the intimal layer, expression of inflammatory-response cellular adhesion molecules (CAMs) and the subsequent attachment of circulating leukocytes, is minimal[42].

There is general agreement that atherosclerosis begins with an inciting injury to the endothelium provoking an inflammatory immune response[57]. When normal homeostasis is not restored, endothelial cell dysfunction continues as the disease progresses[58]. It is the expression of adhesion molecules and the influx

of leukocytes that perpetuate the disease throughout the process. Vascular adhesion molecule-1 (VCAM-1) has been shown to play a major role in leukocyte recruitment, binding to monocytes and T lymphocytes[59]. Further description on the role and mechanisms of adhesion molecules in the inflammatory process will be discussed in Section 2.3. A monocyte crossing the endothelium and entering the tunica intima becomes a tissue macrophage, which then takes up lipids and lipoproteins, in particular oxidized low density lipoprotein (LDL) in the plaque and further transforms into a foam cell[60]. The build up of foam cells is a characteristic of plaques. The foam cells produce pro-inflammatory cytokines which further provoke immune response in the plaque and promote reactive oxygen species[61]. Eventually the foam cells accumulate in the center of the lesion, die, and form a necrotic core within the plaque. Death of the foam cells is attributed to either apoptosis (programmed cell death) or the toxic effects of oxidized lipoprotein uptake[62].

The products of the inflammatory cells within the plaques disrupt the stability of the fibrous cap covering the plaque. Macrophages and smooth muscle cells release proteinases, such as collagenase and elastase, which break down the structural proteins collagen and elastin. The degradation of elastin also disrupts the ability of cells to move though the plaque[61].

2.3. Adhesion Molecules

Cellular adhesion molecules (CAMs) mediate blood -endothelial cell interactions common to all segments of the vasculature under physiological or pathological conditions [62]. They are glycoproteins which have cytoplasmic, transmembrane and extracellular domains[63]. CAMs are expressed by nearly every cell type[55], and are characterized by strong ligand binding. They participate in cell to cell and cell to matrix interactions and in some cases also signalling, migration, motility, gene transcription and differentiation[64].

As was mentioned previously, a hallmark of endothelial dysfunction at the initiation of atherosclerosis is the persistent adherence of circulating leukocytes and their subsequent uptake into the tunica intima[65]. The inflammatory cells are recruited by CAMs. CAMs expressed by the endothelium include intercellular adhesion molecule-1 (ICAM-1), vascular adhesion molecule-1 (VCAM-1), and platelet-endothelial cell adhesion molecule-1 (PECAM-1), integrins, and selectins[66].

Once the adhesion molecules bind with monocytes, macrophages, lymphocytes or platelets, those bound elements become activated themselves, and release proinflammatory cytokines, membrane receptors, and a myriad of enzymes, including the interleukins, tissue necrosis factor alpha (TNF-α), interferon-α, and numerous others. Cytokines have been shown in increase the expression of adhesion molecules including TNF-α, and interleukin-1 β (IL-1β) and increase the binding of leukocytes to the endothelium[67]. The expression of inflammatory proteins creates a positive feedback loop by further inciting uptake

of inflammatory cells, promoting aggregation of oxidized LDL on the endothelial surface and thus causing injury to the endothelium, and excreting further inflammatory mediators[68].

Since VCAM-1 is at the forefront of monocyte recruitment in lesion formation[69] it has been identified as a potential therapeutic target and has been widely studied[70]. In knock out gene studies with mouse models the elimination of VCAM-1 but not ICAM-1 was shown to reduce plaque formation in atherosclerotic mice[71]. *In vitro* studies with monocytes co-cultured with endothelial cells showed that adhesion was reduced when cells were treated with antibodies raised against VCAM-1 and E-selectin, but not P-selectin[61]. Levels of expressed VCAM-1 are used as a measurement in the efficacy of drug therapy[72].

Adhesion molecule P-selectin is expressed on activated endothelial cells and platelets. Targeting P-selectin demonstrated therapeutic efficacy in an atherosclerotic mouse model which are cross bred with a P-selectin null mouse model. Reduction in plaque formation and proliferation of leukocytes was observed. However, the presence of soluble P-selectin in the bloodstream complicates the strategy[73].

Depending on the therapeutic strategy, these adhesion molecules could provide drug targeting candidates. There have been numerous studies using anti-VCAM[74], anti-ICAM-1[75], and the anti-selectins[76] antibodies as targeting vectors which show great potential *in vitro*, however, there has been very little translation of these studies *in vivo* over the last decade. Collaboration with arthritis researchers[70] led to the investigation of another adhesion molecule

candidate, CD44[77], ligand to hyaluronan (HA), a polysaccharide a major component in the extracellular matrix (ECM) of mammalian cells. The interactions of CD44 and HA have been implicated in cancer, autoimmune diseases, and inflammatory processes[78].

2.3.1. Adhesion Molecule CD44

CD44 is a family of adhesion molecules that are characterized by their function, and mainly described as hyaluronan receptors. There are 10 standard isoforms and 10 variant isoforms of CD44, and the most populous is the CD44s isoform. The variation among the forms is found in ECM domain of the structure and accounts for the isoforms variation in function78. CD44 isoform CD44-v6 is highly expressed in the smooth muscle cells of the intima and media of injured arteries[78], CD44 isoforms including CD44-v6 are expressed on the endothelium suggesting regulatory function of growth factors[28] CD44 v10 is expressed by aortic endothelial cells[28]. Isoforms CD44-v3 and CD44-v6 where shown to be expressed on plaque microvessel, whereas CD44H and CD44v6 both express on endothelial cells after exposure to IL-1β and TNF-α. Cd44H, CD44-v5, CD44-v6, CD44-v7/8 isoforms are all expressed on macrophages and are all highly regulated by the cytokines[74]. CD44 and HA were shown to mediate leukocyte endothelial cell adhesion, previously thought to be the sole domain of the selectin family[79]. These studies taken all together indicate that CD44 isoforms are implicated in the pathogenic inflammatory process of atherosclerosis and that their role is highly complex and regulated.

Interruption of the inflammatory process has been studied using CD44 blocked by antibody IM7 (anti-CD44)[80]. Expression of CD44 and its variants was augmented when exposed to pro-inflammatory cytokines within human atheroma, implicating CD44 expression with the pathogenesis of arterial diseases[74]. CD44 was further implicated in the progression of atherosclerosis. Hyaluronan was shown, in a low molecular weight form, to stimulate vascular cellular adhesion molecule (VCAM-1) and proliferation of smooth muscle cells (SMC), whereas high molecular weight forms of HA inhibit SMC proliferation[81]. Atherosclerotic prone ApoE-deficient mice bred with CD44-null mice showed a 50-70% reduction in aortic lesions compared to CD44 heterozygous and wild type mice [82]. These results suggest that CD44 promotes atherosclerosis by both mediating inflammatory cell recruitment to atherosclerotic lesions and by altering smooth muscle function [81].

2.4. Drug Targeting

Drug targeting is a strategy aiming at the delivery of a compound to a particular tissue of the body. Drugs can be delivered singly or in large amounts by using drug carriers. Drug carriers are substances that facilitate time-controlled delivery, organ-specific targeting, protection, prolonged *in vivo* function, and decrease of toxicity of drugs to unspecified tissues. Drug targeting may allow for increased permeability of membrane barriers, allowing for molecular movement between tissues. Ideally, drug targeting would provide a high local concentration of drug at the site of disease and a concentration below levels of toxicity in healthy tissues[81]. Examples of drug carriers are myriad,

including but not limited to, liposomes, micelles, polymeric vesicles, and nano-particles[6].

Normal administration of drugs or therapeutic agents does not allow for concentrated accumulation of drug at diseased sites due to an essentially uniform distribution of drug throughout the body. In order to adequately treat affected sites using traditional systemic administration high doses of drug must be delivered. This not only increases costs, but also can create toxic side effects as normal tissues and organs are needlessly exposed to pharmaceuticals [83]. Encapsulation of drugs for passive targeting, either by liposome [81], niosome [68], or polymeric [81] media has shown increased retention time, decreased therapeutic dose, and reduced toxicity to unspecified tissues.

Targeting schemes include direct application into the affected organ or tissue, passive application to tissues through leaky vasculature-tumors, infarcts, or inflammation. Another scheme is physical targeting, which can be based on manipulating an abnormal pH or temperature at the target by using pH or temperature sensitive drug carriers. Magnetic targeting of drugs to affected areas within the body can be achieved using paramagnetic carriers attached to magnetic drugs and then directed by an external magnetic field[84]. Active drug targeting is generally described as the use of a vector molecule with a high specific affinity toward the affected tissues bound to a drug or drug carrier [21]. Active drug targeting using a monoclonal antibody vector is the approach of this research.

2.4.1. Vesicular Drug Delivery

Among drug carriers listed previously, vesicular drug carriers provide advantages over individual single molecule carriers. They not only allow greater payload of drug to be delivered, but also provide isolation of the drug from the system overall and thereby provide protection immune responses. Vesicle bilayers mimic biological membranes which enhance absorption of encapsulated drugs across cell membranes and into tissues. Vesicular drug delivery allows protection of the encapsulated drugs from enzymatic degradation[85], prolonged circulation time, and therefore a reduced rate of release of drug into the bloodstream[86], and the shielding of an immunogenic drug from recognition by the reticuloendothelial system (RES)[85].

2.4.1.1. Liposomes

Vesicles made from organically-derived amphiphilic (having both hydrophilic and hydrophobic moieties) phospholipids, like those that comprise cell membranes, are the most prevalent and widely researched drug delivery particle[87]. These liposomes, or “fat bodies” from the Greek, were first observed by researchers in the 19th century using lecithin in blood clotting studies. In 1911, Otto Lehmann published a representation of micrograph of what he called ‘artificial cells’ which resembled a dispersion of multi-lamellar liposomes [88]. Even though work with lecithin dispersions continued the properties and potential applications of these dispersions were not described until Dr. Alec Bangham and his colleagues published their seminal work [89]. They described how these particles, formed from the hydration of lipid thin films, retained some of the

hydrating solution that they formed in within their core creating a 'permeability membrane'. Researchers used the self assembly vesicles to study biological membranes and other applications, and these pursuits eventually led them to drug delivery. Liposome applications that developed thereafter, both commercially and within academia, are many and varied including multiple scientific disciplines; medicine, immunology, diagnostics, cosmetics, ecology, cleansing and the food industry [90]. Promising laboratory research did not always translate to commercially viable scale-up within the medical realm, however, and repeatability and stability problems caused early liposome based start-up pharmaceutical companies to fail[91].

Liposomes' interaction with cells has been studied not just for drug targeting purposes but also in developing further understanding of cell-cell interactions. Liposomes' interaction with cells can be characterized in four ways shown in Figure 2.3. First, the liposome may exchange material, either lipids or proteins, with cell membranes. Secondly, liposomes may bind or adsorb with cells, and once bound may be internalized through either endocytosis or phagocytosis. Alternately, the bound liposome may instead fuse with the membrane. Whichever of these possibilities arise is dependent on the size, charge, and makeup of the vesicle[92].

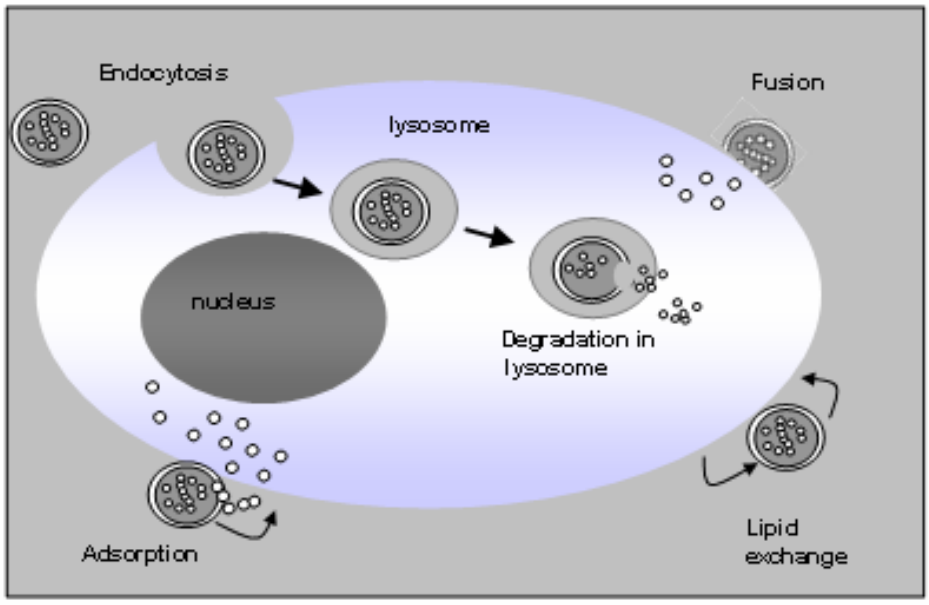

Figure 2.3 Vesicular Interactions with Cells. (Adapted from Lasic [81])

The problem of early and rapid elimination from the bloodstream of the first liposome formulations was solved by the development of the 'Stealth' or 'sterically stabilized' liposomes[93]. The addition of small amounts of a hydrophilic polymer, frequently polyethylene glycol (PEG), extended the half life of a 'classic' liposome from a few minutes to several hours[94]. Researchers have developed several synthesis techniques to enhance desired characteristics. Along with varying methods of synthesis, vesicular drug delivery also varies in physical makeup. Multiple vesicle layers have been shown to enhance release rates significantly when compared to free drug and uni-lamellar vesicle delivery[95].

Development of commercially available vesicle applications, passive and active, have been pioneered by cancer research[96]. One multiple-application technology that is being developed commercially is called DepoFoam™ and is made by the Swiss company SkyePharma. They produce foams of spherical

lipid-bilayer aqueous chambers, or multivescular liposomes that are used to encapsulate drugs, vaccines, DNA, peptides or large particle bio-therapeutics which may be administered locally or systemically[97].

2.4.1.2. Niosomal Drug Delivery

Niosomes are analogues of liposomes synthesized from synthetic surfactants rather than organically derived phospholipids. They are also self assembly vesicles usually composed of a surfactant, cholesterol and a steric stabilizer, such as dicetyl phosphate[98]. Niosomes behave similarly to liposomes *in vivo* by prolonging circulation time of the encapsulated drug and altering chemical distribution within the body [99,100]. However, niosomes have advantages over liposomes as drug carriers, including chemical stability, lower cost, easier storage and handling, and a reduced likelihood of becoming toxic through oxidation [8]. Like liposomes, niosomal encapsulation reduces toxicity of drugs to untargeted tissues in many different applications and therapies. Niosomal drug delivery has been studied using various methods of administration [7] including intramuscular [10], intravenous [101], peroral, [102]and transdermal [103]. Niosomes can be used to solubilize insoluble agents[86]. Nebulized surfactants entrapping all-trans-retinoic acid were delivered as an inhaled aerosol reducing the drug toxicity and altering the pharmacokinetics [84]. In addition, as drug delivery vesicles, niosomes have been shown to enhance absorption of some drugs across cell membranes [26], to localize in targeted organs [17] and tissues [84,104], and to elude the RES [105]. Cellular uptake of niosomes can be via endocytosis [106]**;** however

they have been shown to bind and fuse with cell plasma membranes via cellular receptors when vesicle surface charge is sufficiently negative [26].

Niosome entrapment of methotrexate administered orally and intravenously in a mouse model was shown to increase residence time in the body and decrease clearance[27]. Tumor targeting of niosomal formulations of doxorubicin[26], vincristine sulfate[105], cisplatin[107], camptothecin[24], shown increased residence times and anti-tumor efficacy compared to free drug.

Recent examples of niosomal drug delivery research are varied and include topical vaccination generally[24] and of DNA[108],[106] and treatment of acne[109], alternate insulin delivery methods[2], oral immunizations[110], transdermal anti-inflammatories[111], and ophthalmic applications[112], among others.

2.5. Background and Current Practices in Antibody Mediated Drug Targeting

The discovery of the nature of antibodies and the development and refinement of monoclonal antibody production had a revolutionary effect of the treatment of infectious disease and has provoked the pursuit of numerous targeting strategies in cancer and cardiovascular medicine[113].

Anticancer therapy, and especially tumor targeting, has been the forerunner in the development of liposomal [28], niosomal [32], and other drug delivery systems[32] and is the most widely pursued application of antibody mediated targeted drug delivery [32]. Early clinically approved and commercially available nanoscale (200 nm or smaller) systems for untargeted drug delivery were developed for cancer treatment and include DOXIL®, a liposomal encapsulation of doxorubicin (1995), and Ambisome®, liposomal amphotericin

(1990)[32]. Innovations in vesicle-antibody linking schemes were also driven by cancer researchers. In order to increase circulation time and decrease the rapid clearance of classic liposomes from circulation, polymer groups (usually PEG groups) were added to liposomes surfaces[32]. These liposomes showed favorable passive targeting to tumors and leaky vasculature. The addition of site specific targeting vectors, monoclonal antibodies and fragments most prevalent among them, provided active targeting capabilities to improve therapeutic capacity and decrease non specific tissue interactions. When antibodies were coupled to the vesicle surface of a PEG coated liposome both the ability of the antibody to bind to the surface of the liposome was hindered, as well as its capacity to attach to the targeted antigen site[68]. The PEG groups that inhibited the desired qualities of an immunoliposome provided an attractive site for antibody attachment and increased antibody-antigen site recognition versus attachment of antibodies at the vesicle surface[34].

Liposomal immunotargeting has been used extensively for cancer and cardiovascular applications. Antibody-vesicle conjugation chemistries are varied but there are similar physical configurations of linkers that result in increased efficacy of antigen binding when the ligand is attached distal to the vesicle surface. This increases rotational freedom of the targeting moiety and decreases hindrance by the bulky polyethelyne glycol (PEG) groups at the surface of a 'stealthy' liposome[114]. Attachment of ligand distal to the vesicle on a PEG terminus was found to have increased binding to target cells compared to attachment on the surface[31]. Development of a polyethylene end group on a

phospholipid molecule functionalized with cyanuric chloride allowed for attachment of antibodies without prior derivatization of antibodies [115]. Improved tumor targeting was shown using niosomes with PEG-glucose conjugates using a paramagnetic agent encapsulant[28]. Echogenic liposomes conjugated with targeting antibodies show in vitro promise for simultaneous imaging capabilities and targeted therapeutics [116].

Differing antibody-polymer linkage schemes were developed, usually by creating a functionalized PEG group coupled to a phospholipid molecule ('linker lipid'[92,95,117-126]) and incorporated into the vesicle membrane for subsequent antibody or targeting vector coupling. These schemes included differing formulations of thioether bonds coupling an antibody to the terminal end of a PEG group, either by activating a maleimide group attached to a thiolized antibody [7,8,91,99,100,102,127-131], or hydrazide group reacted with an aldehyde group on an oxidized antibody[10,99,132-135], among others. An end-group functionalized PEG linkage was developed that did not require activation or functionalizing of the antibody[105]. A cyanuric chloride molecule to was added to the head group of a membrane component phospholipid linking a PEG molecule to that, and then another cyanuric chloride molecule to the terminal end of the PEG which would then be coupled to an antibody via nucleophilic substitution[115,136-138].

Although the group subsequently found unfavorable *in vivo* blood circulation times of their immunoliposome (IL) formulation[19,28,29,139], subsequent studies have identified the F_c region of the whole antibodies used as the culprit in provoking an immune response, and promoting rapid clearance of ILs.

Researchers have demonstrated this with liposomes conjugated with anti-HER2 monoclonal antibody fragments (the protein HER2 is a member of the epidermal growth factor family and is over-expressed in breast cancer and implicated in its pathogenesis) [105]. The anti-HER2 IL-were shown to have identical blood residence time as compared to non-targeted sterically stabilized liposomes *in vivo*, and further showed no increased clearance with subsequent administrations. Incubation with cells that over-expressed HER2 had a 700 fold increase in cellular uptake of drug compared to non-targeted liposome[140]. Active targeting of niosomes was shown using glucose targeting with the inclusion of a glucose-palmitoyl glycol chitosan conjugate in a sorbitan monostearate niosome[141]. Improved tumor targeting was shown using niosomes with PEG-glucose conjugates using a paramagnetic agent encapsulant[142]. To our knowledge there is no literature on any other group studying antibody targeting of niosomes.

2.6. Cardiovascular Antibody Mediated Imaging and Therapy

2.6.1. Imaging and Therapy

Diagnostic medical imaging is a prevalent and non invasive technology widely used in obstetric and cardiovascular disciplines, among others. Innovations in technology have transformed ultrasound (US) images from grainy and poorly-resolved to sharp digital imaging[115]. The non invasive nature of US tissue penetration makes it an attractive therapeutic strategy. Active therapeutic targets within the cardiovascular system include atherosclerotic plaques, or other

areas of damage within the vascular walls and bed, infarcts, thrombi and blood elements[115]. US targeted imaging [88] and imaging driven therapy of thrombi has been widely pursued[143]. Contrast agents have been studied not just for the ability to enhance ultrasound (US) imaging but also for thrombolytic potential created by the very high localized pressures created when US exposed contrast agents burst driving their therapeutic load into target thrombi[88]. Ultrasound imaging of a liposomal combination of echogenic contrast agent and drug delivery vehicle has shown also the ability to guide therapy and disrupt thrombi [88,144]. Additionally contrast agents, or 'microbubbles', have been studied as potential gene delivery vectors by exploiting the explosive cavitation of US exposure driven bursting to propel plasmid DNA into vessels[88].

Detection of expressed adhesion molecules as antibody directed contrast agents bind locally can be used to identify inflammation and early detection of cardiovascular pathologies[115]. Atherosclerotic animal models demonstrate the facility of targeted MRI imaging of thrombus producing ruptured plaque to potentially guide therapy[136]. Atherosclerotic plaques can also be imaged using targeted US contrast techniques accessing either expressed inflammatory adhesion molecules on the endothelial surface or activated bound leukocytes through contrast agent antigen receptors[136].

The potential to direct therapy through imaging and simultaneously control drug delivery and release could address several challenges of inflammatory pathologies as greater understanding of the complex chemical and molecular

interactions of inflammatory processes drive plaque buildup, instability and vessel restenosis[115].

2.6.2. Current Research in Vesicle Mediated Drug Delivery in Inflammation and Cardiovascular Disease.

Reviews of cardiovascular targeted drug delivery cover the myriad applications pursued in targeting pharmaceuticals to cardiovascular disease[145]. Thrombus treatments and imaging have been targeted with and without antibody or other protein mediation, and through magnetically driven thrombolytics. Atherosclerotic lesions, circulating blood cells and elements, and endothelial cells have all been addressed as therapeutic targets. In treatment of lung disease, aerosols have been developed to accumulate drug delivery in the lungs[92], as have antibody-mediated delivery to antigens in the lungs[146], to malignant lung disease[145], and immuno-liposomes directed to the pulmonary endothelium[30,147-149]. The mechanisms and techniques of successful targeted and untargeted accumulation of drug delivery vesicles in the pulmonary endothelium are relevant to developing other vascular inflammation strategies.

Imaging of pathogenesis in the heart through targeting has been studied post myocardioal infaction and in myocarditis. Liposomal accumulation has been shown in ischemic heart tissue [150]. Liposomal cardiovascular targeting has been reviewed in detail specifically[32]. While limited to intravascular tissues only, *in vitro* and *in vivo* studies of liposomes and immunoliposome as a drug carriers to many antigens were addressed[151]. Among the topics reviewed was the targeting of vessel wall injury. Multiple pathologies, atherosclerosis, and coronary

thrombosis among them, are initiated by vessel injuries which promote platelet activation and binding. Early detection of the disrupted endothelium through targeting of expressed antigens providing a 'signal' has been studied. This included an *in vitro* examination of targeting extracellular matrix antigens where collagen gaps provide binding sites for liposomes conjugated with antibodies to type 1 collagen, and similarly proven against laminin and fibronectin also. These studies showed good affinity, specificity, and selectivity. Also the liposomal antibody-antigen binding mimicked nature: cell binding studies showed that liposomes conjugated with antibodies provided a dissociation constant (describes the affinity between ligand and protein) on the order of 10^{-9} M, which corresponds to physiological antigen to free antibody binding constants[151].

Human endothelial cells incubated with immunoliposomes conjugated with cell surface antibodies (anti-T antigen A25) were shown to bind at 4˚C and endocytose 30% of bound ILs at 37˚F. Liposomes and ILs were seen to accumulate in an ischemic heart providing imaging and therapeutic targeting potentials to damaged myocardium. Positively charged untargeted liposomes were observed to accumulate in experimentally produced myocardial tissues as early as the 1970s; further studies confirmed further the propensity for liposomes to accumulate in depolarized myocytes and in ischemic tissues in general[151]. These findings provided the groundwork for liposome passive targeting to ischemic tissue and infarcted heart tissue.

Active targeting of anti-myosin conjugated ILs to myocardial tissue was studied *in vivo* and showed good accumulation in the ischemic myocardial tissue.

This effect is limited in traditional liposomes when access is restricted because of lack of blood supply and vesicles are eliminated by the RES before accumulation occurs. As with other traditional liposomes, surface alterations by the incorporation of PEG groups along with antibodies provided targeting and prolonged circulation time showed greater penetration[152].

Another consequence of ischemia is the formation of lesions of the cell membrane. Loss of membrane integrity is further exacerbated upon reperfusion leading to cell death as cell contents are exposed and reperfusion injury ensues. The capacity to target and seal lesions created in hypoxic *in vitro* conditions using cardiocytes with immunoliposomes (ILS) shown to be effective, greatly increasing post hypoxic cell viability after IL incubation. Furthermore, hypoxic and IL treated cells were shown to grow normally in culture after the event[109].

Immuno-liposomes targeted to intercellular adhesion molecule 1 (ICAM-1) were shown to bind to and be internalized by epithelial cells *in vitro*, demonstrating their potential of the anti-ICAM antibody bearing vesicles to deliver an anti-inflammatory drugs to sites of increased ICAM expression [153]. With an aim to combat restenosis following coronary angioplasty, liposomes conjugated with peptide sequences were created to target to glycoprotein IIb-IIIa receptors on activated platelets[34]. Platelet aggregation and deposition is implicated in the pathogenesis of restenosis through deposition of growth factors and inflammatory mediators. To increase circulation time they modified the vesicle surfaces with an oligodextran polymer, analogous to the use of PEG groups to elude the RES [152]. The effect of stress by reactive oxygen species on

endothelial cells is implicated in cardiovascular diseases making antioxidant drugs therapeutic candidates. Antioxidant enzymes such as superoxide dismutase and catalase make good therapeutic candidates but are rapidly eliminated from the bloodstream, inhibiting their efficacy. Muzykantov's group[30] showed that by encapsulating the enzymes, which they coupled to PEGs, the elimination was greatly reduced and the efficacy and bioavailability of the enzymes were increased. Binding to expressed antigens in the endothelium *in vivo* was shown by targeting angiotensin converting enzyme (ACE) and adhesion molecules (ICAM-1 and PECAM-1). Vascular accumulation, endothelial uptake, and increased antioxidant protection were all shown with this targeting scheme[136]. ICAM-1, but not PECAM-1 was shown to be susceptible to pathological stimulus, exhibiting increased expression and uptake in and by endothelial cells. Anti-ICAM1 targeted immunoliposomes of 100-300 nm diameters showed specificity of uptake compared to non specific antibodies or large vesicle targeting[115].

The aim of the literature review was to not only establish a foundation of knowledge in the different disciplines involved in creating a targeted drug delivery system but also to identify the most appropriate carrier system, antigen target, mode of delivery and mechanism of uptake.

3. Project Description

The objective of this project was to develop and test a drug delivery system that could be targeted to vulnerable atherosclerotic plaque. Figure 3.1 shows the interdependent relationship of the physical elements needed to meet this objective. In order to design the system effectively, the affinity of the drug delivery vehicle must be established for both the drug of interest and the drug delivery vector that will be targeting the biological site. The targeting vector is chosen not only for its ability to seek and deliver the drug delivery system to the site of interest but also to help facilitate the uptake of the drug on site. Obviously the efficacy of the drug delivered must be appropriate to treat the affected site.

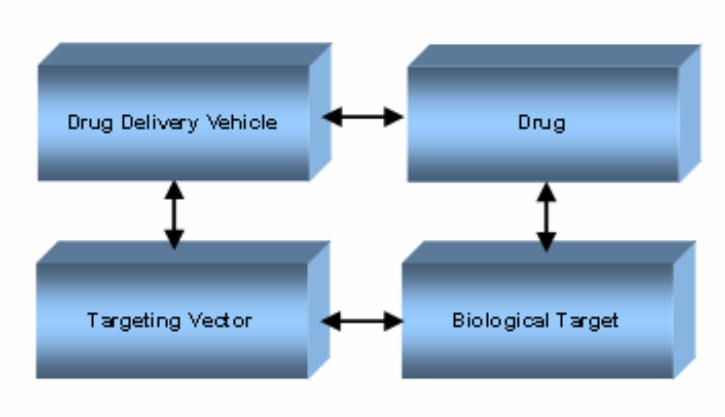

Figure 3.1 Interdependence of Elements of the Drug Delivery System.

The drug delivery vehicle that was chosen for the system is a non ionic surfactant vesicle, or niosome. The vesicle's stability, versatility, biocompatibility, and cost made the choice compelling. Surfactant components available are numerous, allowing versatility in formulation strategies to not only manipulate

stability[136] (the ability to retain the encapsulated component) but also to allow the potential to incorporate various linkers to the vesicle surface[105]. The biological target provides the therapeutic conduit, and therefore should be specific to the disease pathogenesis and if possible, implicit in it. The development of atherosclerosis and the morphological changes in plaque along the progression of the disease provide varied targeting strategies[105]. The inflammatory processes implicated in each progressive step of plaque development and the shift in stability of the plaques have associated biomarkers which provide not only a targeting potential for *in situ* drug delivery, but also a mechanism to interrupt disease progression. Adhesion molecules are mediators in the process of inflammation and make logical therapeutic targets[70].

3.1. Development and Testing of an Immunoniosome

The use of an antibody-conjugated non ionic surfactant vesicle or 'immunoniosome' to target vascular inflammation is an original concept. Niosome research has been largely in the realm of cancer[154], immunization[155], and topical therapies[156]. The process of vesicle development included evaluating the formation and stability of niosomes composed of sorbitan monoester components that had been well described the literature and whose surfactants were commercially available[71]. Liposome literature describes the widespread use of polyethylene glycol (PEG) groups on the surface of liposomes, originally incorporated to elude the immune system, as a desirable site for targeting vector attachment. The addition of PEG may be accomplished by adding the polymers after vesicle formation to linkers attached to phospholipids accessible on the

liposome surface or by creating phospholipid PEG compound molecules and incorporating those as the vesicles form[157]. A similar polymer group was incorporated in one of our sorbitan ester surfactants but the stability of the polyoxyethylene sorbitan monostearate (Tween 61) niosome was not favorable. This led to investigating blending the surfactant components to evaluate the potential to introduce a linking site while maintaining the desired properties of stability and entrapment. Liposome literature reviews described multiple schemes linking proteins to vesicles[141]. Cyanuric chloride has been used in the past to adhere proteins to surfaces and was described as a linker in immunoliposomes[12,28,32,158]. From these ideas I developed the linking chemistry of the polyoxyethylene sorbitan monostearate functionalized with cyanuric chloride in order to provide a protein binding site on the surface of a formed vesicle. This is a novel process and a non-provisional patent application has been filed and published [159]. The resulting immunoniosome (IN), see Figure 3.2, was tested in a fixed synovial lining cell model for specificity, selectivity and binding. Adhesion molecule CD44 was identified as a target antigen implicated in the progression of atherosclerosis[160], so the binding studies were done with anti-CD44 as the targeting vector.

Bovine aortic endothelial cells were used to test the ability of the niosomes to binding to inflammatory cells specifically expressing target antigens. The binding of fluorescent INs to cells was measured using a customized Matlab™ program (see Appendix D), which relates the binding of immunoniosomes to the cells relative to experimental variables.

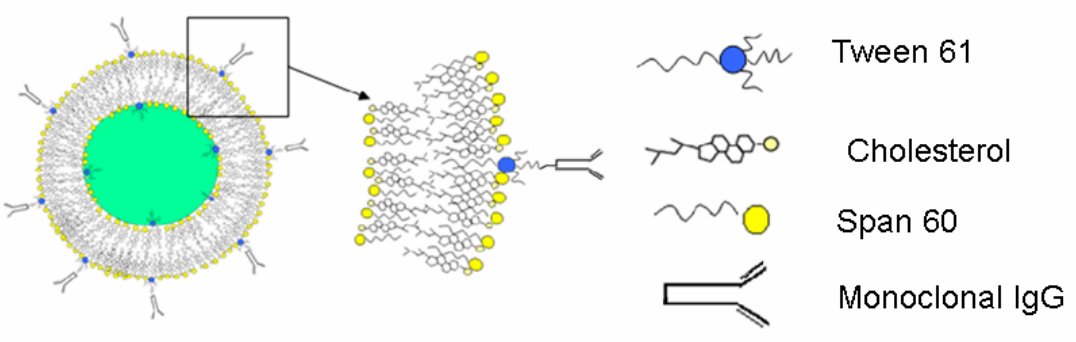

Figure 3.2 Immunoniosome Membrane Structure.

3.2. Binding and Uptake of Vesicles

Uptake of INs by cells was investigated. Prior to the live cell incubation studies, changes in the synthesis process were necessary. Reduction of niosome size by extrusion created niosomes of 200 nm, a size demonstrated as preferential in uptake by atherosclerotic lesions[148]. Additionally, in some studies antibodies were fragmented prior to conjugation and incubation with cells to evaluate the ability of the linkers to attach Fab fragments. Studies showing unfavorable uptake of whole antibody immunoliposomes implicated the conserved Fc region of the antibody[107,161], so in preparation for *in vivo* studies, uptake of Fab conjugated immunoniosomes, as well as the uptake of whole antibody targeted vesicles by cells was tested using confocal and TEM microscopy.

Finally, in order to test the efficacy of the system *in vivo* a protocol for a study using an atherosclerotic mouse model and treated with atorvastatin containing immunoniosomes compared to free drug treatment was developed and approved by the USF Institutional Animal Care and Use Committee (IACUC) and the US Army Medical Research and Material Command Animal Care and use Review Office.

4. Vesicle Development

4.1. Immunoniosome Synthesis Project Description

The development of the immunoniosome took place in four distinct phases. In the first phase, the general formulation of the vesicle had to be identified, synthesized, measured, and tested for viability. Niosome literature and availability of components favored using surfactants from the sorbitan ester family, both for stability, encapsulation capacity, and economy [30]. Vesicles of different compositions of those sorbitan esters, and their encapsulation and retention capacities were evaluated using fluorescent dye as a drug model. Chromatography, particle sizing, fluorescence intensity, and microscopy were employed to purify and measure vesicle formulations[162-164]. Vesicles were stressed with diagnostic levels of ultrasound to evaluate membrane stability. Also of interest was the potential to create a 'tuneable' targeted drug delivery vesicle that would not only be site specific but would have controlled release upon activation with US exposure. The next phase was a refinement of the first, and looked at the potential of blending surfactant components in quantities that retained desired stability properties while providing potential linker candidates. Once the blended formulation was established, the next phase involved the development and evaluation of the linker chemistry. Finally, once the ability of the surfactant linker to bind a monoclonal antibody to the surface of a niosome was established the last phase tested the ability of the resulting

‘immunoniosome’ to bind to a target antigen on a fixed cell using an activated fixed synoviocyte as a cell model of inflammation.

4.2. Material and Methods

4.2.1. Introduction

The ability of lipids to form bilayer vesicles instead of micelles is dependent on the hydrophilic-lipophilic balance (HLB) value of the surfactant, the chemical structure of the components and the critical packing parameter (CCP) which is the relationship between the structure of the surfactant including size of hydrophilic head group, and length of lipophilic alkyl chain (Figure 4.1). The formula is $CCP = \frac{v}{l_c a_0}$ where l_c = the length of the alkyl chain, v = the volume of the hydrophobic chain volume, and a_0= area of the hydrophilic head group[115]. The HLB value can measured experimentally for each surfactant by reversed phase thin layer chromatography[165]. The value represents a relative proportion of the hydrophobic and hydrophobic groups comprising the molecule and provides a guide for evaluating potential vesicle formation. Generally it has been reported that HLB for sorbitan esters are between 4.0-8.0[115]. For of an HLB value of greater than ~6, cholesterol must be added to the surfactant in order for a vesicle to form[166]. The general form of a single bilayer vesicle is shown in the left of Figure 4.1.

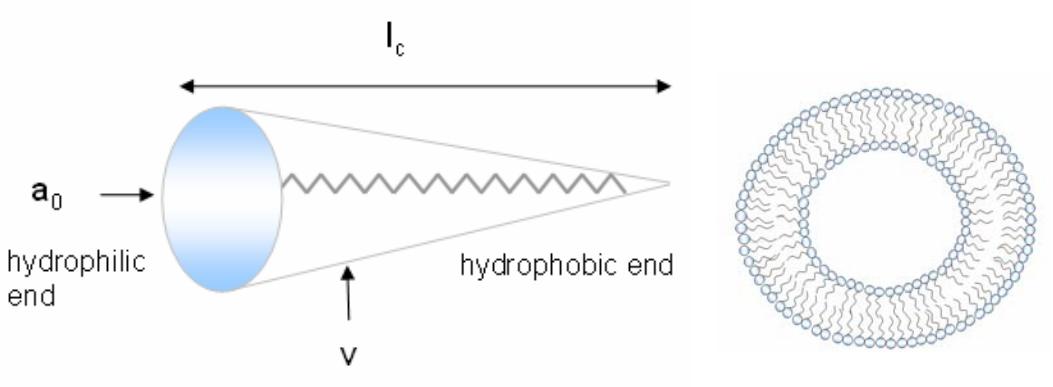

Figure 4.1 Critical Packing Parameter and Bilayer Membrane. Left: Schematic for calculating the critical packing parameter of an amphiphile (Adapted from Uchegbu 1998[115].) Right: Bilayer Membrane Structure

Niosomes are similar to liposomes in structure and methods of synthesis. The fundamental component of both is an amphiphile, a molecule containing both a hydrophobic and hydrophilic moiety, and the structure of the resulting vesicle is formed by a single or multiple bilayer membrane enclosing an aqueous core. There is a wide array of commercially available, inexpensive, biocompatible surfactants that enable specified structural design of vesicles[167]. Niosomes can form from many of these surfactants, and are commonly made by the combination of a single alkyl chain nonionic surfactant and cholesterol, in addition to an ionic electrostatic stabilizer, such as dicetyl phosphate. The addition of cholesterol enables more hydrophobic surfactants to form vesicles and suppresses the tendency of the surfactants to flocculate or form aggregates[167]. The addition of cholesterol has been shown to lend greater stability to the bilayer membrane by raising the gel liquid transition temperature of the vesicle. This stability decreases leakage of the vesicles and stabilizes against osmotic gradients[168].

The formation of single or multiple bilayer (lamellar) vesicles upon hydration is a result of the amphiphilic surfactant's (surface active agent's) interaction with the aqueous solution caused by the high interfacial tension between the water and the hydrophobic alkyl chains. This tension causes the hydrocarbon regions to associate simultaneously as the hydrophilic head groups orient towards the water; the actions of each opposing force culminate in the formation of the vesicle assembly [168]. The thermodynamics of formation dictated by Gibbs free energy (ΔG-ΔH–$\Delta S \geq 0$, at a given temperature) states that in order for the self assembly to go forward there must be sufficient enthalpy (ΔH) to overcome the negative entropy of the system (-ΔS) and the reduction in free energy (-ΔG). The van der Waals attractions, the hydrophobic-hydrophilic interactions, hydrogen bonding, and electrostatic interaction contribute the necessary enthalpy of formation. In order for the association of the molecules to proceed there must be an energy gradient between their associated versus isolated states, and Israelachvili stated that self assembly will proceed as long as the interaction free energy per associated monomer μ_N^0, (where N is the number of associated monomers) is greater that the mean interaction free energy of the isolated monomers; $\mu_N^0 < \mu_1^0$. This is true as long as μ_N^0 decreases with N, with μ_N^0 reaching a limiting value [168]. The energy gradient driven interactions of the molecules described underlie the HLB dependence of vesicle formation mentioned earlier as related to the shape and size of the hydrophilic head groups, and the lengths of the hydrophobic alkyl tails that dictate the HLB balance[169].

4.2.1.1. Gel-Liquid Crystal Transition Temperature

Formation of lamellar vesicles is dependent on not only the components themselves, but also on temperature. The bilayer structures have different phases in which they exist. The gel state is the most ordered, and the liquid crystal state is less ordered. Within the gel phase the alkyl tails of the amphiphiles are crystallized and can not diffuse. In the liquid crystal state there is lateral diffusion of the bilayer components. The liquid crystal phase of a system always exists above the gel phase. In order for niosomal vesicles to form the hydration must be set above the gel-liquid crystal transition temperature of the surfactant[167,169]. The gel phase transition temperature of Span 60 is 57˚C, and therefore the hydration and extrusion temperatures are set to 60˚C[167].

4.2.2. Materials

4.2.2.1. Chemicals

Niosome preparations and surfactant derivatization and treatments were made from sorbitan monostearate (Span 60), sorbitan monopalminate (Span 40), sorbitan monolaurate (Span 20), polyoxyethelene sorbitan monostearate (Tween 61), cholesterol, and dicetyl phosphate (DCP), diisopropylethylamine (DIPEA), cyanuric chloride (CC), Triton-X 100, which all came from Sigma Chemical, St. Louis, MO. Surfactant properties are listed in Table 4.2 in Section 4.2.3.1. Fluorescent dyes, 5(6) carboxyfluorescein (CF) and 5(6) carboxyrhodamine (CR) were obtained from Biotium, Hayward, CA. Phosphate buffered saline (PBS), and Sephadex G50, Histochoice tissue fixative, Hank's Balanced Saline (HBS), Dulbecco's Modified Eagle Medium (DMEM), Bovine serum albumin (BSA) and

goat serum were obtained from Fisher Scientific, Suwannee GA. Collegenase P was obtained from Roche Applied Science, Indianapolis IN. The Alexa Fluor© 488 protein fluorescent labeling kit came from Molecular Probes (A20181).

4.2.2.2. Vesicle Characterization Materials and Methods

Particle analysis included light scattering, single particle optical sensing technology, optical microscopy, chromatography techniques and fluorescence measurements. Fluorescence changes were measured to evaluate encapsulation by the vesicles and leakage over time. The mean particle size and distribution of formed vesicles were determined using an Accusizer 780A optical particle analyzer from Particle Sizing Systems. The algorithm behind the PSS technology combines single-particle light scattering and light extinction technologies. Light scattering is used for particles less than 1 μm in diameter, with a lower limit of 0.5 μm, and light extinction is used for particle greater than 1.0 μm. Small volumes (0.005 - 0.1 ml, depending on concentration) of niosome suspensions are added to the diluting chamber and diluted and cycled through the through the sensor until the concentration of particles is such that they pass through individually, eliminating 'coincidence' of particles. As the particles pass through a uniformly illuminated 'optical particle sensor' they obscure part of the sensor signal which produces an output pulse from a 35mW infrared diode. The pulses represent these discrete particles whose magnitude corresponds to a particle diameter. Figure 4.2 shows a schematic diagram of the auto-dilutor system. The accumulation of the pulses, interpreted by a signal processor, produces a particle size and concentration distribution plot (PSD). Figure 4.3

shows a PSD plot of a polystyrene standard containing a mixture of particles with three different diameters, 0.7, 1.0, and 5 μm. The known sizes and concentrations of the standards allowed for calibration and verification of the instrument.

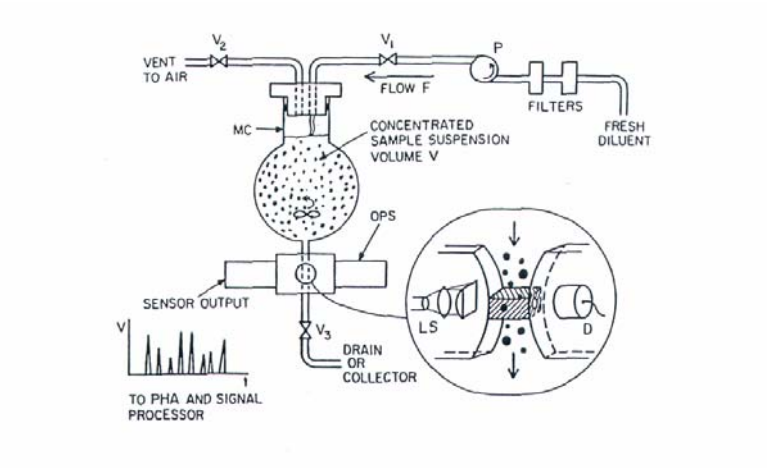

Figure 4.2 Autodilution Scheme of Particle Sizing System. (PSS User manual)

The vesicle suspensions were also characterized by observing the changes of their chromatography elution profiles details of which are described in the GEC purification below. Essentially, the constituents of a vesicle suspension are separated by size as they elute through a packed bed matrix, and those constituents can be measured using UV absorbance or fluorescence intensity. By comparing changes in elution chromatograms the relative stability of the formed vesicles can be monitored.

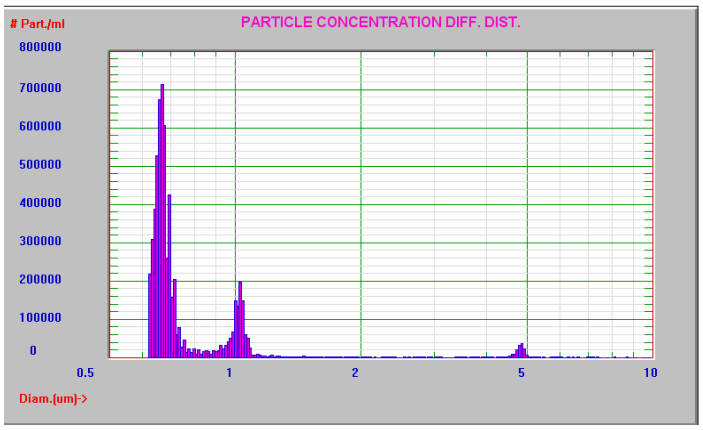

Figure 4.3 Particle Size Distribution Plot of a Mix of Three Sizes of Polystyrene Latex Standards.

Fluorescent dyes were used to study entrapment and retention in the niosomes because of the sensitivity and precision of fluorescent measurements. We were able to observe incremental changes as small as tenths of nano-moles of dyes in suspension. The sensitivity of carboxyfluorescein dye to changes in fluorescence intensity with exposure to light was tested by exposing varied concentrations to as much as five day's exposure to ambient light. The results shown in Figure 4.4 indicate the dye's resistance to decay despite exposure, reassuring us about any potential confounding effects of short term light exposure on signal changes. Nonetheless, dye solutions were always stored away from light in 4˚C.

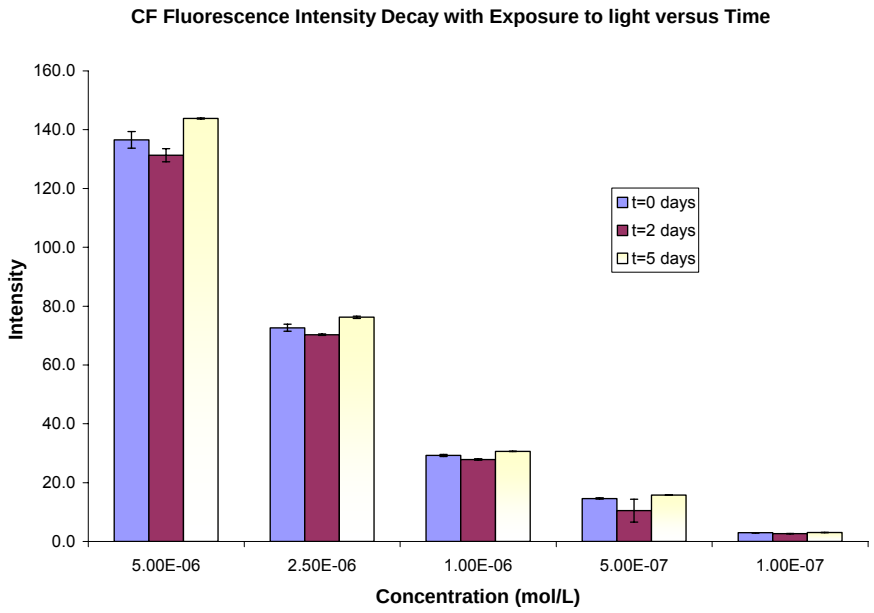

Figure 4.4 Stability of CF. The Decay of Varied Concentration of Carboxyfluorescein.

At low concentrations fluorescence intensity is proportional to dye concentration so encapsulation of dye can be calibrated by use of a standard curve, as shown in Figure 4.5. At higher concentrations the relationship is not linear and measured intensity will decrease with increased concentration due to self quenching as shown in Figure 4.6. Entrapment of dye by niosomes was measured by first disrupting the suspended niosomes with Triton X 100, a non-fluorescing detergent, and then measuring the fluorescence intensity of the dye released by the vesicles into the suspending buffer solution[70]. Light and fluorescence microscopy were also used to verify vesicle formation and disruption.

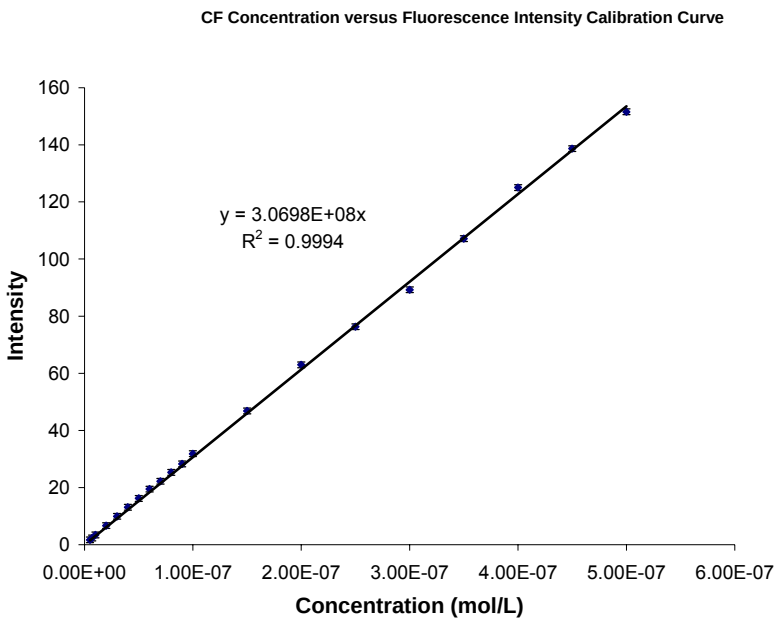

Figure 4.5 Calibration Curve of CF. Carboxyfluorescein Molar Concentration vs. Fluorescence Intensity

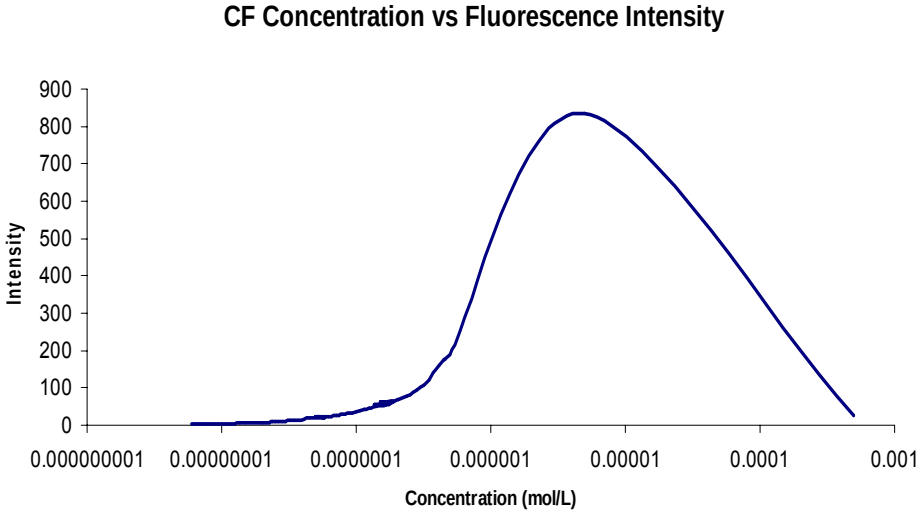

Figure 4.6 Calibration Curve with a Wide Range of Concentrations. Fluorescence Intensity with Respect to a Wide Range of Concentrations of Carboxyfluorescein Dye.

4.2.2.3. Vesicle Purification Materials and Methods

Niosome literature describes several methods of separating formed vesicles from un-encapsulated hydrating solutions and unformed lipids[33]. Among

them are gel exclusion chromatography, dialysis, centrifugation, and ultracentrifugation. Gel exclusion chromatography was chosen as an appropriate bench top method for this research. Gel exclusion chromatography (GEC) is also referred to as size exclusion chromatography, and provides relatively rapid separation of formed vesicles from unformed lipids and unencapsulated dye (or drug). Dialysis is time consuming and only eliminates the free dye and not the unformed lipids. Centrifugation provides only partial separation of unformed lipids, created vesicle disruption, and has limited utility depending on vesicle density. Ultracentrifugation was expensive and largely unavailable for our routine experimentation.

4.2.2.3.1. Gel Exclusion Chromatography

The theory behind GEC is straightforward. Gel filtration media is packed into a column to form a packed bed. The medium is a porous matrix of spherical particles, such as Sephadex G50, that are chemically and physically stable and non reactive. Micrographs of hydrated Sephadex G50 beads at two magnifications are shown in Figure 4.7. The packed bed is equilibrated by flushing with a buffer solution (the mobile phase) such as phosphate buffered saline (PBS). The liquid inside the matrix is referred to as the stationary phase. The void volume refers to the volume of the column not taken up by the matrix. Once a suspended sample is added to the gel matrix, buffer and sample move through the column. Larger particles do not enter the pores of the gel matrix; they move through the column at the same rate as the buffer, and elute within the first column volume. Particles small enough to be caught up in the gel matrix

pores elute later. The separation process takes place as one total column volume of buffer passes through the gel filtration medium. Gel filtration is an isocratic chromatography technique, meaning that separation is achieved without the use of any kind of gradient.

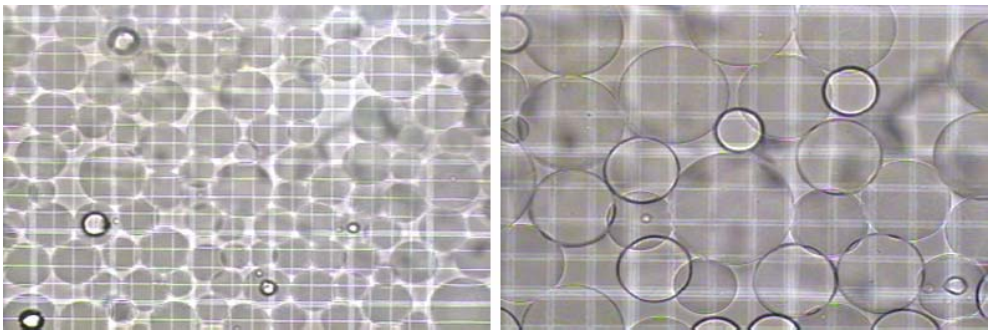

Figure 4.7 Sephadex G50 Hydrated Beads. Left: 100x magnification, right: 200x.

According to the theory the particles or molecules will be separated according to the Stokes radius of the particle. The equation for the Stokes radius is $M = \alpha as$ where M is molecular weight, a is the Stokes radius, and s is the sedimentation coefficient, $\alpha = \frac{6\pi\eta_0 N}{(1-\bar{\upsilon}\rho)}$, where η_0 is the viscosity of the solvent, $\bar{\upsilon}$ is the partial specific volume of the particle, ρ is the density of the solvent, and N is Avogadro's number. Vesicle size can be calculated using the relationship between the volumes of the system; $k_d = \frac{V_e - V_0}{V_t - V_0}$ where V_0 is the void volume, V_e is the elution volume, V_i is the pore volume, and V_t is the total volume, k_d is then the volume fraction of the stationary phase that is available to an eluting species[170].

With GEC, hydrated samples were not only separated and purified, but also the sample's stability and entrapment over time could be evaluated by studying the elution profile of the purified samples as they changed over time. The plot in Figure 4.8 shows an overlay of two elution profiles, or chromatograms, of two niosome suspensions of differing encapsulated PBS concentrations. The abscissa is volume eluted and the ordinate represents the UV absorbance (fluorescence is also measured) of the eluting volume. The first peak is the signal from the niosomes which are eluted in the void volume, and the second from the unencapsulated dye. As a suspension of vesicles deteriorates over time, the first peak decreases and the dye released increases the second peak. Theoretically, a newly purified stable suspension would have no second peak. From the lack of a first peak signal in the 0.1M we discerned that vesicles were not viable at the higher salt concentration due to the osmotic gradient with the eluting buffer.

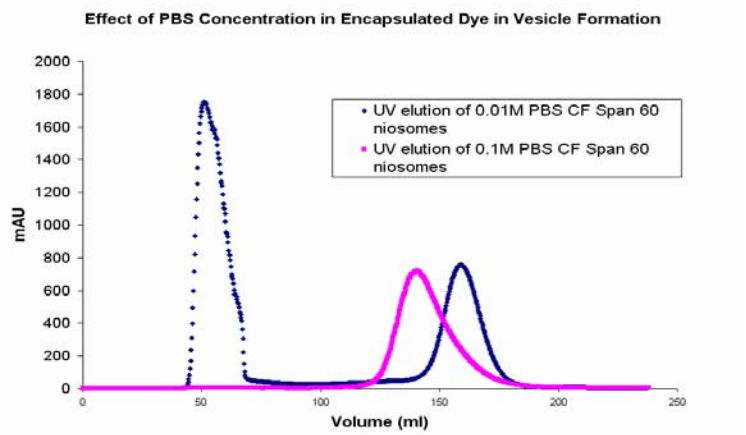

Figure 4.8 Chromatogram of Span 60 Niosomes of Varied PBS Concentrations.

4.2.2.3.2. Fluorescence Intensity

Fluorescent dyes are used as drug models commonly in research because of the high sensitivity of fluorescence spectroscopy, which can be as much as two orders of magnitude more sensitive than absorbance spectroscopy[82]. Fluorescence spectroscopy uses changes in vibrational energy levels of the molecule or substance being measured to assess levels of fluorescence. The sample is excited by exposing it to a known quantity of energy. By absorbing the energy in the form of a photon of light at a particular wavelength the substance changes from a ground electronic state (low energy) to a high frequency state (higher energy). Collisions between highly vibrating molecules cause loss and emission of energy as they drop back down from the excited high energy state to ground state and emit photons[18,25]. Instrumental analysis of the energy absorbed and emitted at particular filter wavelengths provides fluorescence intensity values that can be used to interpret sample concentrations when compared to a standard curve (*e.g.* Figure 4.5.) Initial fluorescence measurements were taken with a single measurement fluorescence spectrophotometer, and later measurements were taken using a fluorescent plate reader which allows for multiple readings to be taken at once. Figure 4.9 shows the effect on vesicle disruption and subsequent release of dye from the vesicles on the concentration of dye in the measuring container (cuvette or plate well). The vessel on the left shows the dye concentration consistent within and outside the formed vesicles after hydration, while the middle shows the vesicles suspended in PBS with dye contained within them, and finally, the right vessel

indicates the release of the dye from the vesicles into the suspending PBS. The dye released from the disrupted vesicles creates the change in signal of the fluorescence (FL) intensity.

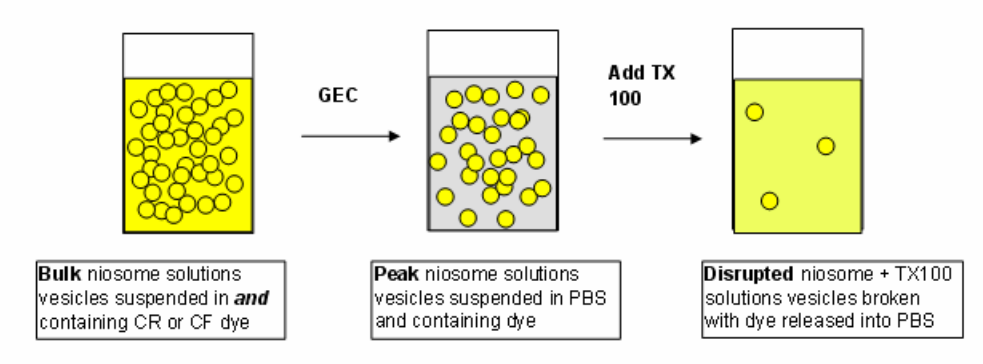

Figure 4.9 Release of Dye from Niosomes.

4.2.2.3.3. UV Absorbance

UV absorbance of materials is commonly used to measure concentration in solutions of proteins and nucleic acids. The theory is straightforward; materials which absorb ultraviolet light (wavelengths from 200-400 nm in the near UV range[171]) have properties which obey the Beer-Lambert Law. The law is expressed in different formulas shown below. The transmittance of light (T) through the material is a ratio of the intensity of the incident light (I_0) and the intensity of the light after passing through it (I_1).

$T = \frac{I_0}{I_1} = 10^{-A} = 10^{-\alpha lc}$, where $A = \log_{10} \frac{I_0}{I_1}$ and $\alpha = \frac{4\pi k}{\lambda}$ so that

$A = \alpha lc$

A is absorbance at a particular wavelength

l is the path length in cm

c is concentration in M

k is the extinction coefficient for the material

λ is the wavelength of the light

So for a material with a known extinction coefficient, at a particular wavelength, and a known path length, molar absorbance is proportional to concentration[148,172,173].

4.2.2.3.4. Ultrasound

Energy can be added to order or to disrupt a system; in our niosome development experiments we used ultrasound for both of those purposes. Sound is the phenomenon we experience perceiving the propagation of pressure waves through air or water. Mechanical vibrations create vibrating pressure waves transferring energy from the source to the pressure waves and to anything the waves contact. Audible (or acoustic) sound frequencies range from 20 Hz to 20KHz. Ultrasound waves are above 20KHz and outside the range of human hearing[141]. Exposure of a biological membrane to ultrasound causes sonoporation which is the temporary, non-destructive perforation of the cell membrane. This transient state enhances permeability of therapeutic agents into cells and tissues[115]. Similarly, the bilayer membrane structure of a self assembly vesicle exhibits a temporary permeability with exposure to acoustic forces[174]. Our suspensions of formed niosomes were exposed to ultrasound in a bath sonicator to reduce lamellarity and size which is a common practice in vesicle synthesis[175]. Experiments were conducted exposing different formulations of niosomes to diagnostic US frequencies to test the potential of US mediated drug release *in vivo*. Intensity levels of US exposure vary for different

medical applications. Power levels greater than 10 W/cm^2 are used in surgical applications; therapeutic US ranges from 0.5-3 W/cm^2, and diagnostic US ranges from 0.1m W/cm^2 to 0.5 W/cm^2 [2, 176].

4.2.2.4. Equipment

Table 4.1. Equipment for Vesicle Development and Synthesis.

Equipment	Manufacturer	Model
Mass balance	Denver Instrument Company	*A-250*
Rotary evaporator	Buchi Laboratory, Switzerland	*Vaccuum Controller V-800* *Buchi-Rotavapor R-200* *Buchi-Heating Bath B-490* *Buchi VacR V-500*
Bath sonicator	Laboratory Supplies CO., INC	Model G1125PIG
Particle sizing	Particle Sizing Systems	Accusizer 780A™
Fluorescence spectrophotometer	Perkin Elmer	LS-3B
Fluorescence Plate Reader	Biotek	Flx800
UV Microscope	Lecia	Type 090-135.002
Inverted Fluorescence Microscope	Olympus	IX71
Chromatography column	GE Healthcare (Amersham Biosciences)	Superdex HiLoad XK 16/60
Chromatography system	GE Healthcare (Amersham Biosciences)	ÄKTAprime
Vortex Mixer	Fisher Scientific	Touch Mixer 231
pH meter		
Echocardiography machine	Acuson	Aspen

4.2.3. Methods

4.2.3.1. Vesicle Synthesis

4.2.3.1.1. Thin Film Hydration Techniques

Traditional thin film hydration techniques were first described in the 1960s[6]. In niosome synthesis this method involves dissolving surfactants, cholesterol and, often, an electrostatic stabilizer (such as dicetyl phosphate) in a non polar solvent, such as chloroform, and then evaporating the solvent and forming a thin film of the dried chemicals on a vessel. Once all solvent is removed, usually by employing a vacuum or nitrogen gas, the addition of an aqueous solution hydrates the thin film. The hydrophobic/hydrophilic interactions of the amphiphilic molecules when exposed to the aqueous environment cause the self-assembly of lipid bilayer vesicles. As the hydrophobic tails orient themselves together, they shield themselves from exposure to the water molecules, and the hydrophilic head groups line up together inwardly and outwardly exposed to the aqueous solution. Figure 4.1 (left) earlier in the text shows a drawing of the orientation of the amphiphiles.

Initially several different formulations were investigated. While different sorbitan ester surfactants were assessed, a consistent ratio of surfactant to cholesterol to dicetyl phosphate was used throughout. The stability of vesicles made using an equimolar ratio of surfactant to cholesterol with the addition of 13% dicetyl phosphate had already been well described[177,178]. A stable vesicle is defined as one which maintains a consistent size and retains a constant level of

encapsulant[178]. The first 'generation' of niosomes had lipid concentrations approximately 10 mM. The concentration refers to the total lipid concentration in the niosome suspension after GEC. It is calculated from the initial concentration of lipids used to make thin films and taking into account the dilution of the suspensions during GEC, and the process loss of vesicle as measured by particle counts. As a general rule the dilution from post hydration to post GEC is 10x and the retention of formed vesicles is approximately 75%.

The lipids were dissolved in chloroform and aliquoted into 50 ml round bottomed flasks. Early films were created by blowing a constant stream of nitrogen gas at 5L/min. Later it was determined that residual chloroform could be further reduced using a vacuum and so the vacuum pump of the rotary evaporator was employed. Once the films dried they were hydrated by adding either 0.01 M PBS, 5.0 mM CF, or 1.0-2.0 mM CR rotating for 1-2 hours in a 60ºC water bath. At regular intervals during hydration, the solutions were agitated on a vortex mixer. Once complete, the solution was sonicated for 5-30 minutes in a bath sonicator at 80 KHz and 80 watts. Residual chloroform was measured by mass balance. After 24 hours, the chloroform remaining was measured to be less than 0.35% of original solvent by mass before hydration. Table 4.2 shows the structures and descriptions of the surfactants investigated in our research. The sorbitan monoesters are a family of alkyl esters of identical head groups and varying alkyl chain length. Polyoxyethylene (PEO) sorbitan monostearate (Tween 61) has the same structure as sorbitan monostearate, as the names suggest, but includes multiple PEO polymer chains on its head group.

The sorbitan monoester (Span) family was investigated because of its well documented facility to form vesicles and its biocompatibility; they are widely used in food, pharmaceutical and cosmetic industries[93].

Table 4.2 Surfactant Structures and Properties.

Surfactant (Trade name)	Description	Structure	Formula, & FW	HLB
Sorbitan monolaurate (Span 20)	Clear viscous liquid (Viscosity 5700 cP at 24.3) Sorbitan ester	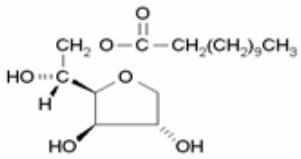	$C_{18}H_{34}O_6$ 346.5	8.6
Sorbitan mono-palminate (Span 40)	Yellowish powder Sorbitan ester	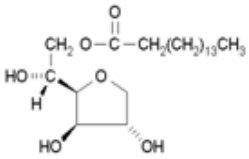	$C_{22}H_{42}O_6$ 402.6	6.7
Sorbitan monostearate (Span 60)	White powder Sorbitan ester	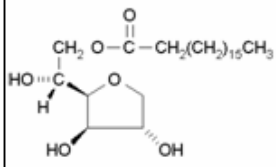	$C_{24}H_{46}O_6$ 430.6	4.7
Polyoxy-ethylene (20) sorbitan monostearate (Tween 61)	Waxy grey-white solid Sorbitan ester ethoxylate	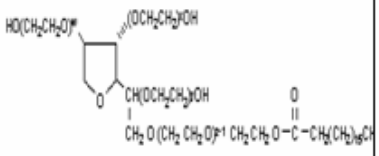	1312	9.6

4.2.3.1.2. GEC Purification

Once the hydration process is completed, 2 ml of 60˚C sample is injected into the sample loop of the chromatography system. A preprogrammed elution method is loaded from a PC. The sample is injected by the system into the column from the sample loop through the injection port as 0.01M PBS is added continuously at 1.0 ml/min. As the elution progresses, the system provides information about temperature, pressure, conductivity, and UV absorbance at 280 nm. The elution method is split into phases where the eluted materials are either captured or sent to waste; in the first phase the sample is introduced to the column. Then the system resets the baseline UV reading to 0. For the first third of the void volume the eluted material is discarded, after which the eluted material containing the separated niosomes is captured in 2 ml fractions. Finally, once the void volume has passed through the column, the eluted material is again sent to waste, and the free dye is flushed from the column. The maximum total volume of the XK 16/60 column is 124 ml. In order to flush completely after a separation, the buffer is run for 2 total column volumes or 240 ml, although the bed packing volume is usually about 100 ml, plus or minus 3-5%.

4.2.3.1.3. UV Absorbance

The Akta prime system incorporated a UV sensor and automatically generated chromatograms for each separation or assessment elution that was run. Although UV is not as sensitive to changes in fluorescent signals as fluorescence microscopy is, the curves provided useful run-by-run comparisons

of different formulations. Unfortunately, the results did not prove as easily quantifiable as those of the fluorescence reading because both the niosomes and the fluorescent dye contained within them contributed to the signal at the niosome elution peak as seen in Figure 4.10. The absorbance of niosomes at 280 nm which contain no absorbing solution can be explained by the presence of double bonds and ring groups in the surfactants.

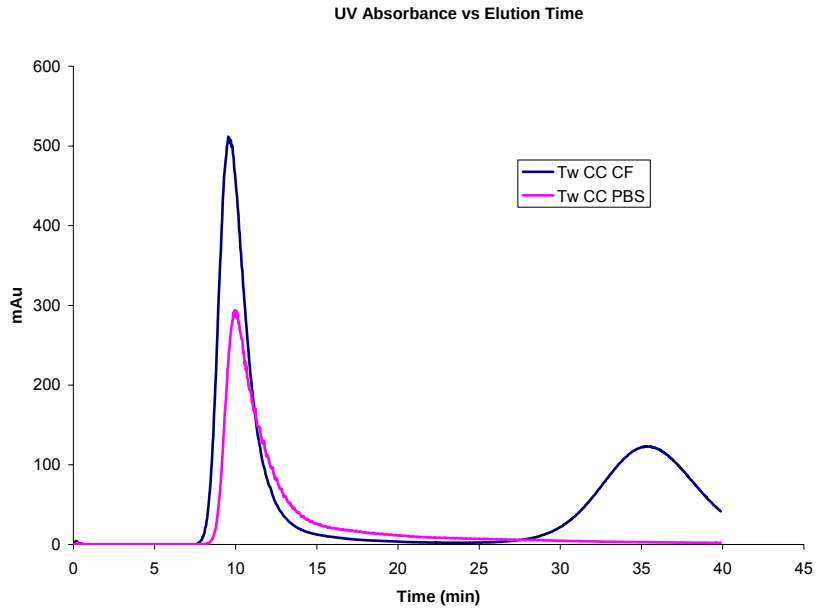

Figure 4.10 Intrinsic UV Absorbance of Niosomes. Tw-CC-CF represents a niosome encapsulating CF dye, and Tw-CC-PBS represents a niosome encapsulating PBS. The Tw-CC-CF curve has a second peak due to the absorbance of free dye. PBS does not absorb UV at 280 nm.

4.2.3.1.4. Niosomes of Differing Surfactant Components

Niosomes made from Span 20, Span 40, Span 60, or Tween 61 as the surfactant component in 1:1:0.105 molar ratio with cholesterol and DCP were made as described encapsulating a 5mM solution of CF. Table 4.3 shows the masses of lipid components used. The encapsulation of the dye was measured by disrupting the vesicles with Triton X 100 in a de-ionized water (DI) solution.

Concentrations of entrapped dye were found by comparing the disrupted niosome fluorescence intensity to a standard curve. Standard curves were created for each type of dye and new dye solution. Particle sized distributions were run for each of the formulations.

Table 4.3 Low Concentration Example of Vesicle Components.

Surfactant mass(g)				Mass (g)		Total mols
Sp20	SP40	Sp60	TW61	cholesterol	DCP	
			0.148	0.0437	0.00635	2.37E-04
		0.01		0.088	0.016	2.80E-04
	0.094			0.088	0.016	4.90E-04
0.081				0.088	0.016	4.91E-04

4.2.3.1.5. Increased Lipid Concentrations

In order to increase the dye entrapment capacity of the niosomes, the lipid concentrations were increased 7.5-10 fold, maintaining the original molar ratios of the components. The GEC methods had to be adapted to the more concentrated hydrated solution.

4.2.3.2. Development of Tween 61-Span 60 Niosome

In order to conjugate a targeting moiety to a niosome, a linking agent had to be conceived of that would either be attached or inserted into the niosomes after they are formed, or to be incorporated within the membrane during formation. The latter approach would not require an additional process step or potentially affect vesicle stability. The surfactant Tween 61 shown in the right side of Figure 4.12 (also seen in Table 4.2) is nearly identical in structure to Span 60 except for the additional incorporation of polyethylene branches on the hydrophilic head group. The polyethylene oxide (PEO) groups on the polar head

of Tween 61 surfactant potentially could be exploited as a linker for antibody conjugation. This linkage is analogous to antibody coupling on the distal end of PEG groups added to immunoliposomes [90,179].

4.2.3.2.1. Tween-Span Mixed Formulations

Based on the results of the stability studies blends of the surfactant component of the vesicles were examined. A combination of Span 60 and Tween 61 was selected with the aim of retaining the desirable qualities of Span 60 stability and retention, while maintaining the option to use the PEO polymer groups from the Tween 61 on the membrane surface for antibody attachment. We looked at combinations of small amounts of Tween 61 (0-10%) incorporated with Span 60 while maintaining the 1:1:0.1 molar ratio of surfactant to cholesterol to dicetyl phosphate. Table 4.4 shows masses of components used to make films of the varied combinations of surfactants. For each formulation the retention of dye over time of the vesicles was compared to the solely Span 60 surfactant composition.

Table 4.4 Masses of Vesicle Components for Varied Tween 61 Surfactant Percentages Ratios per Film.

% Tween	Tween 61 (g)	Span 60 (g)	Cholesterol (g)	DCP(g)
1.00%	0.00089	0.08826	0.10132	0.00752
3.25%	0.0028	0.08417	0.10333	0.00767
5.50%	0.00467	0.08027	0.10525	0.00781
7.75%	0.00643	0.07655	0.10707	0.00795
10.00%	0.00811	0.07300	0.10882	0.00808

4.2.3.3. Functionalization of Tween 61 with Cyanuric Chloride

Tween 61 was functionalized prior to niosome synthesis by activation of the hydroxyl groups on the ends of the PEO chains. In the presence of diisopropyl ethyl amine (DIPEA), Tween 61 and cyanuric chloride were incubated in a nitrogen environment. The overall mechanism is shown in Figure 4.11. The cyanuric chloride undergoes nucleophilic substitution binding to the terminal hydroxyl group of a PEO chain on the Tween 61 molecule. The molar ratio of Tween:CC:DIPEA was 1:0.8:2 [90,180] and a 0.2 g/ml solution was made by combining 1g Tween 61, 0.124 g CC, 0.274 ml DIPEA, and 5 ml chloroform. The Tween 61 and chloroform were combined in a round bottom flask. Cyanuric chloride was added and the DIPEA was withdrawn from a sealed flask using a long sharp metal syringe tip and added directly into the mixture. The flask was rotated in a nitrogen environment for 36 hours. The excess solution was stored and remained stable at -4ºC for several months. The resulting functionalized Tween-CC solution was added to the surfactants and lipids in chloroform prior to forming a thin film.

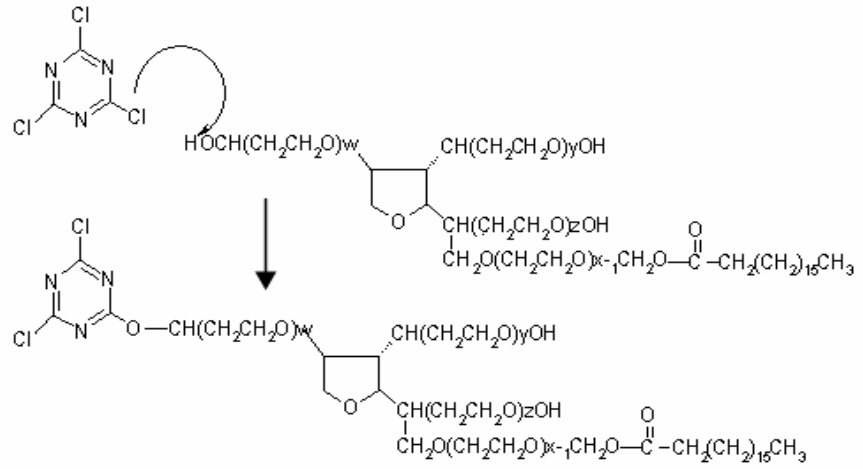

Figure 4.11 Tween 61 Cyanuric Chloride Linking Mechanism.

4.2.3.4. Attachment and Verification of Antibody Conjugation

The GEC purified niosome solutions were adjusted to pH 8.8 by titrating 1 μl at a time of 1 M sodium hydroxide drop-wise while monitoring the pH. IgG monoclonal antibodies (either fluorescently tagged Alexa-488 (AF)-IgGs or anti CD44 IM7) were incubated with the niosomes at a concentration of and gently shaken for 16 hours in the dark. At pH 8.8 the antibody binds to the cyanuric chloride linker distal to the vesicle surface shown in Figure 4.12. Linking of antibodies to either of the available chloride groups has equivalent potential energy, however linking a subsequent antibody to the second available chloride group would require much greater energy of activation, and is not favored when other linkers on other molecules are available[105]. After antibody conjugation the immunoniosome (IN) solution pH is restored to 7.4 using 0.1 M PBS. Concentration of antibodies incubated was 5 μg protein /ml niosomes which is equivalent to 2.78 μg protein/ μmol lipid. Concentration of total lipids in the post GEC niosome solution is 1.8 mM, found by calculation from the original hydration

concentration of 0.0144 M accounting for the 6 times dilution factor and particle retention efficiency during GEC. Viable binding groups of Tween-CC linkage are 52% of the Tween component by calculation. This value is based on the reaction molar ratio (1:0.8 of Tween:CC) and a published binding efficiency (65%) of the reaction of CC with 1.2-Dipalmitoyl-*sn*-glycero-3-phosphoethanolamine polyethylene glycol (DPPE-PEG)[24]. The overall molar percentage of Tween in the total lipid concentration of the niosomes was 4.76%, making the Tween-CC linker 2.47% of total lipids, or 0.045 μmol Tween-CC/ml niosomes. This provides $2.68 * 10^{16}$ binding sites/ml niosomes. Antibody incubation of 5 μg antibodies/ml of niosomes relates to a ratio of greater than 1300:1 Tween-CC binding sites to antibodies.

In order to verify the efficacy of the linker chemistry and establish the ability to bind antibodies to the surface of the vesicles, antibodies were fluorescently tagged and incubated with non fluorescing niosomes for conjugation. Fluorescent tagging of antibodies was done as described in the protocol from a commercially available kit from Molecular Probes.

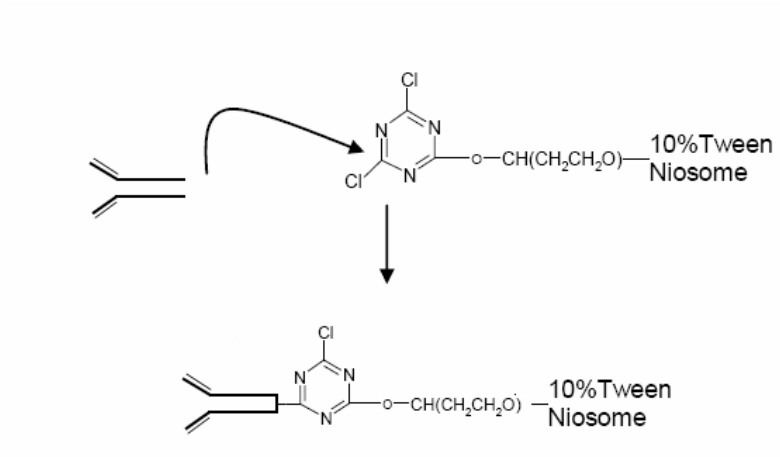

Figure 4.12 Antibody Conjugation.

4.2.3.5. Synovial Lining Cell Culture Methods

Primary cell cultures of bovine synoviocytes were used in niosome incubation experiments. These cells were provided grown and already fixed by a collaborator's laboratory. The following description of the synoviocyte primary culture comes from the resulting publication[70]. The synovial membranes were harvested from the metacarpal phalangeal joints of 3 month old bovines. After washing with phosphate buffered saline (PBS) the tissues were dispersed in 0.1% collagenase P in 4% bovine serum albumin (BSA). Isolated cells were washed with PBS suspended in Dulbecco's DMEM containing 10% fetal calf serum at a concentration of 10^5 cells per ml. The cells were plated in Labtek 8 well micro-slides. Cells were allowed to attach overnight. The media was removed, and the cells washed with PBS and fixed for 2 hours in Histochoice. A subset of fixed cells was immuno-stained with IM7 using standard immunohistochemical techniques.

4.2.3.6. Immunoniosome Synovial Lining Cell Incubation Methods

The fixed cell layers were pre-incubated in 0.01 M PBS with 2% goat serum with or without soluble IM7 antibody for 1 hour at room temperature prior to incubation with immunoniosomes. Cells were rinsed with PBS and incubated for 1 hour at 37 ºC with fluorescent niosomes with or without antibody conjugation. The cells were well rinsed to remove unbound niosomes and examined by fluorescent microscopy. Imaging of cells, cell nuclei, and INs was done with an Olympus 1X71 inverted fluorescent microscope fitted with DAPI and FITC (fluorescein isothiocyanate) filters allowing imaging of the green fluorescent

niosomes and the blue stained cell nuclei. For a given image, a phase contrast picture was captured, and then the light and filters were changed to fluorescent mode to image the cell nuclei using the DAPI filter, and the FITC filter to image the fluorescent niosomes bound to the cells. These images were captured and combined using DP-BWR image analysis software to overlay them.

4.2.3.7. Proof of Concept Cell Binding

To establish proof-of-concept cell binding, bovine synovial membrane lining (SL) cells were plated at 1x 10^3 cells/mm^2 on glass multi-well slides and maintained in DMEM with 20% fetal bovine serum, until cells reached near 90% confluence. The cell layers were washed and fixed for 24 hours in Histochoice fixative and rewashed Hanks Buffered Saline (HBS). The fixed cell layers were pre-incubated in PBS with 2% goat serum with or without soluble IM7 antibody for 1 hour at room temperature to prevent non specific binding. Niosomes used in SL cell studies encapsulated 5(6) carboxyrhodamine 110 (CR), a photo-bleaching resistant fluorescent dye. (Photobleaching is a loss of fluorescence intensity due to exposure to intense light.) Cells were rinsed and incubated for 1 hour at 37 ºC with fluorescent niosomes or fluorescent niosomes derivatized with IM7 (purified IgG). The cells were well rinsed to remove unbound niosomes and were examined by fluorescent microscopy.

4.2.3.8. Statistical Methods

Statistical differences in experimental values were calculated using standard error of the mean (SEM) of at least three repeated measures. The

formula for SEM is the ratio of the standard deviation of a data set divided by the square root of the number of repeated measures, n. The standard deviation of a set of measured values is defined as the square root of the variance. The variance is the summed deviations of the measured values from the mean of those values. If x_i is an observation among n observations and $\bar{x}$ is the mean of all the observations (the sum of all measured values divided by the number of values measured) then the variance is:

$$s^2 = \frac{\sum_{i=1}^{n}(x_i - \bar{x})^2}{n-1}$$ and the standard deviation is therefore;

$$St.Dev = \sqrt{\frac{\sum_{i=1}^{n}(x_i - \bar{x})^2}{n-1}}.$$

The standard error of the mean is $SEM = \frac{St.Dev}{\sqrt{n}}$. The SEM is represented graphically as y-axis error bars in the graphs in this document. P-values are used as another statistical method included in some of the reported data. In hypothesis testing resulting data are evaluated as being different than the mean of the measured values within a range of values. A p-value is defined as the probability of a measure to be different than the mean of the measured values. If a p-value of <0.001 is reported then there is less than 0.1% chance that there is no difference in the means of the measured value versus the comparison value, usually a control [181].

4.2.4. Experimental Designs

4.2.4.1. Vesicle Formulation Assessment

4.2.4.1.1. Sorbitan Ester Formulations

Entrapment efficiency and membrane permeability of varied formulations of niosomes were evaluated. Size reduction through sonication over time was assessed in each formulation. Dye encapsulation capacity was assessed in each formulation. Additionally the effect of sonication on vesicle size and count was evaluated in the different Span compositions. The ability to accurately evaluate the entrapment of dye by niosomes depends on the ability to completely disrupt them.

4.2.4.1.2. Tween-Span US Exposure Stability Study

Based on the results of the studies done on the different surfactant candidates, niosome made from either Tween or Span 60 as the surfactant component were evaluated for stability. The different vesicle formulations were exposed to diagnostic ultrasound at 0, 5, 10 minutes using a transducer and an Accuson Aspen echocardiography machine. Machine settings were kept constant throughout the experiment with the frequency set to 3.5 MHz, the dynamic range set to 70dB, and the initial gain set to 10 dB. During the experiment the mechanical index of the instrument was varied. Mechanical index (MI) is the ratio of the acoustic pressure over the square root of frequency. Therefore max MI corresponds to a maximum acoustic pressure at a given

frequency. The formula is $MI = \frac{P}{\sqrt{f}}$ where P is pressure in MPa, and f is frequency in MHz. The spatial peak temporal average was 46 mW/cm^2, and the total absolute power was 65 mW. Fluorescence readings of the niosomes and suspending fluid were obtained at 5 minute increments over 15 minutes of ultrasound exposure. All vesicle characterization measurements were repeated three times at each 5 minute time increment.

4.2.4.2. Polyoxyethylene Sorbitan Monostearate-Cyanuric Chloride Linker Chemistry

The Tween-CC linkers were prepared as described and tested by first attaching the fluorescently tagged IgG antibodies to non fluorescing niosomes and assessing the vesicle morphology and fluorescence of the resulting suspension, by GEC elution of the vesicle suspension. To further verify the antibody binding to the niosomes, the post GEC purified AF-immunoniosomes were examined with an Olympus 1X71 inverted fluorescent microscope. Approximately 50 μl of immunoniosome suspension was pipetted onto a glass microscope slide and viewed at 10 and 40x using a FITC filter to verify the presence of fluorescent spherical particles. Fluorescent images where captured using the Olympus DP-BSW software.

4.3. Results

4.3.1. Sorbitan Ester Vesicle Formulations

4.3.1.1. Results of the Varied Sorbitan Ester Formulations

The varied formulations were evaluated for entrapment by fluorescent measurements and particle sizing. The entrapment of dye by each formulation is shown in Figure 4.13. The Tween 61 niosome shows the greatest encapsulation of dye, followed by Span 60. Entrapment decreases with decreasing alkyl chain length. Figures 4.14 show that Span 60 forms the greatest number of vesicles after hydration and retains the greatest amount of dye after GEC.

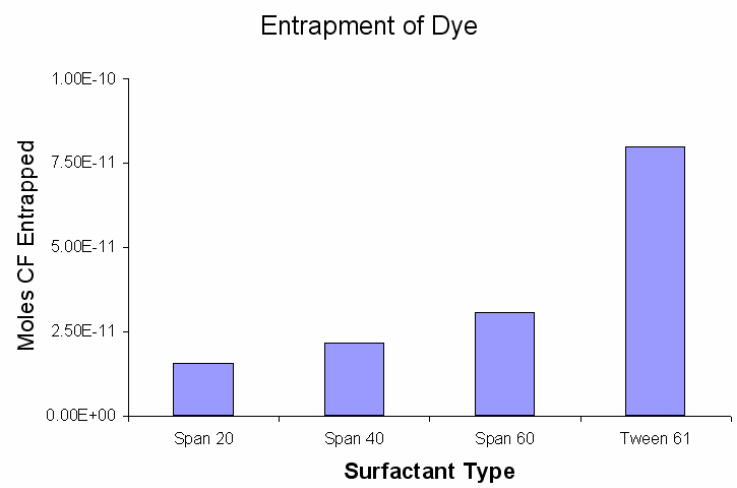

Figure 4.13 Encapsulation of CF by Surfactant Type.

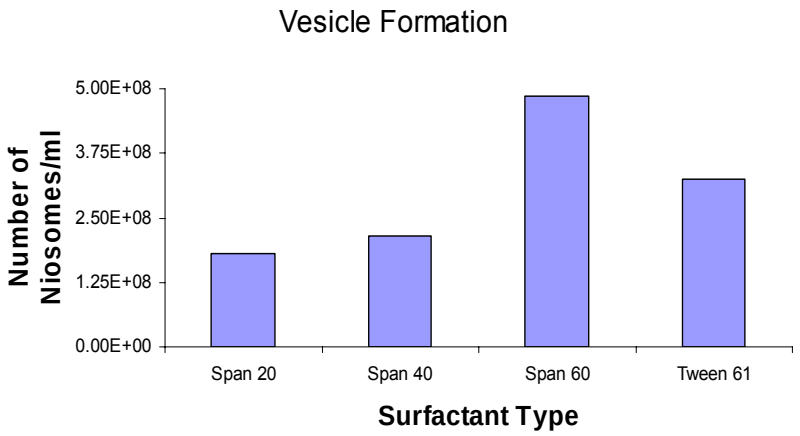

Figure 4.14 Formation of Niosomes after Hydration by Surfactant Type.

In order to reduce vesicle size and lamellar number (number of bilayers) bath sonication over a range of times was tested in the Span 20 and Span 40 niosomes after hydration and before GEC. The data in Figure 4.15 show that vesicle size (number weight mean) decreases and vesicle count increases over sonication time to an asymptotic value. The effect of sonication on the different surfactants is not identical however. The concentration of particles greater than 0.5 μm (the detection limit of particle size analyzer) of the Span 20 vesicles increases and reaches an asymptotic limit with sonication time while the concentration of the Span 40 particles increase to a greater degree and fluctuated more greatly. With both surfactants the mean particle diameter decreases with sonication then levels out. This is to be expected since sonication of vesicles reduces the number of bilayers in the vesicles and disrupts aggregates[182] and is directly seen in the micrograph shown in Figure 4.16 which shows a light microscopy image of a PBS containing niosome sample on a hemocytometer slide before and after sonication which was used to reduce and unify particle size and lamellarity [183].

Figure 4.17 shows the effect on sonication over the entire vesicle size distribution. The curves show the particle size distribution of the unsonicated versus sonicated vesicles of Span 60 niosomes. The size distribution clearly shifts downward after sonication. Based on the results of the Span 20 and Span 40 niosomes it is assumed that a portion of the population of the Span 60 niosomes that are not seen in the post sonication distribution have dropped below the detection limit of the PSS.

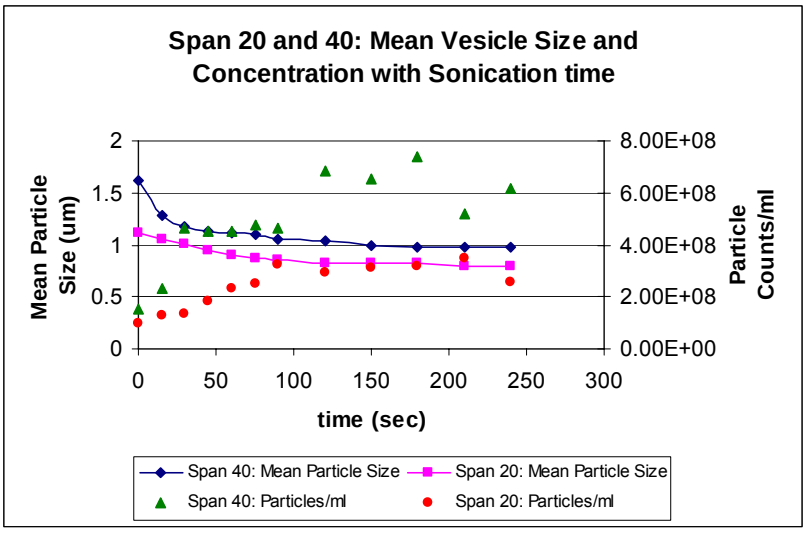

Figure 4.15 The Effect of Sonication Time on Particle Size and Counts.

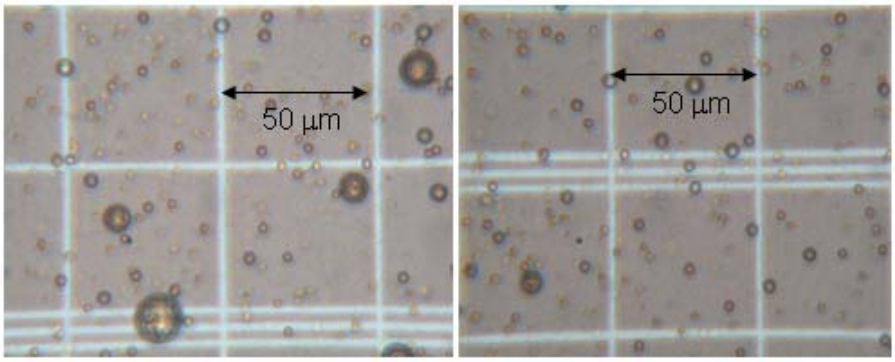

Figure 4.16 Sonication Effects. The Effect of Sonication on Vesicle Size Distribution in Span 60 Niosomes.

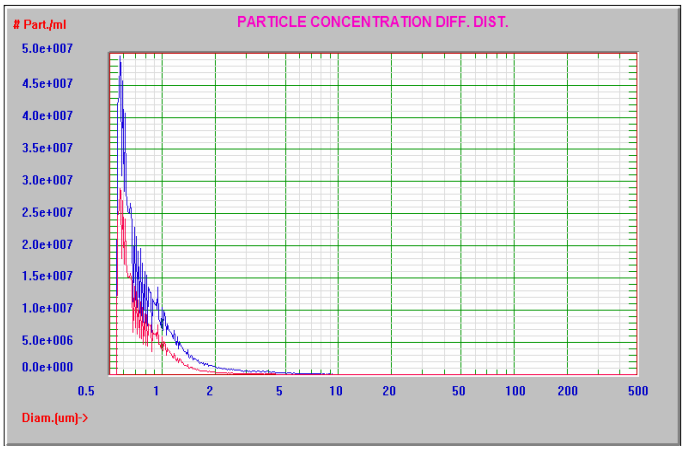

Figure 4.17 PSD Sonication Effects. The graph shows the shift in Particle Size Distribution in a bath sonicated Span 60 nisome sample. The blue curve is the size distribution of the sample before sonication, and the red curve represent the distribution after sonication.

4.3.1.2. Results of Ultrasound Exposure on Niosomes

Ultrasound exposure experiments were conducted on niosomes whose surfactant component was either Tween 61 or Span 60, based on the results of the earlier sorbitan ester experiments, establishing the two as the candidate surfactants. Vesicle suspensions of the different formulations were monitored by particle size distribution and fluorescence intensity measurements. The graphs shown in Figure 4.18 represent the particle size distributions (PSD) of the control and experimental samples over the duration of the experiment. On the left the curves represent the PSDs of the Span 60 niosomes before (blue) and after (red) US exposure. The right side of Figure 4.18 shows the same thing for the Tween 61 niosomes. It is clear by the closeness of the curves in each that the disruptive effect of US on the formed particles was minimal. The particle counts are expressed in numbers per ml of sample.

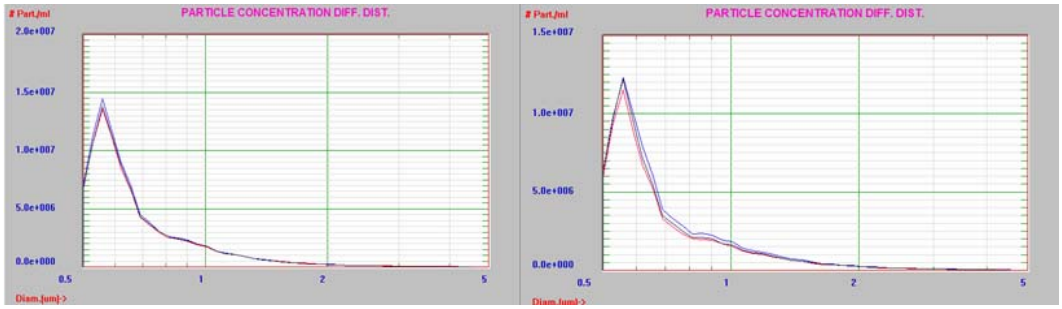

Figure 4.18 PSDs with Respect to US Exposure. Left: Span 60 niosomes; right; Tween 61 niosomes. For each blue is prior to US exposure, and red is after.

In Figure 4.19 the effect of US exposure time is seen to be significantly greater in the Tween 61 niosomes than the Span 60 niosomes. Figure 4.20 indicates that release of dye is shown to increase with increased mechanical index in Tween 61 niosomes, whereas the stability of the vesicles in the Span 60 with MI as shown in Figure 4.21. Taken all together, the stability of the Span 60 niosome and its ability to retain encapsulated materials is demonstrated to be greater than that of the Tween 61. However, for controlled rapid release a Tween 61 vesicle may be desirable.

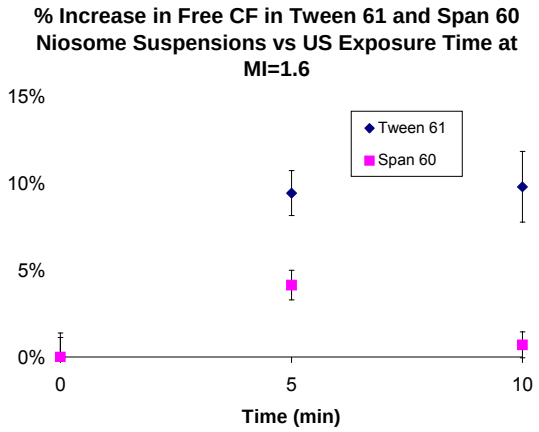

Figure 4.19 The Effect of US Exposure Time on Release of CF. Error bars represent SEM of n>=3.

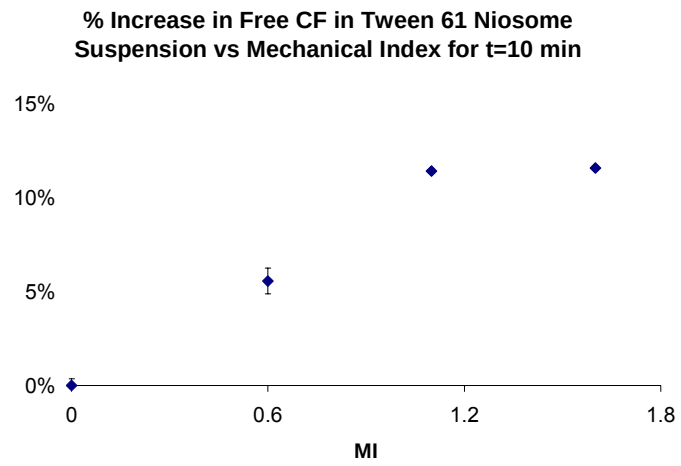

Figure 4.20 The Effect of MI on Released CF in a Tween 61 Niosome. Error bars represent SEM of n>=3.

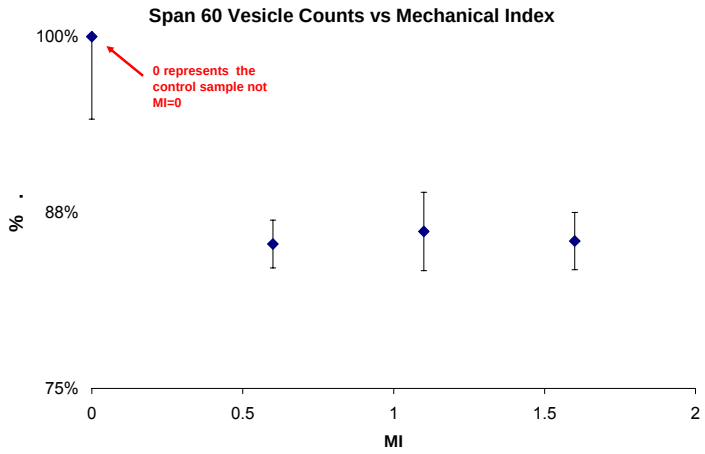

Figure 4.21 The Effect of MI on Particle Retention in the Span 60 Niosomes. Error bars represent SEM of n>=3.

4.3.2. Results of Surfactant Blending

Since the formulation of niosomes with Tween 61 as the sole surfactant component were seen to be less stable than the Span 60 niosomes both statically, and when stressed, the effect of the inclusion of a range of small molar percentages of Tween 61 in a Span 60 niosome on vesicle entrapment capacity and membrane stability was evaluated. This was measured by retention of

entrapped dye over time at 4ºC in a PBS suspension. Although Tween 61 niosomes are reported to have a greater entrapment capacity [184] (which was confirmed by the data shown in Figure 4.13), the observation was that niosomes whose surfactant component was entirely composed of Tween 61 lost three times more encapsulated dye relative to niosome formulations whose surfactant component was purely Span 60 under static conditions holding cholesterol and DCP molar ratios constant as shown in the tabulated values in the right side of Figure 4.22. On the left side of the figure the data indicate that the inclusion of up to 10% by mole of Tween 61 had no significant effect on the retention of dye over the time examined. Statistical differences were judged by evaluating the overlap of standard error of the mean graphically. Also, in order to increase the entrapment capacity of the vesicles, and therefore increase potential drug entrapment, the overall mass of lipids used was increased. The results of the increase can be seen in the overlay chromatogram shown in Figure 4.23.

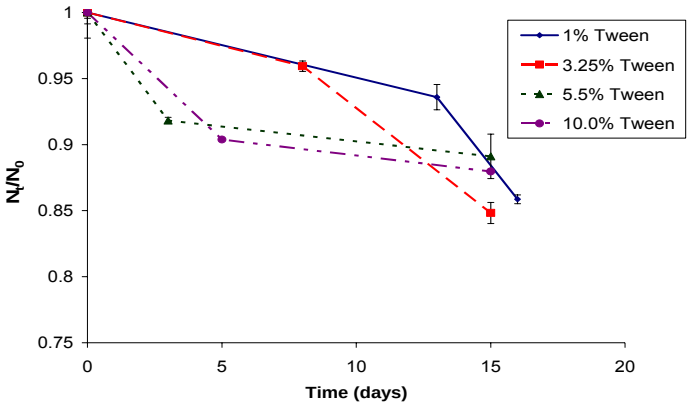

%Tween	% CF Retained
0	88.0%
1	85.9%
3.25	84.8%
5.5	89.1%
10	88.0%
100	62.2%

Figure 4.22 The Retention of CF in Tween 61-Span 60 Niosomes. Left: graphical depiction of the inclusion of 1-10% Tween. Right: Overall retention of dye in various formulations in 15 or more days.

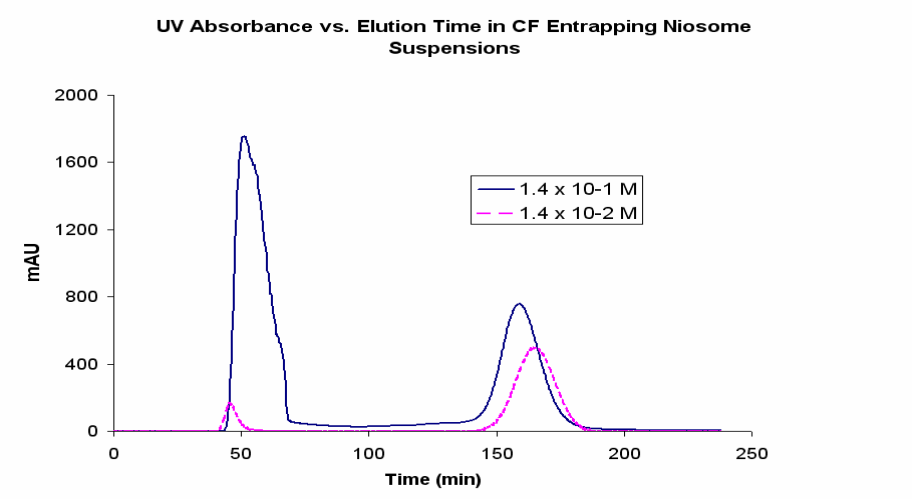

Figure 4.23 Increased UV signal with Increased Lipid Concentration in Tw-CC-CF Niosomes.

4.3.3. Results of Linking Chemistry Development

The verification of the linking chemistry was tested in two ways; first was the assessment of the elution of PBS containing niosomes conjugated to Alexafluor tagged antibodies. After incubation with the antibodies the niosomes were purified using GEC which should have resulted in a suspension of non fluorescing niosomes conjugated to fluorescent antibodies. That purified suspension was eluted through a GEC column and measured by UV absorbance at a wavelength of 280 nm. Figure 4.24 shows a signal in the niosome elution volume. There is also a very slight signal in the antibody elution volume (before 120 ml) which show a few free AF antibodies; the protein and the bound dye would both contribute to the signal at that wavelength.

This indicates that there are negligible numbers of free antibodies in the solution and demonstrates successful attachment of Alexa Fluor tagged IgGs to PBS containing niosomes.

Secondly, the niosome suspension was imaged using fluorescence microscopy as seen in Figure 4.25. Further confirmation of the conjugation of AF antibodies was evident when fluorescent spheres were evident under a fluorescent microscope using a FITC filter. The presence of distinct and discrete spherical fluorescent particles confirms the conjugation of the fluorescent antibodies to the non fluorescing niosomes and the efficacy of the linker to attach the antibodies to the surface of the niosome membrane. The discrete fluorescent spheres appear to be of the same size and relative size distribution of niosomes. These two independent measures indicate successful antibody conjugation of the AF antibodies to non fluorescing niosomes.

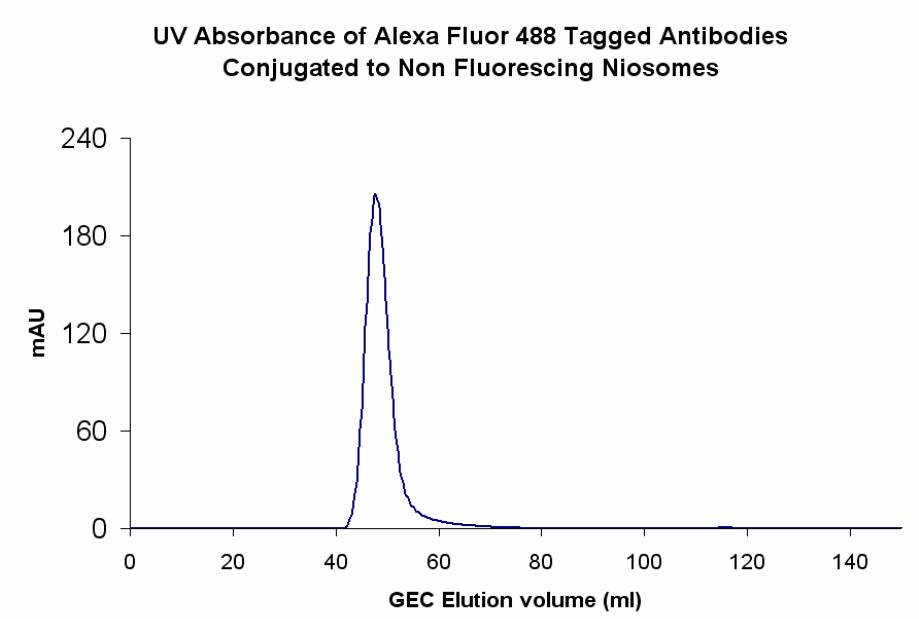

Figure 4.24 Elution of IN with Fluorescent Antibodies.

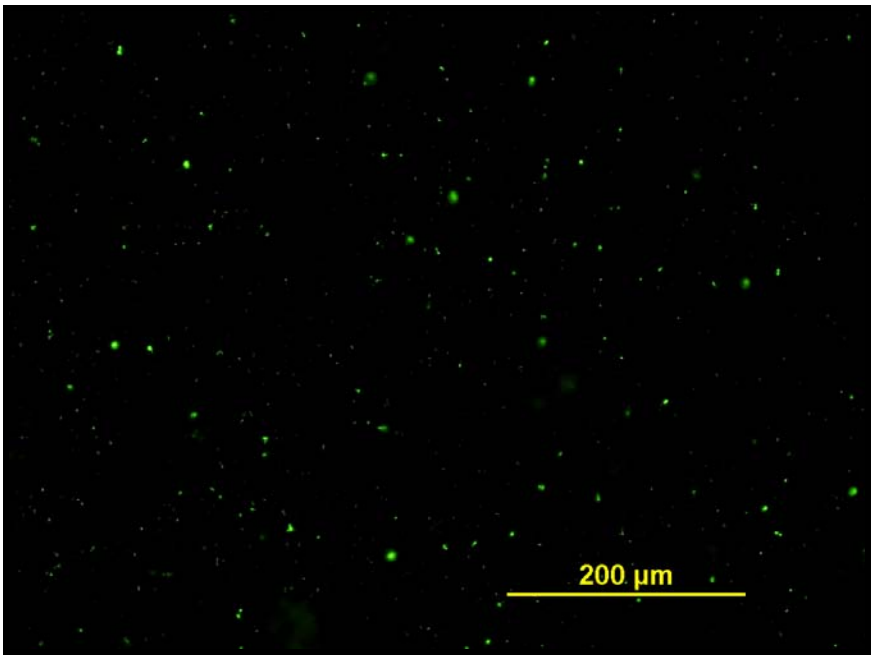

Figure 4.25 Fluorescent micrograph of IN with Fluorescent Antibodies.

The effect of the Tween-CC linker on the 10% Tween 61 niosome was evaluated over 22 days. Figure 4.26 shows an overlay of four separate elutions of the same sample of post-GEC 10%Tween 61 niosomes. Due to slight differences in column packing and suspension injection the chromatograms do not line up perfectly, but do indicate very little variation in the suspension over time.

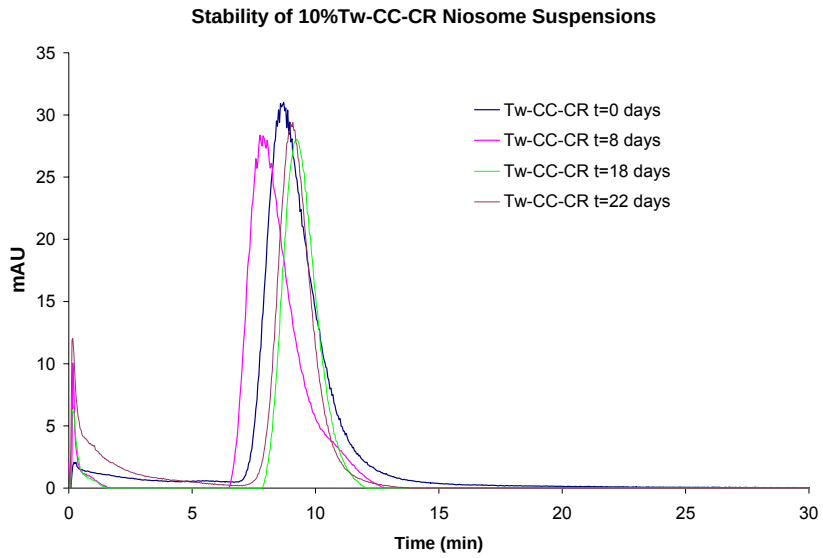

Figure 4.26 Stability of the 10%Tw-CC-CR Post GEC Niosome.

4.3.4. Binding of Immunoniosomes to Synovial Lining Cells

The binding of the immunoniosomes to the target antigen in a fixed cell model was confirmed as follows. The fluorescent and light micrographs shown in Figure 4.27 demonstrate the specificity and selectivity of immunoniosome binding to target antigens. The upper micrograph figures of cells (A, C, and E) correspond exactly to the fluorescent micrographs below them (B, D, and F). Parts A and B of Figure 4.27 correspond to the cells incubated with IM7 tagged niosomes and show binding of the immuno-niosomes evident by the bright spherical shapes attached at cell processes and cell membranes. Whereas the cells pre-incubated with free IM7, shown in C and D, do not show the small spherical attachments due to blocking of the targeted binding sites. This demonstrates the targeting selectivity of antibody antigen binding. In parts E and F, cells have been incubated with unconjugated niosomes. Additionally, the absence of binding in the cells incubated with untagged niosomes, parts E and F,

demonstrates the specificity. In all of the fluorescence images some autofluorescence of cells is evident, but clearly distinct from the brighter point-like images of the fluorescent niosomes. In the left hand side of Figure 4.28, IHC staining techniques show the CD44 expression at the cell processes and at the cell membranes as indicated by the red arrows. Correspondingly, binding of green fluorescent INs in the right hand side of Figure 4.28 is seen at cell processes and membranes.

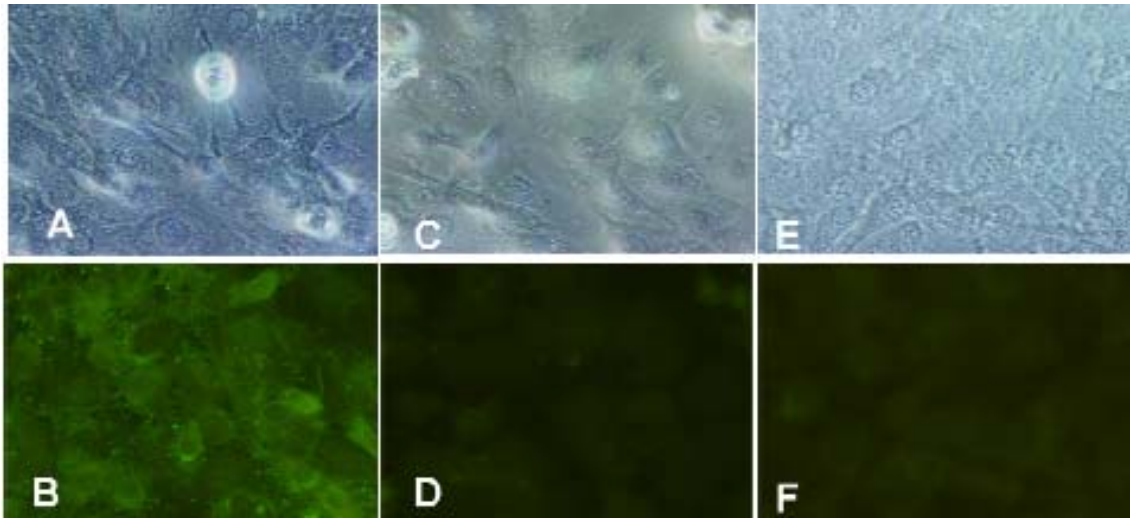

Figure 4.27 Experimental and Control Images of Synovial Lining Cells. The upper slides (A), (C), and (E) show contrast micrographs and the lower slides (B), (D), and (F) are the corresponding fluorescent micrographs of those above them captured using a FITC filter. (A) and (B) show SL cells incubated with IM7-tagged niosomes containing 1 mM CR dye. (C) and (D) are SL cells pre-incubated with free IM7. (E) and (F) are cells incubated with untargeted niosomes (no IM7).

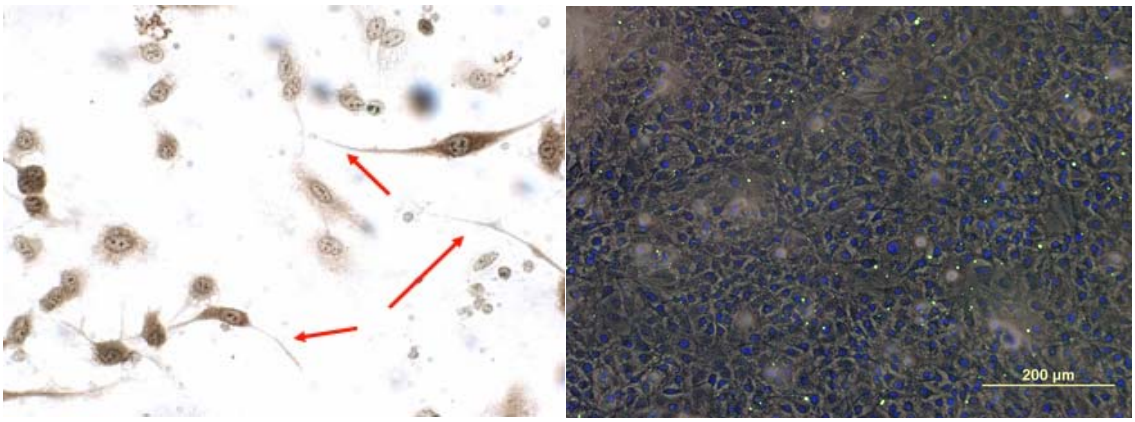

Figure 4.28 Synovial Lining Cells. Left: IHC stained for CD 44 with nuclear counterstaining. Arrows indicate CD44 expressed on cell processes. (40 x magnification Olympus BH 2)

4.4. Discussion

The results of the experiments to this point confirm the capacity to develop monoclonal antibody conjugated niosomes targeted to specific cell receptors. The investigation of members of sorbitan ester family as the candidate surfactant in our vesicle revealed that Span 60 had the best combination of entrapment capacity, stability and retention versus the others studied. However, since the polyoxyethylene polymers on the Tween 61 head group extend distal to the surface of the formed niosome they would provide ideal linking moieties for antibody conjugation. Blending the surfactants in order to retain the desired properties of each surfactant was conceived and the results showed that the inclusion of as much as 10% of Tween 61 within a niosome composed of Span 60 in the surfactant component maintained the desirable stability and retention properties of the 'purely' Span 60 niosome. Sorbitan monostearate based niosomes can be functionalized through inclusion of a cyanuric chloride

derivatized polyoxyethylene monostearate to conjugate monoclonal IgG antibodies to the vesicle surfaces without requiring derivatization of the antibody.

The coupling of IgG antibodies to formed and purified vesicles was verified. The resulting 'immunoniosome' was shown to bind to target antigens in fixed cells. In the fixed SL cell model targeting shows high selectivity and specificity demonstrated by the lack of IN binding to the target antigen when blocked with free antibodies specific to the antigen, and also the inability of untargeted (non antibody conjugated) niosomes to bind to cells. The results of the fixed cell SL binding studies demonstrated that further investigations were warranted to investigate binding and then uptake by inflamed endothelial cells *in vitro* and in *vivo*. The implications for therapeutic treatment of inflammatory diseases is significant not only in the capacity to target chemical therapy to affected tissues but also to block receptors of inflammatory pathways and to interrupt the perpetuating effect of the process [178]. Also, since the attachment of antibodies is independent of the type and generic to any IgG antibody, the system's therapeutic targeting is flexible and may include more than one targeting vector if desired.

In order to pursue live cell uptake experiments the size and particle distribution of INs would have to be addressed. Size reduction protocols using extrusion, and monitored by sub-micron particle sizing, would modify and verify vesicles of size conducive to cellular uptake[177]. Additionally, measurement of optimal antibody coating density would need to be pursued. By using activated fixed aortic endothelial cells (an appropriate model for vascular inflammatory

drug uptake studies) optimizations of the drug targeting system could be conducted prior to pursuing live cell uptake studies. In liposome applications, as few as tens of antibodies or antibody fragments [185] conjugated per vesicle have shown binding and cellular uptake, necessitating the optimization of our immuno-conjugation.

5. Fixed Endothelial Cell and Immunoniosome Binding Studies

5.1. Background

5.1.1. Endothelial Cells Antibody-Targeted Drug Delivery

Endothelial cells are a type of epithelial cell; they are single-layer simple squamous epithelial cells which line blood vessels and are therefore the mediating layer between the blood stream and the tissue that they line. Varying targeting drug delivery strategies have been studied using activated endothelial cells expressing adhesion molecules. Different targeting schemes have been reviewed and/or studied including cardiovascular liposome targeting, nanomedicine, pulmonary targeting of liposomes with antioxidants and anti-thrombotics, and enzymatic therapeutics, also using polymeric nanocarriers. Vesicular or nanocarrier cardiovascular targeting strategies frequently include an endothelial cell model with a target adhesion molecule and the corresponding antigen vector. In the studies described in this section 10%Tween-CC niosomes conjugated with an anti-CD44 antibody were targeted to bovine aortic endothelial cells (BAECs).

The aim was to verify and quantify binding of the INs to activated BAECS under differing experimental variables such as incubation time, concentration of lipid and antibody coating. Throughout these BAEC fixed cell binding experiments the niosome abbreviation IN refers to the formulation defined in Part 4, the blended surfactant niosome with the Tween 61-cyanuric chloride linker,

containing the photobleaching resistant dye, carboxyrhodamine (CR), conjugated to the anti-CD44 antibody, IM7.

5.2. Materials and Methods

5.2.1. Materials and Chemicals

Included in this list are the materials and chemicals new to this phase of the project that were not included in Section 4.2.2.1. Cambrex endothelial cell basal media (EBM), bovine calf serum, penicillin-streptomycin, 0.05% (w/v) Trypsin-EDTA solution, 99% HEPES sodium salt, and 100% ethanol all came from Fisher Scientific, as did all the pipettes, flasks, filters, syringes, and centrifuge tubes. The secondary antibodies used for IHC came from Sigma Chemical as did the Tris buffer, and sodium acetate. Cryo-preserved endothelial cells (BAEC) came from Clonetics, Inc. The IHC ABC staining kit (Cat# PK 7200) came from Vector labs, as did the diamino benzidine (DAB) substrate kit (SK4100), the diamidino-2-phenylindole (DAPI) nuclear mounting stain, and the hard set mounting media. The potassium ferricyanide and uranyl acetate were a kind gift from Ed Haller from the Pathology Department of USF Health. Osmium tetroxide and gelatin came from USF Health Core facilities.

5.2.2. Methods

5.2.2.1. Endothelial Cell Culture

Endothelial cells were grown using classical sterile techniques in 25cm^2 sized cell culture flasks in endothelial basal media supplemented with 10% fetal calf serum, 1% penicillin-streptomycin and 1% non essential amino acids. Cryo-

preserved cells were started on flasks that had been coated with collagen to encourage adhesion. Cell growth media was changed every 2-3 days. The cells were cultured to a confluent monolayer and then sub-cultured into 8 well micro-slides for incubation with INs and subsequent imaging. Cells were sub-cultured by releasing their adherence from flasks with the enzyme trypsin, which is a serine protease of the pancreas which breaks down peptide bonds of the carboxyl groups of amino acids arginine and lysine. The commercially available, purified form of trypsin is used commonly in cell culture to release cells from culture vessel surfaces.

To release the cells from the flasks, first the growth media was removed by pipette, and then the cells were rinsed several times with 37˚C 0.01 M PBS to eliminate the anti-trypsin agents present in the endothelial media. Next 2 ml of 0.05% trypsin was added to the flask and incubated at 37˚C for 5-10 minutes. Release of cells from the surface was monitored using a phase contrast microscope. Once the cells were released, the vessel wall was washed further with PBS, and the suspended cells were centrifuged for 3-4 minutes at 3000 rpm. The trypsin and PBS were removed by pipette from the resulting pellet of cells which were re-suspended in growth media and 400 μl aliquots were added to the individual wells of the micro-slides.

The cells grew to near confluence in 1-2 days. A day prior to incubation with INs, fresh media supplemented with 7 ng/ml TNF-α (an inflammatory cytokine whose role in adhesion molecule expression is described in Section 2.3) was added to the culture to activate the cells and induce the expression of

adhesion molecule CD44. Prior to incubation with INs the cells were fixed overnight with either Histochoice, for IHC staining, or with paraformadehyde, for fluorescence imaging.

5.2.2.1.1. Gelatin Coating Procedure

Coating of culture vessels with either collagen, gelatin or fibronectin helps encourage primary or cryo-preserved endothelial cells to proliferate in initial culturing. A 2% by weight solution of solid gelatin was prepared in pyrogen free deionized (DI) water for flask coating. The DI was heated to 80°C and the gelatin was dissolved in the water. The dissolved gelatin and water were kept at the increased temperature for 10 minutes and then the solution was cooled to about 30˚C and filtered with a 0.22 μm syringe filter. If the solution is allowed to cool too much then filtration becomes very difficult. Then 1.5-2.0 ml of the solution was added to 25 cm^2 culture flasks and incubated at 37˚C for 4 hours or longer. The excess solution was drawn off with a pipette and discarded while working under the sterile hood. Unused gelatin solution can be stored at 4˚C for later use.

5.2.2.2. Cell Fixation

Fixation of cells stabilizes the structure and allows solvents to penetrate the plasma membrane. Paraformaldehyde (PF), which does not fix by cross linking, has been identified as being the best preservative of cell structures. Because PF does not induce autofluorescence it is also a preferred fixative in

fluorescent microscopy applications. Typically concentrations of 2-4% in buffer solution are reported for cell fixation.

5.2.2.3. Immunohistochemical Staining

Immunohistochemistry (IHC) is used to demonstrate the presence and location of antigens in cells or tissues. There are several factors which determine how well the antigen will be detected, chief among them the density and dispersity of the antigens presented on the cells. The fixative type can have an effect on antibody-antigen binding if the cells structure is greatly changed in the fixation process. Detection is also impaired due to the antigen signal versus non specific background binding. This can be offset by using a blocking buffer, usually a non specific protein or serum of the antibody host. The specificity of the antibody used is also important. Monoclonal antibodies give the most specific binding and lowest background, especially when used after a binding buffer treatment.

A subset of the experimental cells which had been TNF-α activated but not incubated with INs underwent IHC staining to verify the expression of the target antigen, CD44. The commercially available kit from Vector Labs that was used employs an immunoperoxidase procedure with avidin-biotin binding. Avadin is a 68 kDa glycoprotein that has a very high affinity (10^{15}/M) to bind to the smaller biotin molecule. This affinity makes the binding essentially irreversible, and is 10^{6} times greater than any antibody-antigen association. The kit is purchased specific to the cell type (e.g. mouse IgG) and primary antibody employed, and the primary antibody is specific to the target antigen to be

detected. The general idea is that the primary antibody will adhere to the antigen that you wish to identify, and a secondary biotinylated antibody will adhere to the primary antibody. The biotin groups on the secondary antibody provide binding sites for the avidin biotinylated enzyme complex containing horseradish peroxidase. Cell nuclei were counterstained with diaminobenzidine (DAB) which provided an orientation of the expressed antigen relative to the rest of the cell. The staining procedure was carried out according to the instructions of the manufacturer.

5.2.3. Incubation Experiments

5.2.3.1. Design of Experiments

The aim of the experiments was to assess the ability to bind the 10%Tween-CC-CR niosome conjugated to IM7 with activated endothelial cells, and to examine the effect of experimental and design variables on binding. Variables examined, shown in Table 5.1, were incubation time, lipid concentration, and antibody coating density. Each variable was given an individual eight well microslide. Whenever PBS is mentioned the concentration was 0.01M unless otherwise indicated.

Table 5.1 Experimental Variables of BAEC-IN Binding Experiments.

Concentration of IgG (ug/ml)	Lipid Conc. (mM)	Incubation Time (hours)
5.00	1.0125 mM	4
0.50	5.0625 mM	2
0.05	10.125 mM	1
Control niosomes (non INs)	10.125 mM	
Control Abs (pre IM7 post IN)	10.125 mM	

After incubation the cells were imaged with fluorescence microscopy to ascertain niosome binding relative to cell binding density by measuring the fluorescence intensity of the green bound niosomes and the blue DAPI stained cell nuclei. A custom made Matlab^{TM} analysis program described in Section 5.2.4.3 allowed for the analysis of the fluorescent images and quantify the fluorescence intensity of binding relative to cell density. The first set of experiments were done at an antibody concentration of 5.0 μg/ml antibody, and then the other antibody densities were examined with optimal variables found in the time and lipid concentration studies.

In order to verify binding independent of the fluorescent techniques a subset of IN incubated BAECs were separately fixed and coated for imaging by scanning electron microscopy (SEM).

5.2.4. Description of Methods

5.2.4.1. Incubation of Niosomes with Endothelial Cells

Cells grown in 8 well micro-slides were fixed with 4% paraformaldehyde diluted in 0.01 M PBS at 4˚C overnight. Prior to incubation the fixative was rinsed from cells three times with PBS. The cells were pre-incubated with 2% goat serum in PBS for 1 hour at 37˚C to prevent non specific protein interactions and then were rinsed three times with PBS. The niosomes were added to the cells and incubated for the designated time. After the IN-cell incubation the cells were rinsed three times with PBS and a drop of DAPI nuclear stain was added to each well. After staining, the wells were removed from the slide and the mounting media was added drop-wise to the slide and a cover slip was placed over the cells and was left to dry before imaging.

5.2.4.2. Fluorescent Microscopy Imaging of Incubated Cells

Fluorescent and phase contrast imaging of cells, cell nuclei, and INs was done as described in Section 4.3.2.6. Each treatment variable was imaged multiple times (3-5) in multiple wells (2-4) at 20x and 40x magnification.

5.2.4.3. Image Analysis

Overlays of fluorescent and phase contrast images were created as described in Section 4.2.3.6 in order to visualize binding. In order to quantify binding the images were analyzed using a customized image analysis Matlab™ (Mathworks) program. Example output and compiled data from the program is included in Appendix D. Essentially a graphic user interface was developed in

which the user first is prompted to import the fluorescent image of the nuclei as shown in Figure 5.1 left. The image includes a scale bar, and the program uses it for calibration. The right side of Figure 5.1 demonstrates the next step as the user is prompted to crop the image (if desired), before setting a threshold value of image intensity. Setting the threshold allows the user to compensate for variability in image clarity and intensity and can be an iterative process with the desired outcome being the identification of the individual nuclei and the removal of background noise, as shown by the image in Figure 5.2. Once the threshold is established, the nuclei are individually identified and counted, shown in the right side of Figure 5.2, by running Process 1. Process 1 measures the area of each identified nuclei and creates minimum, maximum, and average values for the group, and then, using those values, it evaluates whether each one is a single or greater count (Figure 5.3) and then sums the group.

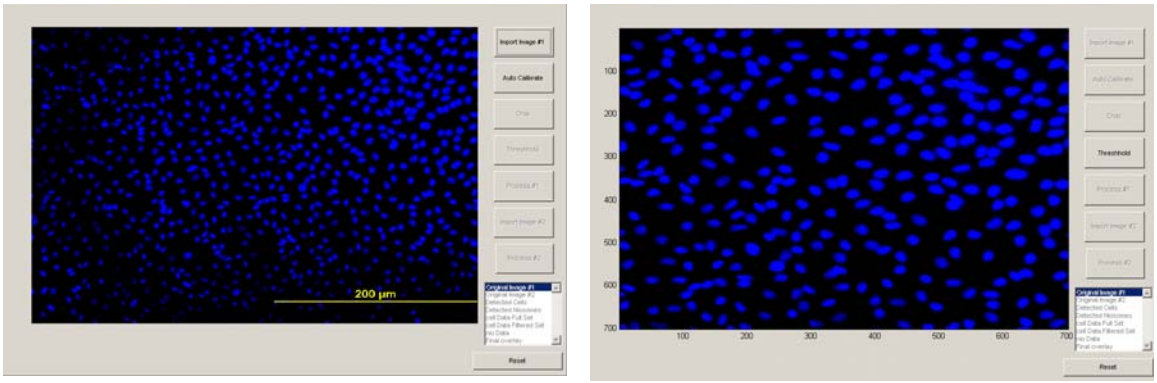

Figure 5.1 Matlab Program Importing and Cropping. Left: Importing of the fluorescent nuclei image. Right: The original image is cropped for analysis.

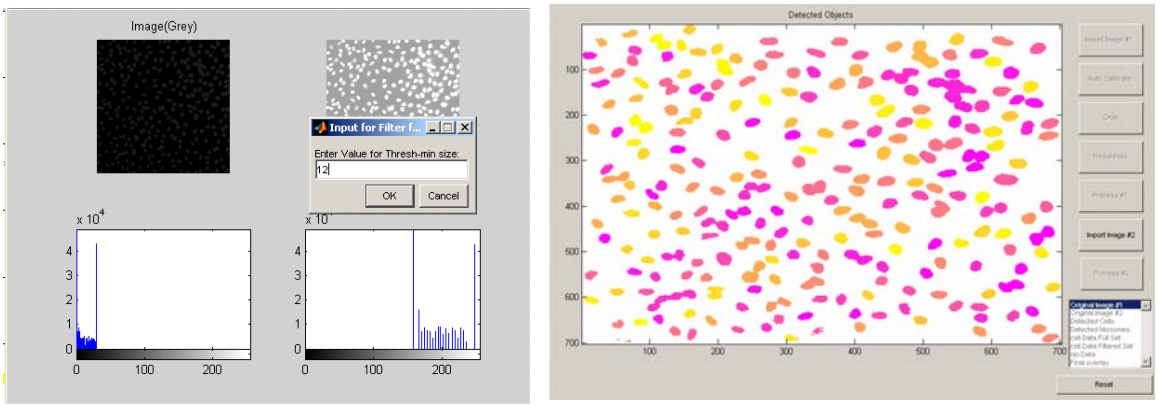

Figure 5.2 Matlab Program Image Sorting. Left: Setting the threshold in process 1. Right: The identified objects are sorted and counted.

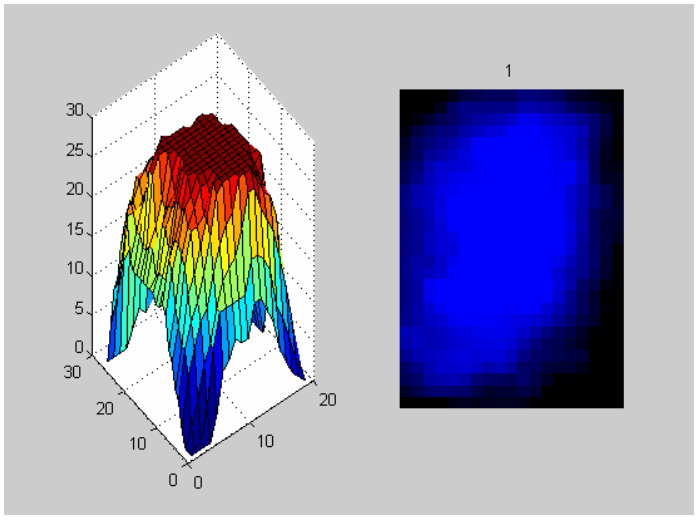

Figure 5.3 Matlab Program Image Analysis.

The fluorescent image of the niosomes which correspond to the same field as the previously imported nuclei image was imported (Figure 5.4 left). The same process of setting a threshold was repeated. Process 2 sorts the niosome images. Once the overall process was finished the program has calculated the number of cells, the total area of cell nuclei and the cell density, the niosome count, and created an overlay image of the two processed fluorescent images as seen in Figure 5.4 right. The discrete counting of niosomes was amended to

calculating fluorescent area of the niosomes instead, reasons for which will be discussed in greater detail in the results section, Section 5.3.1.

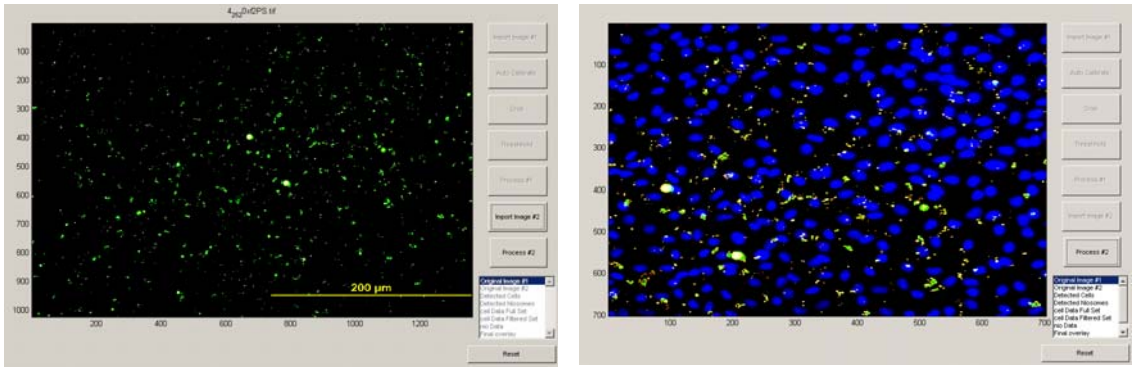

Figure 5.4 Matlab Program Fluorescent Nuclei and IN Overlay. Left: Importing the IN fluorescent images. Right: Overlay of processed images

5.2.4.4. Scanning Electron Microscopy

Scanning electron microscopy was used to verify the binding of niosomes to cells independent of the fluorescent measures, and to assess the patterns of surface binding of niosomes to endothelial cells. The cells were grown on square glass cover slips to allow for fixation and metal coating prior to SEM imaging. Before incubation with INs, the BAECs were rinsed with 37˚ C PBS several times to remove serum proteins, and then were fixed with 2.5% glutaraldehyde in PBS overnight at 4˚C. The fixed cells were rinsed three times with PBS (cells may be stored at 4˚C in PBS at this point, if required). Cells were then incubated with niosomes at 37˚C for the designated times and rinsed with PBS three times again afterwards. A 1.5% potassium ferricyanide-1% osmium tetroxide solution

was prepared under a fume hood in DI and added to the cells to incubate in the dark for 1 hour[1].

Once the osmium fixation step was completed, the cells were rinsed three times with a 0.1 M sodium acetate buffer. The lipids of the niosome membranes were fixed with the addition of a 1.5% uranyl acetate solution in 0.1 M Tris buffer for an hour. Before the dehydration began, the fixative was rinsed three times with sodium acetate buffer. Dehydration was done in a graded series for 5 minutes per treatment starting with 30% ethanol, then 70%, 95%, and 100% twice. Once the cells were dehydrated, they were substituted with a 1:1 preparation of hexamethyldisilazane (HMDS) and 100% ethanol for five minutes followed by two five minute treatments of pure HMDS. The coverslips of fixed cells and niosomes were dried under the fume hood. After this fixation process they were mounted on stubs and sputter coated by Ed Haller in the USF Health core facilities lab. The SEM imaging was done with Betty Loorman of the Biological Electron Microscope Facility of the Biology Department at USF on a JOEL JSM 35 scanning electron microscope.

[1] Extreme care must be taken working with these strong fixatives which can rapidly fix mucous membranes at low concentrations, and all contact with liquid and fumes must be avoided. Dispose of chemicals in a dedicated OsO_4 container.

5.3. Results

5.3.1. Endothelial Cell-Immunoniosome Images

5.3.1.1. Fluorescent Micrographs

Figure 5.5 shows the IHC stained BAECs with nuclear counterstain after activation with TNF-α. White arrows indicate expressed CD44 on cell surfaces and processes. Correspondingly, the two images in Figure 5.6 shows the green fluorescent niosomes attached to the cell processes and surfaces at different magnifications. Both images represent INs conjugated to 5μg/ml IM7 antibodies and incubated for 2 hours prior to imaging.

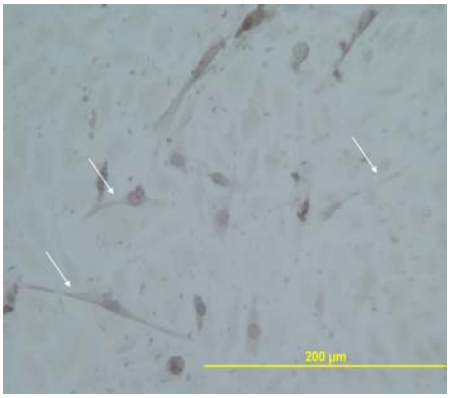

Figure 5.5 Immunohistochemical stain for CD44.

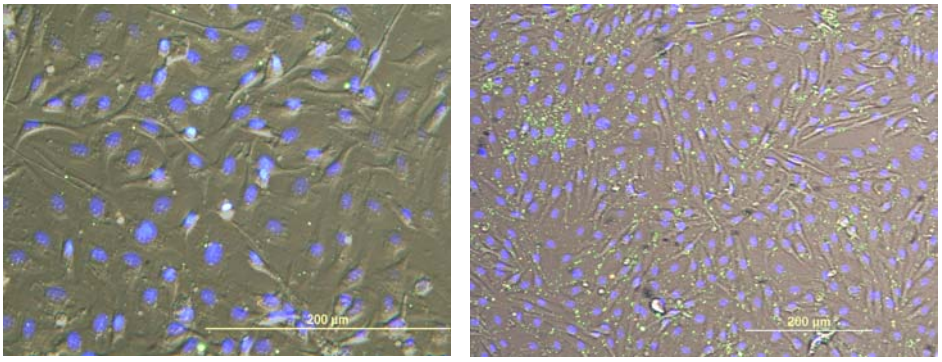

Figure 5.6 Fluorescent and Contrast Overlay of BAECs and INs. Left: 40x magnification. Right 20x.

5.3.1.2. Scanning Electron Micrograph Images

The left side of the SEM image shown in Figure 5.7 shows fixed cells incubated with INs, and the right side is a control of the same group of cells that were not incubated with INs. The vesicles seen on the cell surface of the left image are spherical and appear to be approximately the same size as the post GEC niosomes. The comparison was made by matching the vesicles to the 1 μm white line above the 10 μm scale line as shown.

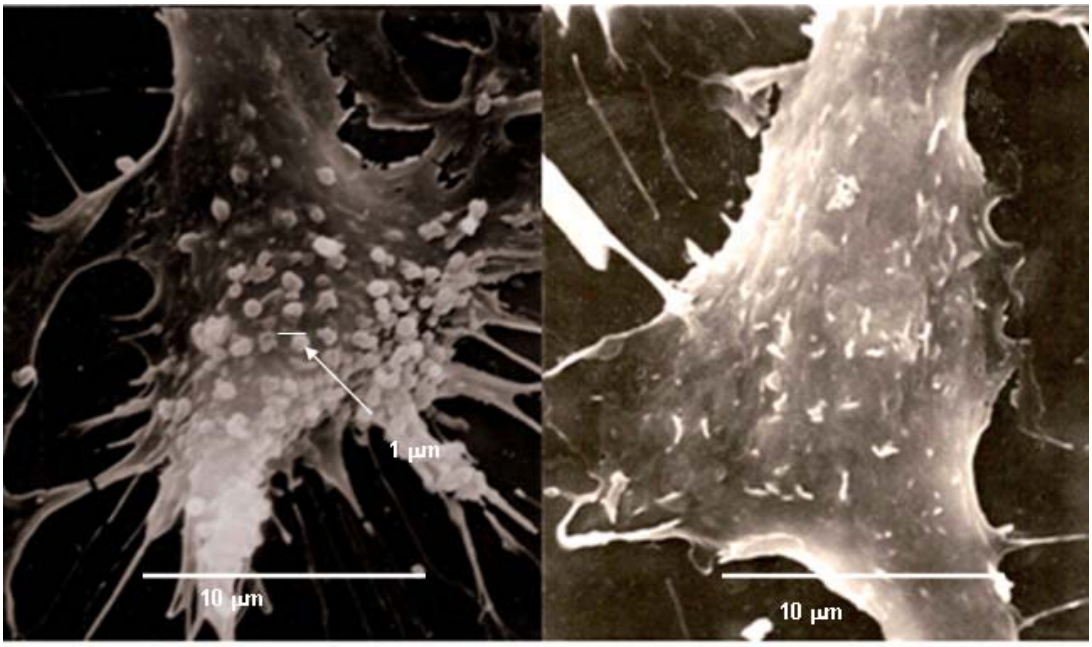

Figure 5.7 Scanning Electron Micrographs of BAECs. Left: INs bound to cell surfaces. Right: Control.

The graph in the left side of Figure 5.8 shows the effect of lipid concentration on relative binding density at different incubation times. The graph in the right side of Figure 5.8 displays the same data relative to incubation time at the different lipid concentrations, and the control data shown there reflect the

incubation of non targeted niosomes (without conjugated antibodies) at the maximum lipid concentration.

Figure 5.9 shows the affect of antibody concentration on the relative binding of INs to fixed BAECs. In all graphs the error bars represent the standard error of the mean with n>=3.

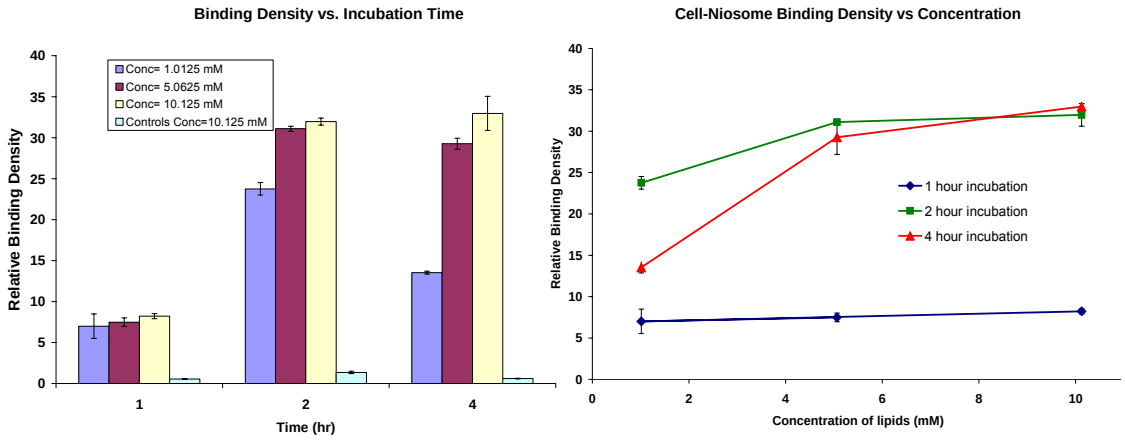

Figure 5.8 Binding Density with Respect to Time and Concentration. Left: Binding density with respect to lipid concentration at different incubation times. Right: Binding with respect to time at different lipid concentrations as compared to controls. All p<0.01 as compared to controls.

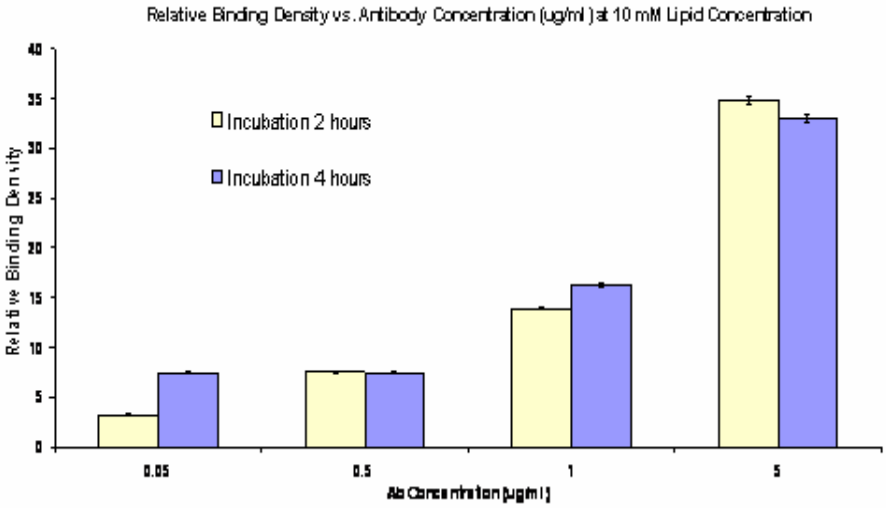

Figure 5.9 Binding Density with Respect to Antibody Concentration. Graph shows relative binding density at 1 and 2 hour incubation times.

5.4. Discussion

The aim of the experiments was to establish definitively that the drug targeting system would bind to fixed endothelial cells at the target antigen. The IHC staining of Figure 5.5 indicates that CD44 was expressed on the fixed bovine endothelial cells at the cell processes and surface. The two fluorescent micrograph-overlay images shown in Figure 5.6 indicate binding of the vesicles in those regions. Furthermore, examination of the SEM images in Figure 5.7 shows that vesicles of the right size and shape were observed bound to cell surfaces and that similarly shaped features were not observed in the control image. The binding of the vesicles to cell surfaces is observed in both cases to be non-homogeneous, and the accumulation of multiple vesicles concentrated in small areas as compared to relatively sparse binding in other areas led us to believe that discrete counting of bound INs by fluorescent measures would be inaccurate. The original Matlab^{TM} routine created a ratio of discrete counts of cell nuclei to discrete counts of niosomes. Once the SEM data revealed that niosomes may be bound closely together in groups making individual counting unlikely, the analysis was reconfigured to measure fluorescence intensity by area of binding and the data are shown to reflect binding area relative to controls.

The graph in Figure 5.8 left shows that the binding of INs at 1hour incubation time is independent of concentration of lipids. The binding intensity at 1 hour corresponded exactly to what was observed in the synovial lining studies. At increased incubation times the binding increased at the 5 mM lipid concentration, but little increased binding was observed in either an increase in

incubation time or in an increase in lipid concentration. The graph of Figure 5.8 right shows the same data with the controls included to clarify the effect of time on binding density with respect to each of the lipid concentrations. The control data at each incubation time represent non-immunoniosomes incubated at the maximum lipid concentration.

Immunoniosome binding relative to different coatings of antibody concentrations is shown in Figure 5.9. With increasing antibody concentrations, increased relative binding was observed, although at the lower antibody concentrations there appeared to be no variation in binding at 4 hours. Binding of INs at 1 hour was not studied based on the previous data. Additional testing of binding relative to concentrations of antibodies between 1-5 μg/ml may yield an optimum point.

In conclusion, the results shown indicate that INs bind to activated fixed endothelial cells specifically and in a non homogeneous pattern. The binding relative to time and lipid concentration increased to a limiting value but antibody concentration did not for the concentrations studied. For the treatments studied, 5 mM at 2 hours appears to be optimum in binding density while conserving material. Further studies will be conducted to investigate uptake up by live endothelial cells *in vitro* to prepare for *in vivo* animal studies. Section 6 describes the uptake of IM7 conjugated immunoniosomes in live cells.

6. Live Endothelial Cell Uptake Studies

6.1. Background

6.1.1. Live Endothelial Cells in Targeted Drug Delivery

Live endothelial cells have been used as a cell model for testing drug targeting efficacy for many applications including immunoliposomes targeting inflammation and for delivering anti-thrombolytics, and echogenic immunoliposomes for imaging and targeting. The cells have been used in flow experiments for tumor targeting, using antibody fragments, and to address targeting of quiescent versus proliferating cells. Uptake of antibody targeted drug delivery vesicles is highly dependent on the target antigen, as previously described (Section 2.3). In order to further investigate the IM7 conjugated immunoniosome as an effective treatment against inflammation the uptake of the vesicles into cells needed to be verified using live cells. Additionally, since accumulation, permeability, and uptake of vesicle by cells has been well established as being size dependent the size of the vesicles would need to be reduced. A study involving liposomes suggests that the preferential size for uptake by atherosclerotic lesions is 200 nm. Size reduction of niosomes has been reviewed[115] and includes probe sonication, extrusion through polycarbonate filters, micro-fluidization, and high pressure homogenization. Extrusion gave the best size control while maintaining comparable levels of encapsulation.

Microscopic methods used for investigating IN uptake by activated BAECs were confocal microscopy and transmission electron microscopy (TEM). With confocal microscopy fluorescent images are captured in multiple x-y planes in a z direction. The result provides three-dimensional information about cellular uptake of a fluorescent vesicle. TEM provides very high magnification and resolution because the energy source from which the image is formed is a beam of electrons rather than light, which has a resulting wavelength (in a vacuum and at a small angle) 3 orders of magnitude lower than that of light.

6.1.2. Dynamic Light Scattering

Dynamic Light Scattering (DLS), also referred to as photon correlation spectroscopy, is used widely to measure the size and distribution of dispersed particles by measuring the changes in laser light projected through the particles. The random movement of small particles in a suspension is called Brownian motion, and is caused as particles collide with molecules from their surroundings and diffuse randomly. When polychromatic light hits small suspended particles, the light is scattered in many directions; this is referred to as Raleigh scattering. However, when monochromatic light is shined into a solution of particles undergoing Brownian motion, the light hitting the moving particles undergoes a Doppler shift when changing wavelength, which can be measured. The change in wavelength is related to the size of the particle that the light hit.

Particles undergoing Brownian motion travel at different speeds related to their size; smaller particles move faster than larger ones. This relationship is

defined by the Stokes-Einstein equation. First, the Einstein relation describes diffusion of particles:

$D = \mu_p k_B T$; where D is the diffusion constant, μ_p is the mobility of the particles, k_B is Boltzmann's constant (a physical constant which relates energy and temperature;1.38 x 10^{-23} J/K) , and T is the temperature in K. Under conditions of low Reynolds number (the ratio of inertial to viscous forces) the mobility is related inversely to the drag coefficient, γ, where under Stokes Law, spherical particles of a radius r:

$\gamma = 6\pi\eta r$; η is the viscosity of the media in which the particle is dispersed. Therefore taken together, the Stokes-Einstein equation becomes

$D = \frac{k_B T}{6\pi\eta r}$ Diffusion coefficient units are in m^2/s . The hydrodynamic radius is then found by:

$r_H = \frac{k_B T}{6\pi\eta D}$.

Through these relations, given viscosity and absorption of suspending media, and the temperature of system, the DLS system algorithms measure particle size and/or molecular weight of a suspension through the use of a digital correlator. The correlator measures how closely two signals are over a period of time. Correlation is a statistical technique for reducing noise and finding a real signal within it; it measures the degree by which a signal is not random when it would appear to be. The second order equation is:

$G(\tau) = \frac{I(t_0)I(t_0+\tau)}{I(t_\infty)^2}$ where the function relates the product of the intensity at t_0 by the intensity at t_0 increased by some value τ as a ratio to the square of the intensity overall squared.

6.1.3. Monoclonal Antibody Fragments

Another important consideration in effective targeted drug delivery is the persistence of the system within the bloodstream. Vesicle encapsulation of drugs has been shown to increase circulation time, improve bio-distribution, and prolong therapeutic plasma levels *in vivo* versus free drug administrations. If the drug delivery vesicle or targeting vector provokes an immune response within the body and subsequent rapid clearance from the blood stream there may not be sufficient time or payload of drug delivered to be efficacious. Concern about the rapid and increasing clearance of immunoliposomes *in vivo* with subsequent intravenous injections was solved when antibody fragments were substituted for whole antibodies.

While antibodies have been discussed in earlier sections, a description of the physical structure was not given in detail. An antibody is a glycoprotein of molecular weight 150 kDa which is made up of two general types of polypeptide chains, two heavy chains and two light chains. The light chains are about 25 kDa each, and each heavy chain is about 50 kDa. There are five subcategorizes of antibodies, IgA, IgE, IgD, IgM, and IgG. These differ by their heavy chains types and structural makeup. The chains are held together by a series of disulfide bonds. Figure 6.1 shows the general structure of an antibody with respect to the

different chains. An IgG, which is the subgroup of interest for this research, is composed of either of two types of light chains, κ or λ, and the γ_1 heavy chains, which designate the subgroup.

The antigen binding (variable) region is indicated at the top of Figure 6.1, and is specific to the exact antigen to which the antibody binds. The regions below are conserved, and consistent by antibody type. The area between them is referred to as the hinge region. Overall above the hinge is referred to as the $F(ab')_2$, and below the Fc region. The immune response to the immunoliposomes was provoked by the Fc region of the antibody and was negated when Fab fragments were used. As Figure 6.1 indicates, fragmentation of antibodies can include a single or a coupled Fab antigen binding group, in fact many more configurations and combinations have been studied and engineered for use in biopharmaceuticals, biosensors and diagnostics.

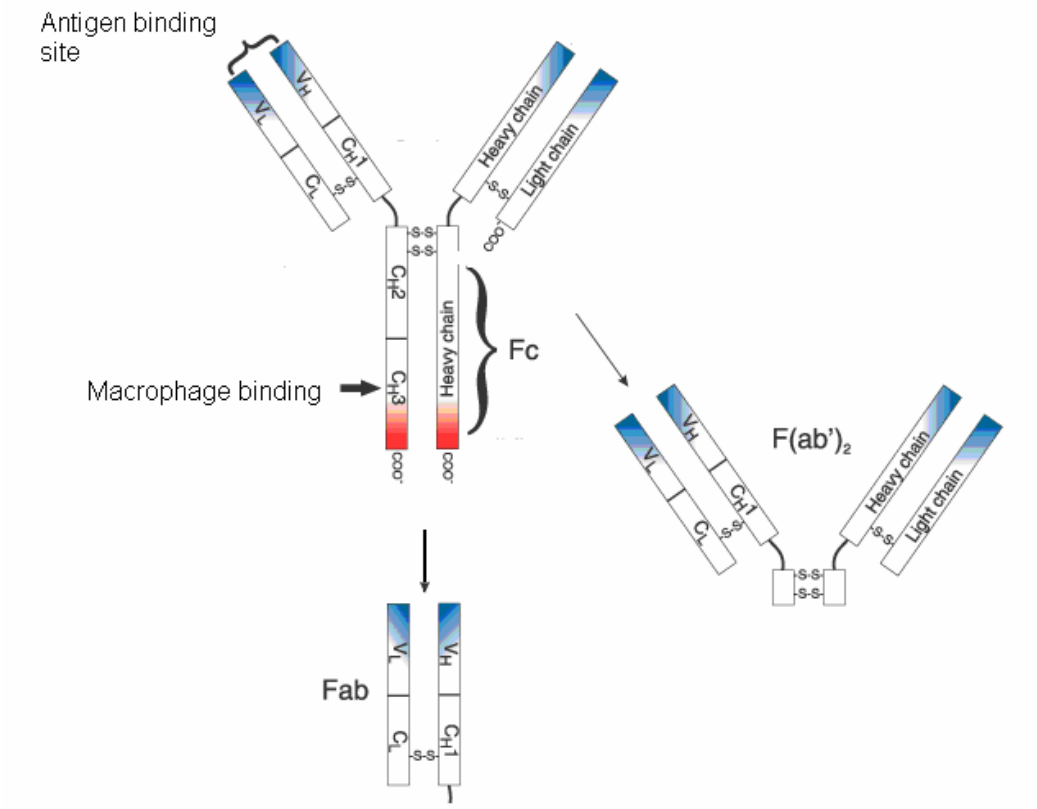

Figure 6.1 IgG Antibody Structure. (Source: Invitrogen)

Fragmentation of antibodies is done using proteolysis reactions (degradation of protein by enzymes) using enzymes such as papain, or pepsin or ficin, and then subsequent purification steps are taken to separate Fc segments and non-fragmented whole antibodies from the desired Fab or $F(ab')_2$ fragments.

6.2. Materials and Methods

6.2.1. Materials and Chemicals

Included in this list are the materials, chemicals, and equipment new to this phase of the project that were not included in the previous sections. Polycarbonate filters and polystyrene latex particle standards where obtained from Sigma Chemical. The antibody fragmentation kit (Immunopure ® IgG1 Fab

and F(ab')$_2$ 44880) was purchased from Pierce Biotechnology. Propidium iodide nuclear stain (H-1300) was obtained from Vector Labs. The gold particles were a gift from Ed Haller, USF Health Pathology. Embed media and components for TEM (and assistance) were provided, kindly, by Dr Karl Muffly.

Table 6.1 Equipment for Uptake Studies.

Equipment	Manufacturer	Model
Lipid Extruder and Assembly	Northern Lipids	Thermobarrel 10 ml
Water bath	Fisher	Isotemp Open-Bath Circulator
Submicron Dynamic Light Scattering Instrument	Malvern	Nano-S
Confocal Microscope	Leica	SP3

6.2.2. Methods

6.2.2.1. Extrusion of Niosomes

Prior to extrusion the niosomes were prepared through the hydration step and then frozen overnight. Freezing and thawing the vesicle preparations prompts hydration of the lipids and equal distribution of encapsulated materials.

The niosomes were extruded using a bench top stainless steel 10 ml Thermobarrel Lipex^{TM} Extruder. Figure 6.2 shows the extruder and indicates the functional parts. In order to set up the extrusion process the extruder must be disassembled so that the filter package can be put in place. Two polycarbonate filters were stacked on top of a mesh disk and a support disk within the cavity of the filter support base and secured under an o-ring. A drop or two of de-ionized

(DI) water was added between each filter while stacking to ensure good seating. The correct alignment of the filters is crucial to the extrusion process; poor alignment increases extrusion time and may necessitate changing filters before the extrusion sequence is complete. The barrel of the extruder was replaced and secured with wing nuts.

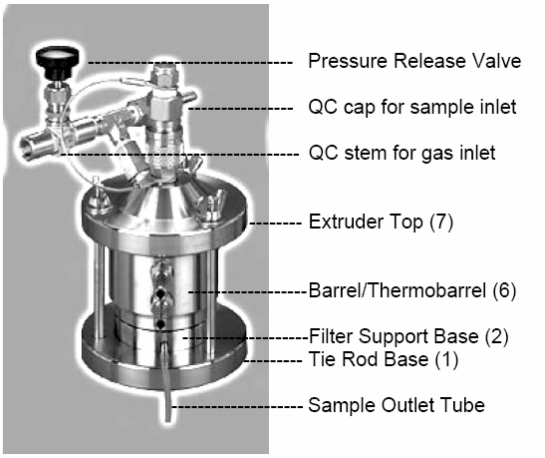

Figure 6.2 Extruder Assembly. (Source: Northern Lipids Extruder Handbook)

The vesicle suspension was pushed through the polycarbonate filters using high pressure nitrogen gas (N_2) supplied through high pressure lines. The direct pressure into the system from the N_2 tank was controlled through a valve on the delivery tubing which is coupled to the gas inlet.

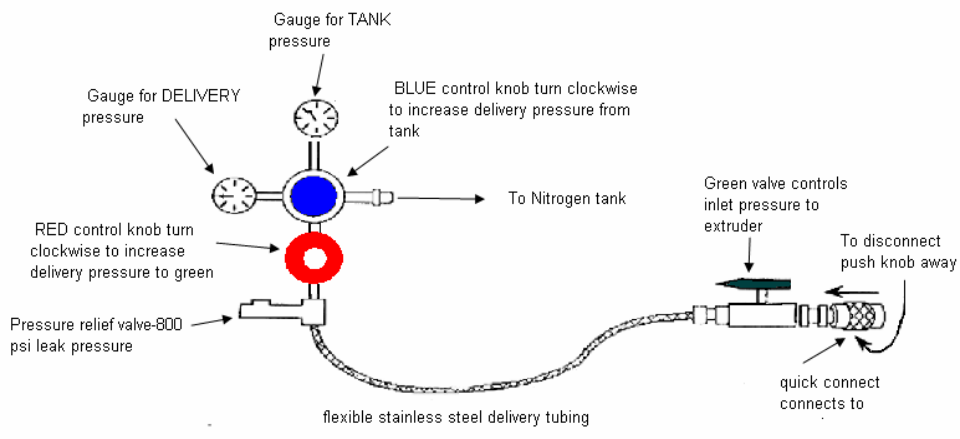

Figure 6.3 Nitrogen Delivery to Extruder. (Adapted from Northern Lipids Extruder Handbook.)

The water jacket of the extruder was supplied 60˚C DI water by a heated water bath which was circulated by a peristaltic pump. Once the circulating water equilibrated the extruder temperature, the filter assembly was conditioned by expressing 8-10 ml of heated PBS through it. The pressure of the PBS delivery was relatively low; setting the pressure to 200 psig, and rapidly opening and closing the valve was sufficient to expel the liquid.

Once the filters are conditioned, the heated niosome suspension was pipetted into the sample inlet. Control of the niosome suspension temperature is important because extrusion must be done above the gel-to-liquid crystalline phase transition temperature of the surfactant component (or in the case of phospholipids, the component with the saturated alkyl tail) as described in Section 4.2.1.1. The temperature of the sample added to the inlet was allowed to equilibrate for a moment before starting the extrusion (this is repeated at each successive step). The valve was opened to allow the pressure to push the niosome suspension through the filters. The extruded sample was expressed

from the outlet tube once the extrusion process was underway. If sample was not expressed within a few seconds, the pressure was increased until the solution began to flow from the tube. The maximum pressure set by the manufacturer was 800 psig. Once the extruded sample was captured, the system pressure was vented by opening the pressure relief valve, and the sample was returned to the inlet. This process was repeated ten times and loss from the process was usually less than 10%. After extrusion, the niosome sample was ready for the GEC process.

6.2.2.2. Dynamic Light Scattering Measurements

Dynamic light scattering was used to measure the size of the extruded and purified vesicle suspensions using a Malvern Instruments Nanosizer S. Since the PSS particle analyzer (Section 4.2) had a lower detection limit of 0.5 μm diameter particles, the new instrument was required to monitor the size and stability of the extruded vesicles. The Malvern system provides size, molecular weight, and dispersity data using dynamic light scattering measurements with autocorrelation function. The data results in a poly dispersity index which is a measure of the width of the particle size distribution peak of the sample. The instrument allowed measurements of post GEC particles suspended in PBS. Operating parameters were programmed for measuring samples specifically in a standard operating procedure (SOP) in the instrument software (DTS). The material properties, refractive index and UV absorbance of the material to be measured and the dispersant are input. Refractive index was measured on a refractometer, and the UV absorbance of the niosome suspension at red laser

wavelength (633 nm) was measured using a UV spectrophotometer. These values are used to allow the conversion of the intensity distribution to a volume or number distribution.

Outputs from individual measurements include intensity and volume particle size distributions, cumulants and distribution fit curves, intensity and volume statistics, and the correlation data. Calibration of the system was done with polystyrene latex standards. Figure 6.4 shows the intensity PSD of a 60 nm and 220 nm mixture of polystyrene latex particle standards, and the Figure 6.5 shows the correlation function curve. The PSS system (as described in Section 4.2.2.2) provided actual counts of particles, due to the single particle sensing measurement algorithm, whereas the Malvern instrument provides a distribution relative to a measured population-the area under the curve of the size distribution of the Nanosizer data is always 100%, and the area under the curve of the PSS size distribution is the number of particles measured and counted by the instrument. Due to the difference in the underlying physics of these particle characterization tools, their data did not align well. Despite claims to the contrary by the manufacturer, dispersions of vesicles between 700-1000 nm did not measure accurately or repeatedly in the Malvern instrument, at any dilution. This would probably be due to the size limitation of Brownian motion.

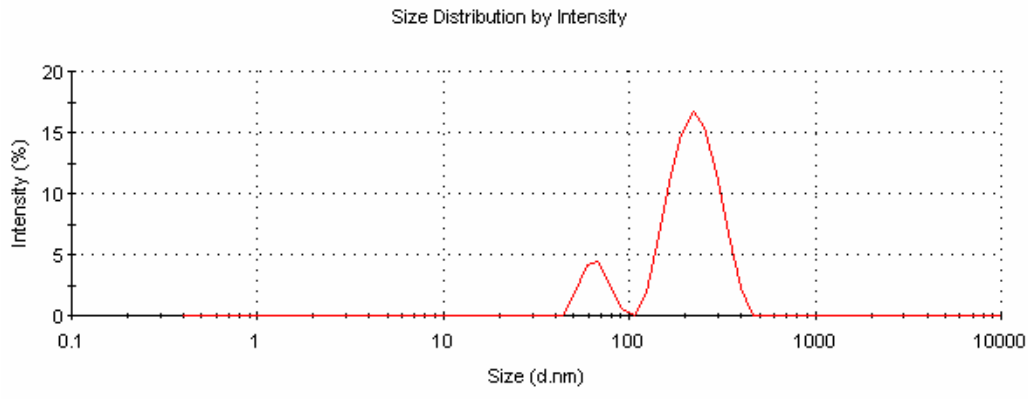

Figure 6.4 Particle Size Distribution of 60 nm and 220 nm Standards.

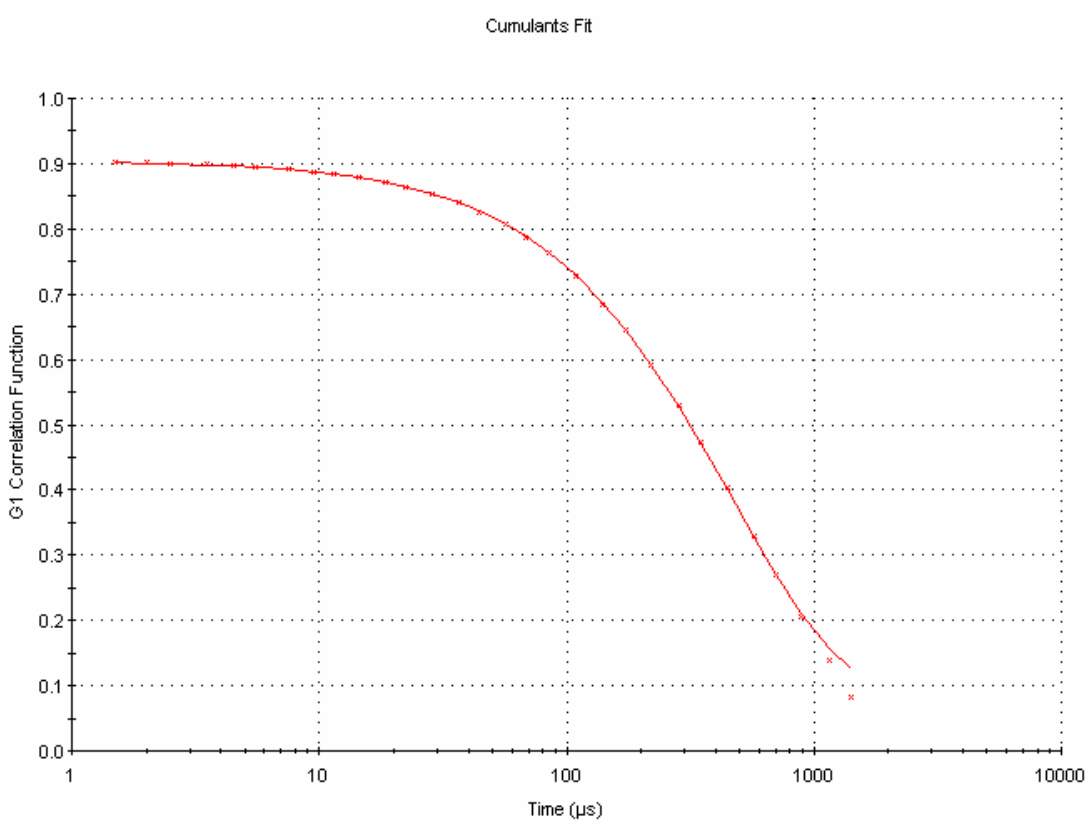

Figure 6.5 Correlation Function Curve of the Standards.

6.2.2.3. Antibody Fragmentation

Antibodies were fragmented using a commercially available kit from Pierce according to the manufacturer's instructions. While the components of the columns and buffers are proprietary, essentially the process is the pH dependent digestion of the hinge proteins of the antibody by the thiol protease enzyme ficin (MW 25 kDa) in the presence of the amino acid cysteine. At a concentration of 1 mM cysteine, ficin will produce $F(ab')_2$ fragments, and at a concentration of 10 mM cysteine, ficin will produce Fab fragments. The digestion reaction takes place in a column and the resulting fragments are eluted out in different fractions using different buffers. The UV absorption of the fractions was measured and a balance of proteins found that the initial yield was 70%. The protein concentrations were measured using extinction coefficients of $\varepsilon_{Fab}= 7.5 \times 10^4$, and $\varepsilon_{IgG}= 22.1 \times 10^4$ using Beers Law (see Section 4.2).

6.2.2.4. Endothelial Cell Culture and Fixation Techniques

Cells were cultured and activated as previously described in section 5.2. For confocal studies the cells were grown on 8 well micro-slides, for TEM the cells were grown on cover slips to allow for embedding into the resin. Prior to incubation with live cells, the INs were filtered for sterility using a 0.2 μm syringe filter to eliminate possible contaminants.

For the TEM studies a dilute solution of 15 nm spherical gold particles was encapsulated in 10% Tw-CC niosomes which were extruded, purified with GEC, and conjugated to IM7 antibodies in the usual manner. The gold particles were

used in the niosomes to provide a strong signal during the TEM imaging. Prior to IN incubation, the cells were well rinsed with warmed PBS.

6.2.2.5. Fixation Techniques for Confocal Microscopy

Fluorescent IN suspensions were diluted 1:1 in serum free endothelial media (to avoid unwanted protein interactions) and incubated with live bovine aortic endothelial cells (BAECs) at 37˚C for varied times. After incubation the vesicle-media mixture was discarded and the cells were rinsed three times with room temperature PBS and then were fixed with 1% paraformaldehyde in PBS for 15 minutes. After fixation, the cells were PBS rinsed again and incubated with 0.1% Triton X 100 solution for three minutes, to encourage membrane permeability for the nuclear stain, propidium iodide, which was left to penetrate for 30 minutes. Once the staining was complete, the cells were rinsed again, and the wells were removed. A few drops of hard setting mounting solution were added to each slide and a glass coverslip was placed over the cells and allowed to harden overnight.

6.2.2.6. Fixation Techniques for Transmission Electron Microscopy

Incubation of cells with INs with the gold containing INs was done as described for the confocal studies. Once the incubation was complete the cells were rinsed three times with room temperature PBS. Cells were fixed with a 2.5% solution of glutaraldehyde for 15 minutes at room temperature. Fixation of cells for TEM was similar to that of the SEM procedure. A 1.5% potassium ferricyanide/1% osmium tetroxide solution in DI water was added to the rinsed

cells and left to fix for an hour in the dark. The cells were rinsed three times for 10 minutes each in 0.1M sodium acetate buffer. The lipid membranes were stabilized by fixing in a 1.5% solution of uranyl acetate in a 0.1 Tris buffer, pH 6.3 for 30 minutes and then were rinsed three times with DI water.

Once the final fixation step was complete the cells went through a series of dehydration steps. A series of ethanol in water was added as follows for 5 minutes each, 30%, 70%, 95%, and 100% ethanol for 15 minutes. After the alcohol series, the cells were cleared with 100% propylene oxide for 15 minute, and then a mixture of 100% propylene oxide mixed 1:1 with the embedding media. The embedding media was mixed together per the instructions from the EMS Technical Data Sheet for Araldite 502/EMBED-812 Embedding media as follows: Embed-812 -13.75 g, Araldite 502 -8.5 g, DDSA -27.5 g, DMP-30-0.9 g. The cells were embedded in the 1:1 mixture and allowed to dry overnight, and then was capsulated in pure embedding media. The embedded cells were sectioned with a diamond knife and fixed onto copper grids stained with 8% uranyl acetate and lead citrate.

6.2.3. Confocal Microscopy

The confocal images were captured with a Leica SP2 using 40x oil objectives with FITC and rhodamine filters. The argon laser (blue light for green labels) provided wavelengths 458-514 nm, and the helium neon laser (red light for far red labels) provided light at a wavelength of 633 nm. The Leica confocal software (LCS) was used for imaging and for post-image capture processing.

Once the fluorescently stained cell nuclei images were visually confirmed and focused by viewing through the microscope eyepiece, the image capture software was set up. The two photomultiplier (PMT) gains and offsets were set for clarity and reduction of background noise, where possible. Figure 6.6 shows the image acquisition screen where the settings are adjusted in the software.

Table 6.2 shows the PMT gain and offset and z position settings for the samples examined.

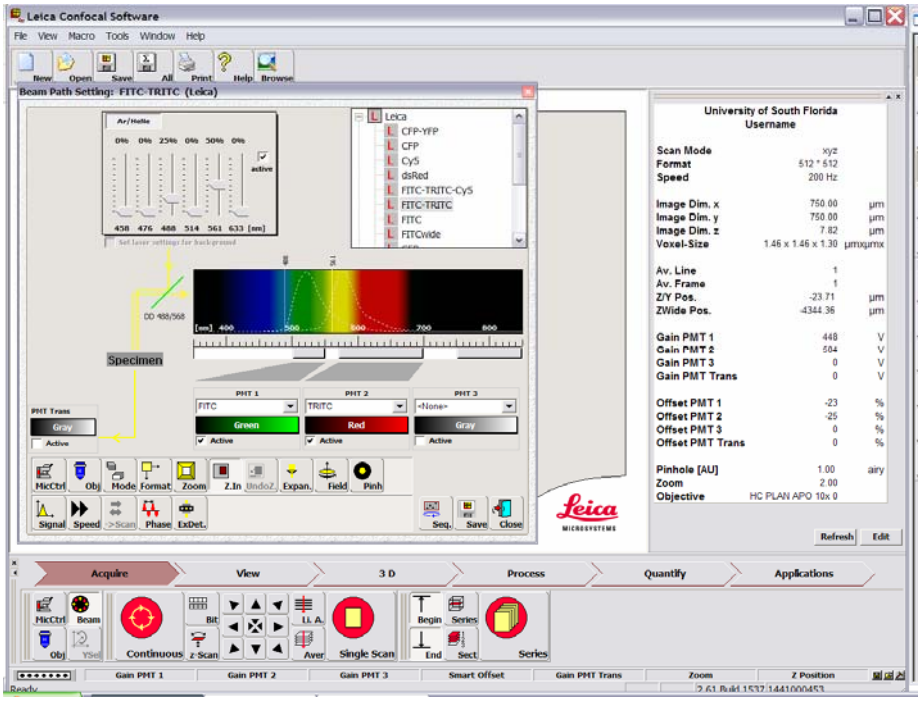

Figure 6.6 Leica Confocal Software Image Acquisition Window.

Table 6.2 Confocal Settings.

Sample	PMT 1		PMT 2		Z/Y Position
	Gain	Offset	Gain	Offset	(microns)
Control	632	-11%	616	-7%	-42
20min-dim	520	-15%	464	-4%	-49
20min-brt	549	-14%	568	-14%	-28
1hour-run1	862.3	-5.10%	847	-3.60%	-29
1hour-run2	862.3	-5.10%	847	-3.60%	-29

Once the settings are established the image capture stack has to be defined prior to going into scan mode. Figure 6.7 shows the schematic for setting the z/y position in the LCS software. By scrolling through the image using the z position the bottom and top positions were set to mark the start and end of the captured stack.

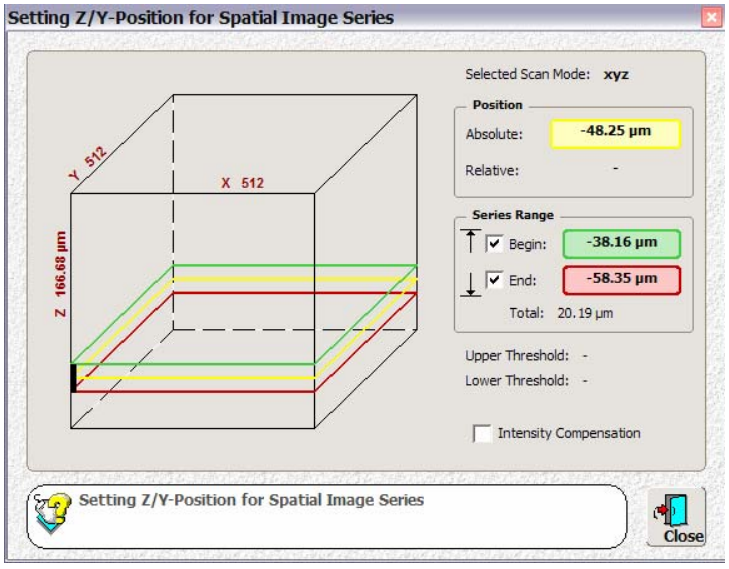

Figure 6.7 Spatial Setting for Scan Mode Imaging.

6.3. Experimental Designs

Extrusion experiments were evaluated by taking aliquots of sample at each extrusion pass. These samples were examined for size and entrapment of dye by GEC elution and DLS. The GEC elution profiles were created by fluorescent measurements of sequentially eluted fractions. Particle size distribution was measured by DLS to see the effect of extrusion passes on vesicle formation and dispersity.

For the confocal uptake studies with whole antibodies conjugated to fluorescent immuniosomes incubation times examined were 20 mins, 1 hour, 2 hours, and a control of 2 hours at 4˚C to check for non specific binding. Confocal images of INs conjugated to IM7 Fab fragments were measured at 1 hour. TEM incubation time was 1 hour. All antibody or fragment coating was at a done at concentrations of 5 μg/ml.

6.4. Results

6.4.1. Extrusion Results

In Figure 6.8 the fluorescence chromatograms show the GEC elution of each sample. The first peak represents the fluorescent signal from the niosomes (partially quenched due to concentration) and the second peak represents the unencapsulated free dye. Figure 6.9 shows the particle size distribution of the niosome fractions captured during GEC.

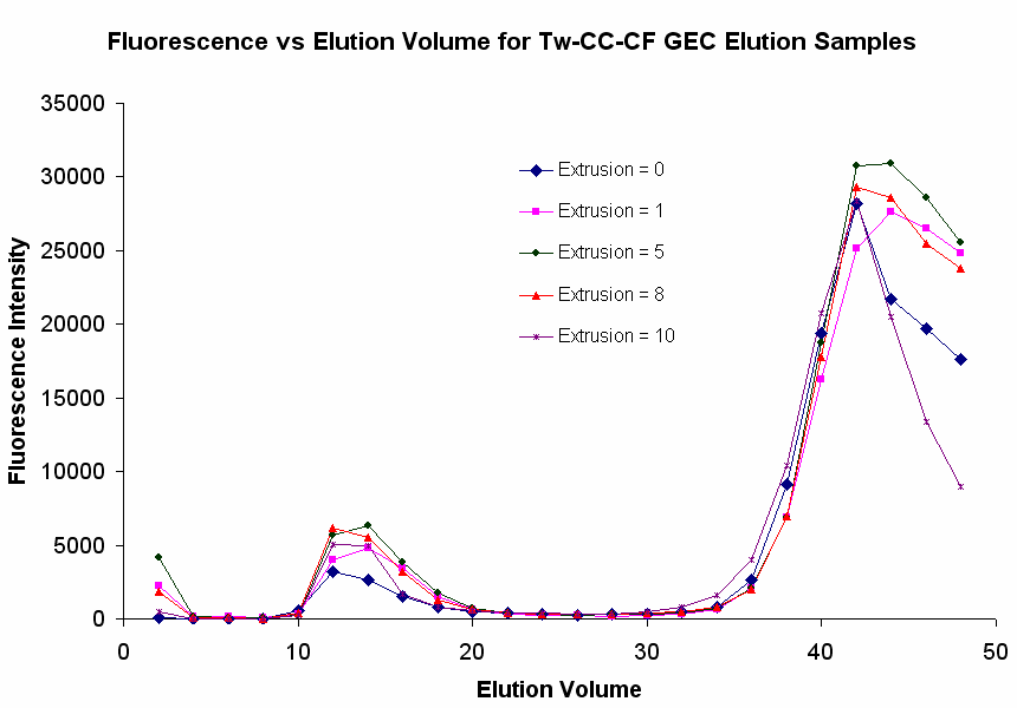

Figure 6.8 Elution of Extrusions 0-10 for a 10% TW-CC-CF Hydration Sample.

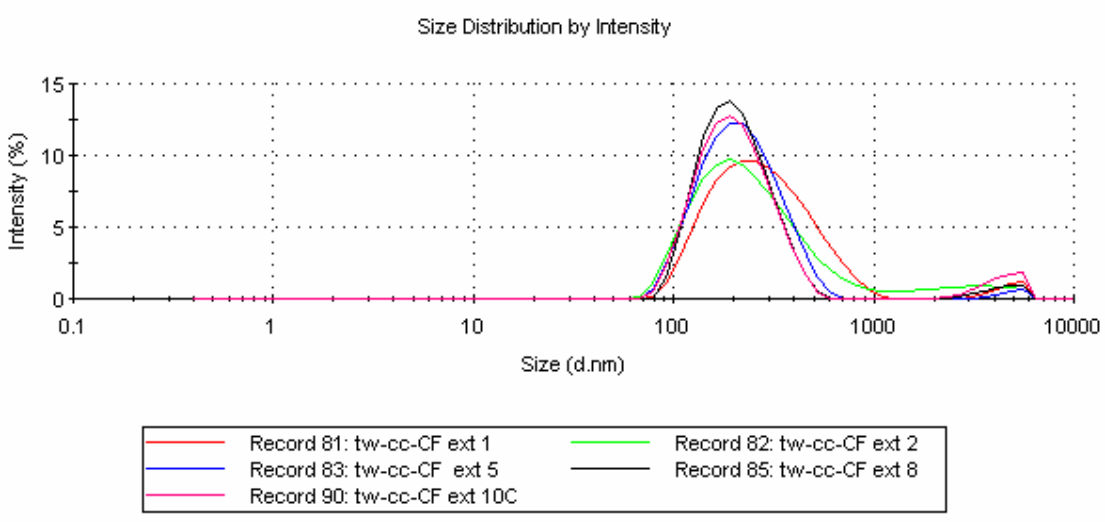

Figure 6.9 Dynamic Light Scattering Data of Extruded Samples.

The cell nuclei are stained red in the confocal images, and the INs are green. All images shown are at the maximum area of cell nuclei. Figure 6.10 shows the 20 min incubation. The z value represents the depth within the stack that the

image represents. Figure 6.11 shows the 1 hour incubation, and Figure 6.12 is the 2 hour incubation. The control cells are shown in Figure 6.13. These figures represent incubations with whole antibody bound INs. The LCS software provided a post imaging function called slice that allowed for a cross section of x-z or y-z plane to be viewed. The narrow images shown in Figure 6.14 are individual cross sections for each incubation slide already shown. The final confocal image is seen in Figure 6.15 representing the incubation of BAECs with fragment conjugated immunoniosomes.

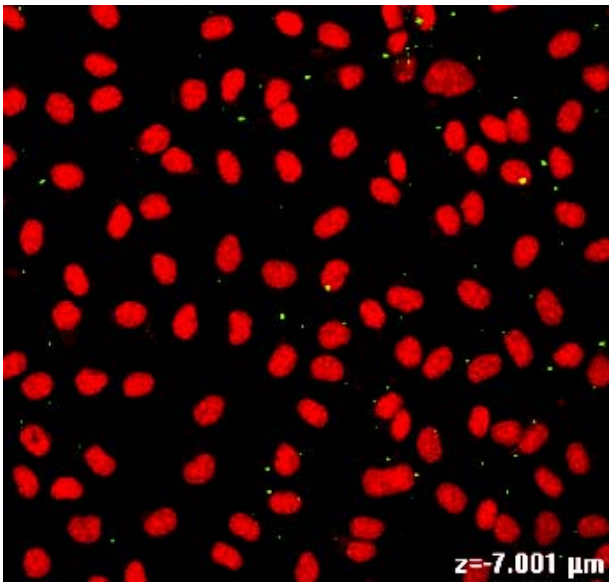

Figure 6.10 Confocal BAECs 20 Minute Incubation. Image at -7.001 mm (Range of stack: 0,-12.537 mm)

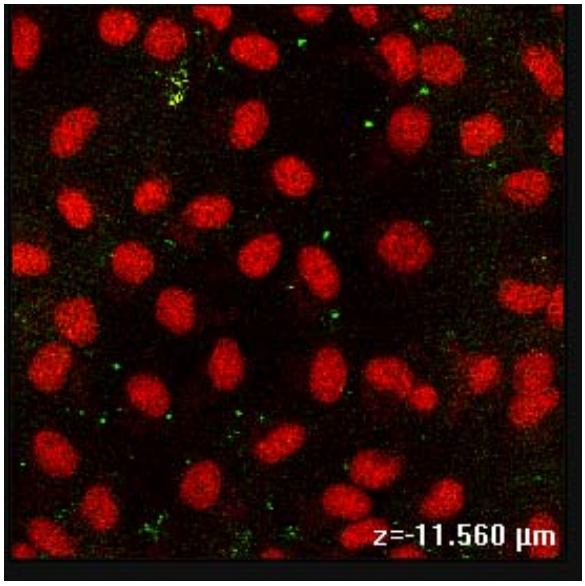

Figure 6.11 Confocal BAECs I Hour Incubation. Image at -11.56 mm (Range of stack: 0,-20.00 mm)

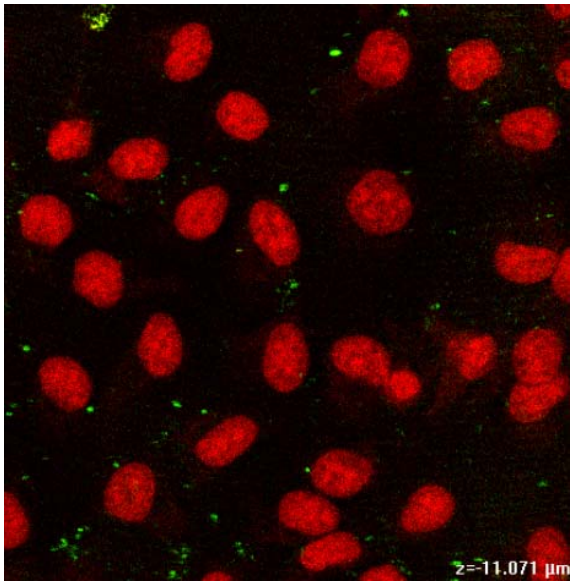

Figure 6.12 Confocal BAECs 2 Hour Incubation. Image at -11.07 mm (Range of stack: 0, 20.03 mm)

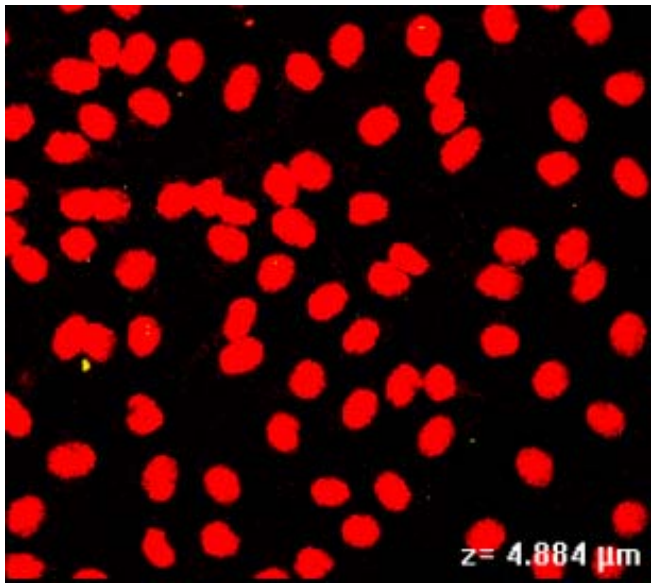

Figure 6.13 Confocal BAECs Control. Incubation at 4° C for 2 hrs. Image at 4.88 mm (Range of stack: 11.07,0 mm)

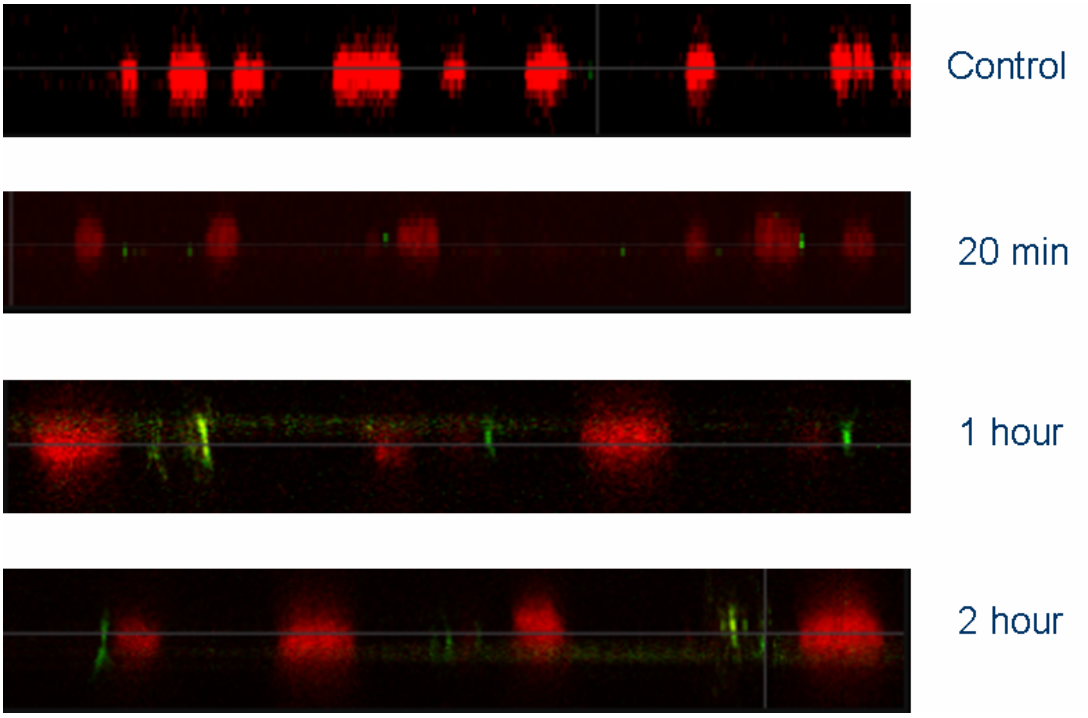

Figure 6.14 Confocal Cross Sections.

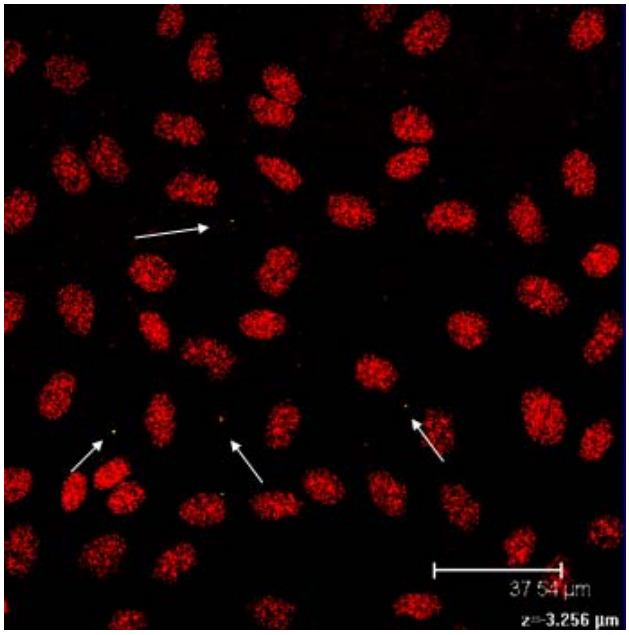

Figure 6.15 Fab-IN BAEC Confocal Image.

6.4.2. TEM

Figure 6.16 shows the TEM image a single endothelial cell captured from the incubation of INs containing gold particles with BAECs. The arrows indicate the niosomes bound to the surface of the endothelial cell.

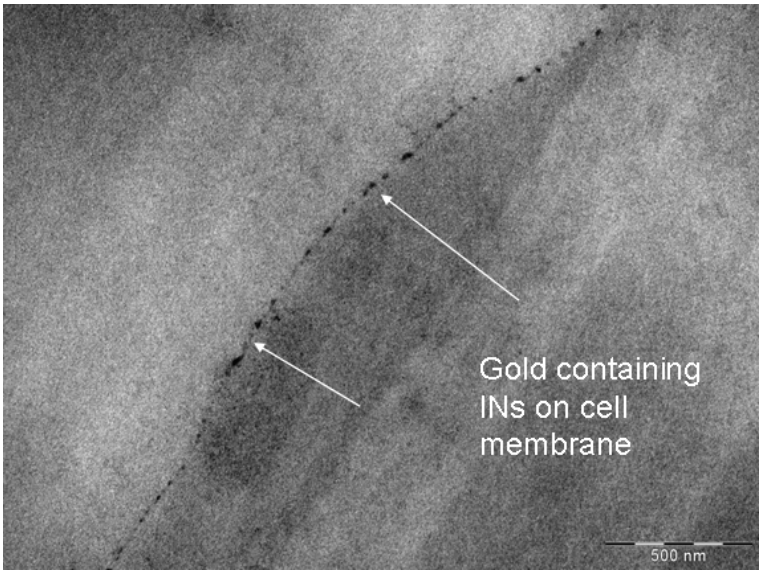

Figure 6.16 TEM of Au-INs.

6.5. Conclusions

The extrusion studies indicated that eight passes through the system is preferable for these vesicles versus the suggested ten passes used in the synthesis of liposomes. Each successive extrusion pass up until the eight showed an increase in the formed niosome signal of Figure 6.8, and correspondingly showed a taller and sharper peak in the dynamic light scattering data of Figure 6.9. In each data set, reduction of niosome formation and peak was seen in the tenth pass sample.

The confocal images suggest uptake of immunoniosomes by live endothelial cells. Penetration of IM7-niosomes continues between 20 min and 1 hour, but does not appear to increase appreciatively thereafter. The cross section images raise the possibility that INs are attaching to the junctions between the cells, although there are niosomes visible in some images near nuclei. Controls show no binding at 4˚C. Absolute verification of location of the vesicles either within or on the surface of the cell remains to be done. Membrane staining was attempted to clarify the imaging, but since the nature of the vesicle membrane is analogous to that of a cell membrane, cross staining did not allow for the desired distinction of IN position using that technique. An independent measure is needed to confirm uptake such as radio labeling of vesicle components or encapsulated material.

The IN-Fab incubation showed very sparse binding. This may be due to disruption of the antigen couple of the fragment dissociating when exposed to the binding pH. Using the $F(ab')_2$ fragments instead of the single Fab's may provide

binding closer to that of the whole antibodies and should better preserve the antigen binding sites. As it stands although the potential for fragment use is demonstrated, the fragment binding requires optimization.

The TEM image shows adhesion to the surface of cell by the gold INs, none were observed within the cell, however a very small sample of cells were identified in the media, and an improvement of the cell embedding technique may allow for clearer data.

7. Conclusions and Contributions

7.1. Introduction

The research that this document represents created a new drug delivery system with a novel linking chemistry targeted to treat a very significant pathological condition, atherosclerosis. The long term goal of this research was to create, test, and optimize a drug delivery carrier with a targeting vector that could be used to treat the vulnerable plaque of atherosclerosis and test it experimentally *in vivo* in an atherosclerotic animal model.

The fixed cell binding results of this research strongly demonstrate and ability of the immunoniosome to bind to a target antigen and to do so selectively and specifically. The uptake results do not definitively demonstrate the exact fate of the IM7 conjugated niosomes when bound to inflammatory endothelial cells. There has been sufficient demonstration within the body of liposome literature to establish that the correct antigen-antibody couple will enable the uptake of antibody bearing vesicles into the endothelium through endocytosis. Further studies evaluating uptake of immunoniosomes by endothelial cells will need to be pursued.

Regardless of uptake, the binding of niosomes bearing drug payload has the potential for therapeutic effect by virtue of localization and antigen binding site blocking. If a drug bearing particle is localized to a pathological site, *in situ* drug

release will provide higher concentration of drug at the desired location than a systemic delivery would. Also, a critical factor in the progression of inflammatory diseases, and the build up of atherosclerotic plaque, is the destructive proliferation of inflammatory cells at the sites of chronic inflammation. By blocking the binding of inflammatory cells and the cell uptake sites, their accumulation within the tissues would be mitigated. Whether the targeted vesicles are taken up by the cells through endocytosis, or remain on the surface of the inflammatory site, the potential for treatment remains.

The immunoniosome system was evaluated in this research for use in targeting inflammatory processes; it would not necessarily be limited to that application. The system is capable of encapsulating a solution of either hydrophilic or hydrophobic drug, and of binding to any IgG and, except where limited by size or surface hindrances, any protein. With these capacities, many different applications of the system are possible and remain to be pursued. The creation of the Tween 61-cyanuric chloride linker provides a highly reactive binding moiety which can undergo nucleophilic substitution reactions easily and without prior derivatization of the binding species. The potential of the system to be used for other applications is significant.

7.2. Contributions

The contributions of this research to the field of targeted drug delivery include the synthesis and characterization of a novel formulation of an antibody targeted non ionic surfactant vesicle drug carrier. There is no information in the literature describing niosomes composed of a blend of surfactants as a tool to

simultaneously maintain required physical properties while creating linking moieties. The creation of an antibody linker by the functionalization of a polyoxyethylene sorbitan monostearate molecule is novel, as is the creation of the polyoxyethylene sorbitan monostearate-cyanuric chloride linker molecule. There is no reported use of non ionic surfactant vesicles designed for active targeting with monoclonal antibodies.

7.3. Future Work

Future work in the vesicle characterization of this research includes the further investigation of uptake of INs by activated endothelial cells, and a refinement of the antibody fragment binding process. Entrapment of an HMG CoA reductase inhibitor drug, atorvastatin, will be pursued prior to the onset of the *in vivo* animal study. The protocol for the study has already been developed and granted approval by the USF IACUC and the US Army Medical Research and Material Command Animal Care and use Review Office. Table 7.1 outlines the experimental design of the research.

The atherosclerotic animal model that will be used in the experiments is a knock out mouse which lacks the ligand apolipoprotein E (apoE) which promotes lipoprotein clearance. The apoE- deficient mice are bred using homologous recombination in embryonic stem cells to be susceptible to developing atherosclerosis.

The animals will be fed a high fat diet to encourage the formation and progression of atherosclerotic lesions and plaque. After the 8-10 week feeding

period, the treatment phase lasts 6 weeks. Treatments of experimental groups are outlined in Table 7.1.

Table 7.1 Future Work: *In Vivo* Atherosclerotic Mouse Study

Treatment Group (n=6 for all)	Treatment
Test low	1. Surfactant vesicle coated with antibody fragments and containing drug atorvastatin (test substance-low drug concentration)
Test high	2. Surfactant vesicle coated with antibody fragments and containing atorvastatin (test substance-high drug concentration)
Control targeted non drug	3. Surfactant vesicle coated with antibody fragments and containing buffered saline solution
Control non targeted with drug	4. Surfactant vesicle without antibody containing atorvastatin
Control free drug low	5. Free drug atorvastatin low concentration (control)
Control free drug high	6. Free drug atorvastatin high concentration (control)
Control injection	7. Buffered saline (control)

Treatments will be administered by tail vein injection, and weekly blood samples will be taken by submandibular bleeding to assess blood cholesterol, triglycerides, and atherosclerotic markers (e.g. C-reactive protein). Weekly body weight will also be measured.

At the end of the treatment period, the mouse aortas will be evaluated for differences in plaque progression, the bio-distribution of the atorvastatin drug in the animal's organs will be assessed, and the lipid blood levels will be studied. The expectation from this study is that the targeted drug treatment group will show a reduction of plaque progression relative to the free drug groups and

controls. Additionally the study may demonstrate the extrahepatic effects of the statin on the build up of plaques, since statin treatment does not affect the production of cholesterol in the liver in the mouse model.

References

1. Waldmann TA. Immunotherapy: past, present and future. *Nat Med* 2003;9:269-77.

2. Torchilin VP. Drug targeting. *European Journal Of Pharmaceutical Sciences* 2000;11:S81-S91.

3. Wright S, Huang L. Antibody-directed liposomes as drug-delivery vehicles. *Advanced Drug Delivery Reviews* 1989;3:343.

4. Kohler G, Milstein C. Continuous Cultures Of Fused Cells Secreting Antibody Of Predefined Specificity. *Nature* 1975;256:495-497.

5. Riechmann L, Clark M, Waldmann H, Winter G. Reshaping Human-Antibodies For Therapy. *Nature* 1988;332:323-327.

6. Bangham AD, Standish MM, Watkins JC. Diffusion Of Univalent Ions Across Lamellae Of Swollen Phospholipids. *Journal Of Molecular Biology* 1965;13:238-.

7. Bramwell VW, Perrie Y. Particulate delivery systems for vaccines. *Critical Reviews In Therapeutic Drug Carrier Systems* 2005;22:151.

8. Choi MJ, Kim JH, Maibach HI. Topical DNA vaccination with DNA/Lipid based complex. *Current Drug Delivery* 2006;3:37.

9. Perkins WR, Vaughan DE, Plavin SR, Daley WL, Rauch J, Lee L, Janoff AS. Streptokinase entrapment in interdigitation-fusion liposomes improves thrombolysis in an experimental rabbit model. *Thrombosis And Haemostasis* 1997;77:1174-1178.

10. Date AA, Naik B, Nagarsenker MS. Novel drug delivery systems: potential in improving topical delivery of antiacne agents. *Skin Pharmacology And Physiology* 2006;19:2.

11. Gabizon A, Shmeeda H, Horowitz AT, Zalipsky S. Tumor cell targeting of liposome-entrapped drugs with phospholipid-anchored folic acid-PEG conjugates. *Advanced Drug Delivery Reviews* 2004;56:1177-1192.

12. Ding BS, Dziubla T, Shuvaev VV, Muro S, Muzykantov VR. Advanced drug delivery systems that target the vascular endothelium. *Molecular Interventions* 2006;6:98-112.

13. Barry BW. Novel mechanisms and devices to enable successful transdermal drug delivery. *European Journal Of Pharmaceutical Sciences: Official Journal Of The European Federation For Pharmaceutical Sciences* 2001;14:101.

14. Kaur IP, Chhabra S, Aggarwal D. Role of cyclodextrins in ophthalmics. *Current Drug Delivery* 2004;1:351.

15. Torchilin VP, Klibanov AL. Immobilization Of Proteins On Liposome Surface. *Enzyme And Microbial Technology* 1981;3:297-304.

16. Fonseca C, Moreira JN, Ciudad CJ, de Lima MCP, Simoes S. Targeting of sterically stabilised pH-sensitive liposomes to human T-leukaemia cells. *European Journal Of Pharmaceutics And Biopharmaceutics* 2005;59:359-366.

17. Zalipsky S, Mullah N, Qazen M. Preparation of poly(ethylene glycol)-grafted liposomes with ligands at the extremities of polymer chains Liposomes, Pt D, 2004:50-69.

18. Volkel T, Holig P, Merdan T, Muller R, Kontermann RE. Targeting of immunoliposomes to endothelial cells using a single-chain Fv fragment directed against human endoglin (CD105). *Biochimica Et Biophysica Acta-Biomembranes* 2004;1663:158-166.

19. Park JW, Benz CC, Martin FJ. Future directions of liposome- and immunoliposome-based cancer therapeutics. *Semin Oncol* 2004;31(6) Suppl 13:196-205.

20. Nobs L, Buchegger F, Gurny R, Allemann E. Current methods for attaching targeting ligands to liposomes and nanoparticles. *Journal Of Pharmaceutical Sciences* 2004;93:1980-1992.

21. Sapra P, Allen TM. Ligand-targeted liposomal anticancer drugs. *Progress In Lipid Research* 2003;42:439-462.

22. Cattel L, Ceruti M, Dosio F. From conventional to stealth liposomes a new frontier in cancer chemotherapy. *Tumori* 2003;89:237-249.

23. Park JW, Hong K, Kirpotin DB, Colbern G, Shalaby R, Baselga J, Shao Y, Nielsen UB, Marks JD, Moore D, Papahadjopoulos D, Benz CC. Anti-HER2 Immunoliposomes: Enhanced Efficacy Attributable to Targeted Delivery. *Clin Cancer Res* 2002;8:1172-1181.

24. Park JW, Kirpotin DB, Hong K, Shalaby R, Shao Y, Nielsen UB, Marks JD, Papahadjopoulos D, Benz CC. Tumor targeting using anti-her2 immunoliposomes. *Journal Of Controlled Release* 2001;74:95-113.

25. Maruyama K, Takizawa T, Takahashi N, Tagawa T, Nagaike K, Iwatsuru M. Targeting efficiency of PEG-immunoliposome-conjugated antibodies at PEG terminals. *Advanced Drug Delivery Reviews* 1997;24:235.

26. Hansen CB, Kao GY, Moase EH, Zalipsky S, Allen TM. Attachment Of Antibodies To Sterically Stabilized Liposomes - Evaluation, Comparison And Optimization Of Coupling Procedures. *Biochimica Et Biophysica Acta-Biomembranes* 1995;1239:133-144.

27. Allen TM, Brandeis E, Hansen CB, Kao GY, Zalipsky S. A New Strategy For Attachment Of Antibodies To Sterically Stabilized Liposomes Resulting In Efficient Targeting To Cancer-Cells. *Biochimica Et Biophysica Acta-Biomembranes* 1995;1237:99-108.

28. Torchilin VP. Targeting Of Drugs And Drug Carriers Within The Cardiovascular-System. *Advanced Drug Delivery Reviews* 1995;17:75-101.

29. Torchilin VP. Immunoliposomes and PEGylated immunoliposomes: possible use for targeted delivery of imaging agents. *Immunomethods* 1994;4:244-58.

30. Muzykantov VR. Targeting of superoxide dismutase and catalase to vascular endothelium. *J Control Release* 2001;71:1-21.

31. Muro S, Muzykantov VR. Targeting of antioxidant and anti-thrombotic drugs to endothelial cell adhesion molecules. *Curr Pharm Des* 2005;11:2383-401.

32. Torchilin VP. Targeting of liposomes within cardiovascular system. *Journal Of Liposome Research* 1997;7:433-454.

33. Voinea M, Manduteanu I, Dragomir E, Capraru M, Simionescu M. Immunoliposomes directed toward VCAM-1 interact specifically with activated endothelial cells - A potential tool for specific drug delivery. *Pharmaceutical Research* 2005;22:1906-1917.

34. Lestini BJ, Sagnella SM, Xu Z, Shive MS, Richter NJ, Jayaseharan J, Case AJ, Kottke-Marchant K, Anderson JM, Marchant RE. Surface modification of liposomes for selective cell targeting in cardiovascular drug delivery. *Journal Of Controlled Release* 2002;78:235-247.

35. Association AH. Heart Disease and Stroke Statistics : 2007 Update In: Association AH, ed.: American Heart Association, Dallas, Texas, 2007.

36. Kiortsis DN, Filippatos TD, Mikhailidis DP, Elisaf MS, Liberopoulos EN. Statin-associated adverse effects beyond muscle and liver toxicity. *Atherosclerosis* 2007;195:7.

37. Siest G, Jeannesson E, Visvikis-Siest S. Enzymes and pharmacogenetics of cardiovascular drugs. *Clinica Chimica Acta* 2007;381:26.

38. Choudhury RP, Lee JM, Greaves DR. Mechanisms of disease: macrophage-derived foam cells emerging as therapeutic targets in atherosclerosis. *Nat Clin Pract Cardiovasc Med* 2005;2:309-15.

39. Kempe S, Kestler H, Lasar A, Wirth T. NF-kappaB controls the global pro-inflammatory response in endothelial cells: evidence for the regulation of a pro-atherogenic program. *Nucleic acids research* 2005;33:5308-19.

40. Canault M, Peiretti F, Kopp F, Bonardo B, Bonzi M-F, Coudeyre J-C, Alessi M-C, Juhan-Vague I, Nalbone G. The TNF alpha converting enzyme (TACE/ADAM17) is expressed in the atherosclerotic lesions of apolipoprotein E-deficient mice: Possible contribution to elevated plasma levels of soluble TNF alpha receptors. *Atherosclerosis*;In Press, Corrected Proof.

41. Hürlimann D, Enseleit F, Ruschitzka F. Rheumatoide Arthritis, Inflammation und Atherosklerose. *Herz* 2004;29:760-8.

42. Libby P. Inflammation in atherosclerosis. *Nature* 2002;420:868-874.

43. Fuster V, Corti R, Badimon JJ. The Mikamo Lecture 2002 - Therapeutic targets for the treatment of atherothrombosis in the new millennium - Clinical frontiers in atherosclerosis research. *Circulation Journal* 2002;66:783-790.

44. Viles-Gonzalez JF, Fuster V, Badimon JJ. Links between inflammation and thrombogenicity in atherosclerosis. *Current Molecular Medicine* 2006;6:489-499.

45. Venes D. Taber's Cyclopedic Medical Dictionary. Philadelphia: F.A. Davis Co, 2001.

46. Marieb EN. Human Anatomy & Physiology San Francisco: Benjamin Cummings, 2001.

47. Fuster V, Moreno PR, Fayad ZA, Corti R, Badimon JJ. Atherothrombosis and High-Risk Plaque: Part I: Evolving Concepts. *J Am Coll Cardiol* 2005;46:937-954.

48. Little WC, Constantinescu M, Applegate RJ, Kutcher MA, Burrows MT, Kahl FR, Santamore WP. Can coronary angiography predict the site of a subsequent myocardial infarction in patients with mild-to-moderate coronary artery disease? *Circulation* 1988;78(5) Pt 1:1157-66.

49. Brown BG, Gallery CA, Badger RS, Kennedy JW, Mathey D, Bolson EL, Dodge HT. Incomplete lysis of thrombus in the moderate underlying atherosclerotic lesion during intracoronary infusion of streptokinase for acute myocardial infarction: quantitative angiographic observations. *Circulation* 1986;73:653-61.

50. Ambrose JA, Tannenbaum MA, Alexopoulos D, Hjemdahl-Monsen CE, Leavy J, Weiss M, Borrico S, Gorlin R, Fuster V. Angiographic progression of coronary artery disease and the development of myocardial infarction. *J Am Coll Cardiol* 1988;12:56-62.

51. Giroud D, Li JM, Urban P, Meier B, Rutishauer W. Relation of the site of acute myocardial infarction to the most severe coronary arterial stenosis at prior angiography. *Am J Cardiol* 1992;69:729-32.

52. Stevens RJ, Douglas KMJ, Saratzis AN, Kitas GD. Inflammation and atherosclerosis in rheumatoid arthritis. *Expert Reviews in Molecular Medicine* 2005;7:1.

53. Corti R, Hutter R, Badimon JJ, Fuster V. Evolving concepts in the triad of atherosclerosis, inflammation and thrombosis. *J Thromb Thrombolysis* 2004;17:35-44.

54. Tschoepe D, Stratmann B. Plaque stability and plaque regression: new insights. *Eur Heart J Suppl* 2006;8:F34-39.

55. Mullenix PS, Andersen CA, Starnes BW. Atherosclerosis as inflammation. *Annals Of Vascular Surgery* 2005;19:130-138.

56. Croce K, Libby P. Intertwining of thrombosis and inflammation in atherosclerosis. *Curr Opin Hematol* 2007;14:55-61.

57. Libby P, Ridker PM. Inflammation and atherothrombosis from population biology and bench research to clinical practice. *J Am Coll Cardiol* 2006;48(9) Suppl:A33-46.

58. Libby P, Ridker PM, Maseri A. Inflammation and atherosclerosis. *Circulation* 2002;105:1135-1143.

59. Stary HC, Chandler AB, Dinsmore RE, Fuster V, Glagov S, Insull W, Jr., Rosenfeld ME, Schwartz CJ, Wagner WD, Wissler RW. A Definition of Advanced Types of Atherosclerotic Lesions and a Histological Classification of Atherosclerosis : A Report From the Committee on Vascular Lesions of the Council on Arteriosclerosis, American Heart Association. *Circulation* 1995;92:1355-1374.

60. Guray U, Erbay AR, Guray Y, Yilmaz MB, Boyaci AA, Sasmaz H, Korkmaz S, Kutuk E. Levels of soluble adhesion molecules in various clinical presentations of coronary atherosclerosis. *International Journal of Cardiology* 2004;96:235.

61. Goodison S, Urquidi V, Tarin D. CD44 cell adhesion molecules. *Mol Pathol* 1999;52:189-196.

62. Blankenberg S, Barbaux S, Tiret L. Adhesion molecules and atherosclerosis. *Atherosclerosis* 2003;170:191-203.

63. Meager A. Cytokine regulation of cellular adhesion molecule expression in inflammation. *Cytokine & Growth Factor Reviews* 1999;10:27-39.

64. Obrien KD, Allen MD, McDonald TO, Chait A, Harlan JM, Fishbein D, McCarty J, Ferguson M, Hudkins K, Benjamin CD, Lobb R, Alpers CE. Vascular Cell-Adhesion Molecule-1 Is Expressed In Human Coronary Atherosclerotic Plaques - Implications For The Mode Of Progression Of Advanced Coronary Atherosclerosis. *Journal Of Clinical Investigation* 1993;92:945-951.

65. Cybulsky MI, Iiyama K, Li HM, Zhu SN, Chen M, Iiyama M, Davis V, Gutierrez-Ramos JC, Connelly PW, Milstone DS. A major role for VCAM-1, but not ICAM-1, in early atherosclerosis. *Journal Of Clinical Investigation* 2001;107:1255-1262.

66. Tsouknos A, Nash GB, Rainger GE. Monocytes initiate a cycle of leukocyte recruitment when cocultured with endothelial cells. *Atherosclerosis* 2003;170:49-58.

67. Woollard KJ, Chin-Dusting J. Therapeutic targeting of p-selectin in atherosclerosis. *Inflamm Allergy Drug Targets* 2007;6:69-74.

68. Mastrobattista E, Storm G, van Bloois L, Reszka R, Bloemen PGM, Crommelin DJA, Henricks PAJ. Cellular uptake of liposomes targeted to intercellular adhesion molecule-1 (ICAM-1) on bronchial epithelial cells. *Biochimica Et Biophysica Acta-Biomembranes* 1999;1419:353-363.

69. Ehrhardt C, Kneuer C, Bakowsky U. Selectins - an emerging target for drug delivery. *Advanced Drug Delivery Reviews* 2004;56:527-549.

70. Hood E, Gonzalez M, Plaas A, Strom J, VanAuker M. Immuno-targeting of nonionic surfactant vesicles to inflammation. *International Journal of Pharmaceutics* 2007;339:222.

71. Pure E, Cuff CA. A crucial role for CD44 in inflammation. *Trends In Molecular Medicine* 2001;7:213-221.

72. Koopman G, Taher TEI, Mazzucchelli I, Keehnen RMJ, van der Voort R, Manten-Horst E, Ricevuti G, Pals ST, Das PK. CD44 isoforms, including the CD44 V3 variant, are expressed on endothelium, suggesting a role for CD44 in the immobilization of growth factors and the regulation of the local immune response. *Biochemical And Biophysical Research Communications* 1998;245:172-176.

73. Singleton PA, Bourguignon LYW. CD44v10 interaction with Rho-Kinase (ROK) activates inositol 1,4,5-triphosphate (IP3) receptor-mediated Ca2+ signaling during hyaluronan (HA)-induced endothelial cell migration. *Cell Motility And The Cytoskeleton* 2002;53:293-316.

74. Krettek A, Sukhova GK, Schonbeck U, Libby P. Enhanced expression of CD44 variants in human atheroma and abdominal aortic aneurysm - Possible role for a feedback loop in endothelial cells. *American Journal Of Pathology* 2004;165:1571-1581.

75. DeGrendele HC, Estess P, Picker LJ, Siegelman MH. CD44 and its ligand hyaluronate mediate rolling under physiologic flow: A novel lymphocyte-endothelial cell primary adhesion pathway. *Journal Of Experimental Medicine* 1996;183:1119-1130.

76. Gee K, Kryworuchko M, Kumar A. Recent advances in the regulation of CD44 expression and its role in inflammation and autoimmune diseases. *Archivum Immunologiae Et Therapiae Experimentalis* 2004;52:13-26.

77. Krettek A, Sukhova GK, Schonbeck U, Libby P. Enhanced Expression of CD44 Variants in Human Atheroma and Abdominal Aortic Aneurysm: Possible Role for a Feedback Loop in Endothelial Cells. *Am J Pathol* 2004;165:1571-1581.

78. Cuff CA, Kothapalli D, Azonobi I, Chun S, Zhang Y, Belkin R, Yeh C, Secreto A, Assoian RK, Rader DJ, Pure E. The adhesion receptor CD44 promotes atherosclerosis by mediating inflammatory cell recruitment and vascular cell activation. *J. Clin. Invest.* 2001;108:1031-1040.

79. Rapoport N, Pitt WG, Sun H, Nelson JL. Drug delivery in polymeric micelles: from in vitro to in vivo. *Journal Of Controlled Release* 2003;91:85-95.

80. Crommelin DJA, Scherphof G, Storm G. Active targeting with particulate carrier systems in the blood compartment. *Advanced Drug Delivery Reviews* 1995;17:49.

81. Lasic DD. Liposomes : from physics to applications / D.D. Lasic. Amsterdam ; New York Elsevier, 1993.

82. Antohe F, Lin L, Kao GY, Poznansky MJ, Allen TM. Transendothelial movement of liposomes in vitro mediated by cancer cells, neutrophils or histamine. *Journal Of Liposome Research* 2004;14:1-25.

83. Lasic DD. Novel applications of liposomes. *Trends In Biotechnology* 1998;16:307-321.

84. Lasic DD, Martin FJ. Stealth Liposomes. CRC Press, 1995:320.

85. Zhong H, Deng Y, Wang X, Yang B. Multivesicular liposome formulation for the sustained delivery of breviscapine. *International journal of pharmaceutics* 2005;301:15-24.

86. Allen TM, Cheng WW, Hare JI, Laginha KM. Pharmacokinetics and pharmacodynamics of lipidic nano-particles in cancer. *Anticancer Agents Med Chem* 2006;6:513-23.

87. Baillie AJ, Florence AT, Hume LR, Muirhead GT, Rogerson A. The Preparation And Properties Of Niosomes Non-Ionic Surfactant Vesicles. *Journal Of Pharmacy And Pharmacology* 1985;37:863-868.

88. Uchegbu IF, Florence AT. Nonionic Surfactant Vesicles (Niosomes) - Physical And Pharmaceutical Chemistry. *Advances In Colloid And Interface Science* 1995;58:1-55.

89. Blazek-Welsh AI, Rhodes DG. Maltodextrin-based proniosomes. *AAPS pharmSci [electronic resource]* 2001;3:E1.

90. Arunothayanun P, Turton JA, Uchegbu IF, Florence AT. Preparation and in vitro in vivo evaluation of luteinizing hormone releasing hormone (LHRH)-loaded polyhedral and spherical tubular niosomes. *Journal Of Pharmaceutical Sciences* 1999;88:34-38.

91. Rentel CO, Bouwstra JA, Naisbett B, Junginger HE. Niosomes as a novel peroral vaccine delivery system. *International Journal Of Pharmaceutics* 1999;186:161-167.

92. Desai TR, Finlay WH. Nebulization of niosomal all-trans-retinoic acid: an inexpensive alternative to conventional liposomes. *International Journal Of Pharmaceutics* 2002;241:311-317.

93. Gopinath D, Ravi D, Karwa R, Rao BR, Shashank A, Rambhau D. Pharmacokinetics of zidovudine following intravenous bolus administration of a novel niosome preparation devoid of cholesterol. *Arzneimittel-Forschung-Drug Research* 2001;51:924-930.

94. Baillie AJ, Coombs GH, Dolan TF, Laurie J. Nonionic Surfactant Vesicles, Niosomes, As A Delivery System For The Antileishmanial Drug, Sodium Stibogluconate. *Journal Of Pharmacy And Pharmacology* 1986;38:502-505.

95. Oommen E, Tiwari S, Udupa N, Ravindra K, Uma D. Niosome entrapped ß-cyclodextrin methotrexate complex as a drug delivery system. *Indian Journal of Pharmacology* 1999; 31
279-284

96. Azmin MN, Florence AT, Handjani-Vila RM, Stuart JF, Vanlerberghe G, Whittaker JS. The effect of niosomes and polysorbate 80 on the metabolism and excretion of methotrexate in the mouse. *Journal Of Microencapsulation* 1986;3:95.

97. Gude RP, Jadhav MG, Rao SGA, Jagtap AG. Effects of niosomal cisplatin and combination of the same with theophylline and with activated macrophages in murine B16F10 melanoma model. *Cancer Biotherapy & Radiopharmaceuticals* 2002;17:183.

98. Luan L-b, Zhu J-b, Yu W-p, Wei K-b. Studies on the preparation of camptothecin niosomes. *Yao Xue Xue Bao = Acta Pharmaceutica Sinica* 2002;37:59.

99. Jain S, Vyas SP. Mannosylated niosomes as carrier adjuvant system for topical immunization. *The Journal of Pharmacy and Pharmacology* 2005;57:1177-84.

100. Jain S, Singh P, Mishra V, Vyas SP. Mannosylated niosomes as adjuvant-carrier system for oral genetic immunization against Hepatitis B. *Immunology Letters* 2005;101:41.

101. Ning M, Guo Y, Pan H, Zong S, Gu Z. Preparation and characterization of EP-liposomes and Span 40-niosomes. *Die Pharmazie* 2006;61:208.

102. Jain S, Sharma RK, Vyas SP. Chitosan nanoparticles encapsulated vesicular systems for oral immunization: preparation, in-vitro and in-vivo characterization. *The Journal Of Pharmacy And Pharmacology* 2006;58:303.

103. Alsarra IA, Bosela AA, Ahmed SM, Mahrous GM. Proniosomes as a drug carrier for transdermal delivery of ketorolac. *European Journal Of Pharmaceutics And Biopharmaceutics* 2005;59:485-490.

104. Uster PS, Allen TM, Daniel BE, Mendez CJ, Newman MS, Zhu GZ. Insertion of poly(ethylene glycol) derivatized phospholipid into pre-formed liposomes results in prolonged in vivo circulation time. *Febs Letters* 1996;386:243-246.

105. Bendas G, Krause A, Bakowsky U, Vogel J, Rothe U. Targetability of novel immunoliposomes prepared by a new antibody conjugation technique. *International Journal Of Pharmaceutics* 1999;181:79-93.

106. Luciani A, Olivier JC, Clement O, Siauve N, Brillet PY, Bessoud B, Gazeau F, Uchegbu IF, Kahn E, Frija G, Cuenod CA. Glucose-receptor MR imaging of tumors: study in mice with PEGylated paramagnetic niosomes. *Radiology* 2004;231:135-42.

107. Bendas G, Rothe U, Scherphof GL, Kamps J. The influence of repeated injections on phan-nacokinetics and biodistribution of different types of sterically stabilized immunoliposomes. *Biochimica Et Biophysica Acta-Biomembranes* 2003;1609:63-70.

108. Dufes C, Gaillard F, Uchegbu IF, Schatzlein AG, Olivier J-C, Muller J-M. Glucose-targeted niosomes deliver vasoactive intestinal peptide (VIP) to the brain. *International Journal Of Pharmaceutics* 2004;285:77.

109. Harvey CJ, Pilcher JM, Eckersley RJ, Blomley MJK, Cosgrove DO. Advances in utrasound. *Clinical Radiology* 2002;57:157-177.

110. Dayton PA, Ferrara KW. Targeted imaging using ultrasound. *Journal Of Magnetic Resonance Imaging* 2002;16:362-377.

111. Coussios CC, Holland CK, Jakubowska L, Huang SL, MacDonald RC, Nagaraj A, McPherson DD. In vitro characterization of liposomes and Optison (R) by acoustic scattering at 3.5 MHz. *Ultrasound In Medicine And Biology* 2004;30:181-190.

112. Maruyama K, Suzuki R, Takizawa T, Utoguchi N, Negishi Y. Drug and gene delivery by "bubble liposomes" and ultrasound. *Yakugaku Zasshi* 2007;127:781-7.

113. Botnar RM, Perez AS, Witte S, Wiethoff AJ, Laredo J, Hamilton J, Quist W, Parsons EC, Vaidya A, Kolodziej A, Barrett JA, Graham PB, Weisskoff RM, Manning WJ, Johnstone MT. In vivo molecular imaging of acute and subacute thrombosis using a fibrin-binding magnetic resonance imaging contrast agent. *Circulation* 2004;109:2023-2029.

114. Spragg DD, Alford DR, Greferath R, Larsen CE, Lee K-D, Gurtner GC, Cybulsky MI, Tosi PF, Nicolau C, Gimbrone MA, Jr. Immunotargeting of liposomes to activated vascular endothelial cells: A strategy for site-selective delivery in the cardiovascular system. *PNAS* 1997;94:8795-8800.

115. Uchegbu IF, Vyas SP. Non-ionic surfactant based vesicles (niosomes) in drug delivery. *International Journal Of Pharmaceutics* 1998;172:33-70.

116. Ulbrich H, Eriksson EE, Lindbom L. Leukocyte and endothelial cell adhesion molecules as targets for therapeutic interventions in inflammatory disease. *Trends In Pharmacological Sciences* 2003;24:640-647.

117. Gianasi E, Cociancich F, Uchegbu IF, Florence AT, Duncan R. Pharmaceutical and biological characterisation of a doxorubicin-polymer conjugate (PK1) entrapped in sorbitan monostearate Span 60 niosomes. *International Journal Of Pharmaceutics* 1997;148:139-148.

118. Gopinath D, Ravi D, Rao BR, Apte SS, Rambhau D. 1-O-alkylglycerol vesicles (Algosomes): their formation and characterization. *International Journal Of Pharmaceutics* 2002;246:187-197.

119. Naresh RAR, Udupa N. Niosome encapsulated bleomycin. *Stp Pharma Sciences* 1996;6:61-71.

120. Naresh RAR, Udupa N, Devi PU. Niosomal plumbagin with reduced toxicity and improved anticancer activity in BALB/C mice. *Journal Of Pharmacy And Pharmacology* 1996;48:1128-1132.

121. Uchegbu IF, Double JA, Kelland LR, Turton JA, Florence AT. The activity of doxorubicin niosomes against an ovarian cancer cell line and three in vivo mouse tumour models. *Journal Of Drug Targeting* 1996;3:399-409.

122. Parthasarathi G, Udupa N, Umadevi P, Pillai GK. Niosome encapsulated of vincristine sulfate: improved anticancer activity with reduced toxicity in mice. *Journal of drug targeting* 1994;2:173-82.

123. Gaikwad SY, Jagtap AG, Ingle AD, Ra SG, Gude RP. Antimetastatic efficacy of niosomal pentoxifylline and its combination with activated macrophages in murine B16F10 melanoma model. *Cancer Biotherapy & Radiopharmaceuticals* 2000;15:605.

124. Dimmock JR, Vashishtha SC, Patil SA, Udupa N, Dinesh SB, Devi PU, Kamath R. Cytotoxic and anticancer activities of some 1-aryl-2-dimethylaminomethyl-2-propen-1-one hydrochlorides. *Die Pharmazie* 1998;53:702.

125. Parthasarathi G, Udupa N, Parameshwaraiah N, Pillai GK. Altered biological distribution and decreased neuromuscular toxicity of niosome encapsulated vincristine. *Indian Journal Of Experimental Biology* 1996;34:124.

126. Kerr DJ, Rogerson A, Morrison GJ, Florence AT, Kaye SB. Antitumour activity and pharmacokinetics of niosome encapsulated adriamycin in monolayer, spheroid and xenograft. *British Journal Of Cancer* 1988;58:432.

127. Lezama-Davila CM. Vaccination of C57BL/10 mice against cutaneous leishmaniasis. Use of purified gp63 encapsulated into niosomes surfactants vesicles: a novel approach. *Memorias Do Instituto Oswaldo Cruz* 1999;94:67.

128. Gupta PN, Mishra V, Rawat A, Dubey P, Mahor S, Jain S, Chatterji DP, Vyas SP. Non-invasive vaccine delivery in transfersomes, niosomes and liposomes: a comparative study. *International Journal Of Pharmaceutics* 2005;293:73.

129. Vyas SP, Singh RP, Jain S, Mishra V, Mahor S, Singh P, Gupta PN, Rawat A, Dubey P. Non-ionic surfactant based vesicles (niosomes) for non-invasive topical genetic immunization against hepatitis B. *International Journal of Pharmaceutics* 2005;296:80.

130. Yoshioka T, Skalko N, Gursel M, Gregoriadis G, Florence AT. A non-ionic surfactant vesicle-in-water-in-oil (v/w/o) system: potential uses in drug and vaccine delivery. *Journal of drug targeting* 1995;2:533-9.

131. Brewer JM, Alexander J. The Adjuvant Activity Of Nonionic Surfactant Vesicles (Niosomes) On The Balb/C Humoral Response To Bovine Serum-Albumin. *Immunology* 1992;75:570-575.

132. Shahiwala A, Misra A. Studies in topical application of niosomally entrapped Nimesulide. *Journal Of Pharmacy And Pharmaceutical Sciences* 2002;5:220-225.

133. Agarwal R, Katare OP, Vyas SP. Preparation and in vitro evaluation of liposomal/niosomal delivery systems for antipsoriatic drug dithranol. *International Journal Of Pharmaceutics* 2001;228:43-52.

134. Fang JY, Hong CT, Chiu WT, Wang YY. Effect of liposomes and niosomes on skin permeation of enoxacin. *International Journal Of Pharmaceutics* 2001;219:61-72.

135. Choi MJ, Maibach HI. Liposomes and niosomes as topical drug delivery systems. *Skin pharmacology and physiology* 2005;18:209-19.

136. Yoshioka T, Sternberg B, Florence AT. Preparation And Properties Of Vesicles (Niosomes) Of Sorbitan Monoesters (Span-20, Span-40, Span-60 And Span-80) And A Sorbitan Triester (Span-85). *International Journal Of Pharmaceutics* 1994;105:1-6.

137. Liu T, Guo R. Preparation of a highly stable niosome and its hydrotrope-solubilization action to drugs. *Langmuir* 2005;21:11034-9.

138. Florence AT, Arunothayanun P, Kiri S, Bernard MS, Uchegbu IF. Some rheological properties of nonionic surfactant vesicles and the determination of surface hydration. *Journal Of Physical Chemistry B* 1999;103:1995-2000.

139. Bendas G. Immunoliposomes - A promising approach to targeting cancer therapy. *Biodrugs* 2001;15:215-224.

140. van Royen N, Voskuil M, Hoefer I, Jost M, de Graaf S, Hedwig F, Andert JP, Wormhoudt TAM, Hua J, Hartmann S, Bode C, Buschmann I, Schaper W, van der Neut R, Piek JJ, Pals ST. CD44 Regulates Arteriogenesis in Mice and Is Differentially Expressed in Patients With Poor and Good Collateralization. *Circulation* 2004;109:1647-1652.

141. Chono S, Tauchi Y, Deguchi Y, Morimoto K. Efficient drug delivery to atherosclerotic lesions and the antiatherosclerotic effect by dexamethasone incorporated into liposomes in atherogenic mice. *Journal of drug targeting* 2005;13:267-76.

142. Hood E, Leekumjorn S, Bhethanbotla V, VanAuker MD. Entrapment Efficiency and Membrane Permeability of Non Ionic Surfactant Vesicles. AIChE 2003 Annual Meeting. San Francisco, CA: AIChE, 2003.

143. Bouwstra JA, vanHal DA, Hofland HEJ, Junginger HE. Preparation and characterization of nonionic surfactant vesicles. *Colloids And Surfaces A-Physicochemical And Engineering Aspects* 1997;123:71-80.

144. Israelachvili JN. Intermolecular and surface forces : with applications to colloidal and biological systems. London ; Orlando.: Academic Press, 1985.

145. Bioscience A. Gel Filtration: Amersham Bioscience, GE Healthcare.

146. Christofidou-Solomidou M, Scherpereel A, Wiewrodt R, Ng K, Sweitzer T, Arguiri E, Shuvaev V, Solomides CC, Albelda SM, Muzykantov VR. PECAM-directed delivery of catalase to endothelium protects against pulmonary vascular oxidative stress. *American Journal Of Physiology-Lung Cellular And Molecular Physiology* 2003;285:L283-L292.

147. Otsubo T, Maruyama K, Maesaki S, Miyazaki Y, Tanaka E, Takizawa T, Moribe K, Tomono K, Tashiro T, Kohno S. Long-circulating immunoliposomal amphotericin B against invasive pulmonary aspergillosis in mice. *Antimicrobial Agents And Chemotherapy* 1998;42:40-44.

148. Muro S, Muzykantov VR. Targeting of antioxidant and anti-thrombotic drugs to endothelial cell adhesion molecules. *Current Pharmaceutical Design* 2005;11:2383-2401.

149. Murciano JC, Muro S, Koniaris L, Christofidou-Solomiclou M, Harshaw DW, Albelda SM, Granger DN, Cines DB, Muzykantov VR. ICAM-directed vascular immunotargeting of antithrombotic agents to the endothelial luminal surface. *Blood* 2003;101:3977-3984.

150. Massou S, Albigot R, Prats M. Carboxyfluorescein fluorescence experiments. *Biochemical Education* 2000;28:171-173.

151. Hollas JM. Modern Spectroscopy. Chichester, UK: John Wiley & Sons, 2004:451.

152. Ng KY, Liu Y. Therapeutic ultrasound: Its application in drug delivery. *Medicinal Research Reviews* 2002;22:204-223.

153. Lin HY, Thomas JL. PEG-Lipids and oligo(ethylene glycol) surfactants enhance the ultrasonic permeabilizability of liposomes. *Langmuir* 2003;19:1098-1105.

154. Arunothayanun P, Bernard MS, Craig DQM, Uchegbu IF, Florence AT. The effect of processing variables on the physical characteristics of non-ionic surfactant vesicles (niosomes) formed from a hexadecyl diglycerol ether. *International Journal Of Pharmaceutics* 2000;201:7-14.

155. Uchegbu IF. Synthetic Surfactant Vesicles: Niosomes and Other Non-Phospholipid Vesicular Systems. Amsterdam: Harwood Academic Publishers, 2000:248.

156. Manosroi A, Wongtrakul P, Manosroi J, Midorikawa U, Hanyu Y, Yuasa M, Sugawara F, Sakai H, Abe A. The entrapment of kojic oleate in bilayer vesicles. *International Journal Of Pharmaceutics* 2005;298:13-25.

157. Allen TM, Agrawal AK, I. A, C.B. H, S. Z. Antibody-mediated targeting of long-circulating (Stealth®) liposomes. *Journal of Liposome Research* 1994;4:1-25.

158. Chiu GNC, Bally MB, Mayer LD. Targeting of antibody conjugated, phosphatidylserine-containing liposomes to vascular cell adhesion molecule 1 for controlled thrombogenesis. *Biochimica et Biophysica Acta (BBA) - Biomembranes* 2003;1613:115.

159. VanAuker MD, Plaas A, Hood E. Immunotargeting of non ionic surfactant vesicles, 2006.

160. Moghimi SM, Hunter AC, Murray JC. Nanomedicine: current status and future prospects. *Faseb Journal* 2005;19:311-330.

161. Harasym TO, Bally MB, Tardi P. Clearance properties of liposomes involving conjugated proteins for targeting. *Advanced Drug Delivery Reviews* 1998;32:99.

162. Muro S, Gajewski C, Koval M, Muzykantov VR. ICAM-1 recycling in endothelial cells: a novel pathway for sustained intracellular delivery and prolonged effects of drugs. *Blood* 2005;105:650-658.

163. Muro S, Dziubla T, Qiu WN, Leferovich J, Cui X, Berk E, Muzykantov VR. Endothelial targeting of high-affinity multivalent polymer nanocarriers directed to intercellular adhesion molecule 1. *Journal Of Pharmacology And Experimental Therapeutics* 2006;317:1161-1169.

164. Muro S, Schuchman EH, Muzykantov VR. Lysosomal enzyme delivery by ICAM-1-targeted nanocarriers bypassing glycosylation- and clathrin-dependent endocytosis. *Molecular Therapy* 2006;13:135-141.

165. Trapani G, Altomare C, Franco M, Latrofa A, Liso G. Determination Of Hydrophile-Lipophile Balance Of Some Polyethoxylated Nonionic Surfactants By Reversed-Phase Thin-Layer Chromatography. *International Journal Of Pharmaceutics* 1995;116:95-99.

166. Lawrence MJ, Lawrence SM, Chauhan S, Barlow DJ. Synthesis and aggregation properties of dialkyl polyoxyethylene glycerol ethers. *Chemistry And Physics Of Lipids* 1996;82:89-100.

167. Conn PM. Cell culture San Diego Academic Press, 1990:424

168. Doyle A, Griffiths JB. Cell and tissue culture for medical research [electronic resource] Chichester, UK; New York, NY: Wiley, 2000.

169. Mather JP, Roberts PE. Introduction to Cell and Tissue Culture : Theory and Technique: Plenum Press, 1998.

170. Tiukinhoy SD, Khan AA, Huang SL, Klegerman ME, MacDonald RC, McPherson DD. Novel echogenic drug-immunoliposomes for drug delivery. *Investigative Radiology* 2004;39:104-110.

171. Schiffelers RM, Molema G, ten Hagen TLM, Janssen A, Schraa AJ, Kok RJ, Koning GA, Storm G. Ligand-targeted liposomes directed against pathological vasculature. *Journal Of Liposome Research* 2002;12:129-135.

172. Klibanov AL, Maruyama K, Beckerleg AM, Torchilin VP, Huang L. Activity Of Amphipathic Poly(Ethylene Glycol)-5000 To Prolong The Circulation Time Of Liposomes Depends On The Liposome Size And Is Unfavorable For Immunoliposome Binding To Target. *Biochimica Et Biophysica Acta* 1991;1062:142-148.

173. Litzinger DC, Buiting AMJ, van Rooijen N, Huang L. Effect of liposome size on the circulation time and intraorgan distribution of amphipathic poly(ethylene glycol)-containing liposomes. *Biochimica et Biophysica Acta (BBA) - Biomembranes* 1994;1190:99.

174. Hajibagheri MA. Electron Microscopy Methods and Protocols: Humana Press 1999.

175. Sartor M. Dynamic Light Scattering: to determine the radius of small beads in Browniam motion in a solution. San Diego: University of California, 2002:21.

176. Morrison ID, Ross S. Colloidal Dispersions: Suspensions, Emulsions, and Foams. John Wiley and Sons, Inc, 2002.

177. Cosgrove T. Colliod Science: Principles, methods and applications: Blackwell PUblishing Ltd., 2005:288.

178. Zetasizer nano series user manual: Malvern Instruments 2003.

179. Namdeo A, Jain NK. Niosomal delivery of 5-fluorouracil. *Journal Of Microencapsulation* 1999;16:731-740.

180. Lu B, Zhang JQ, Yang H. Nonphospholipid Vesicles of Carboplatin for Lung Targeting
Drug Delivery 2003;10: 87 - 94

181. Johnson RA. Miller & Freund's Probability & Statistics for Engineers. Englewood Cliffs, NJ: Prentice Hall, Inc, 1994.

182. Holliger P, Hudson PJ. Engineered antibody fragments and the rise of single domains. *Nature Biotechnology* 2005;23:1126-1136.

183. Cullis PR, Mayer LD, Bally MB, Madden TD, Hope MJ. Generating and loading of liposomal systems for drug-delivery applications. *Advanced Drug Delivery Reviews* 1989;3:267.

184. vanHal DA, Bouwstra JA, vanRensen A, Jeremiasse E, deVringer T, Junginger HE. Preparation and characterization of nonionic surfactant vesicles. *Journal Of Colloid And Interface Science* 1996;178:263-273.

185. Plump AS, Smith JD, Hayek T, Aaltosetala K, Walsh A, Verstuyft JG, Rubin EM, Breslow JL. Severe Hypercholesterolemia And Atherosclerosis In Apolipoprotein-E-Deficient Mice Created By Homologous Recombination In Es Cells. *Cell* 1992;71:343-353.

Appendices

Appendix A. Particle Sizing Systems Data and Software Output

The images below are Particle Sizing Systems Accusizer software output from a 3 size polystyrene latex standard for size and count calibration of instrument. The axes scales can be set, and the y axis can display units of number of particles counted (# Part.) or numbers of particles counted per ml of sample injected for analysis (# Part./ml as shown). For a given injection volume the cumulative number of counts can be found in the volume fraction calculation menu in the display menu. To obtain the number of particles per ml divide the calculated number of particles listed in the volume fraction calculation by sample volume injected. For example in the sample below 0.025 ml was injected. The calculated # is 147011. The total number per ml is 5.88 x 10^6 particles per ml.

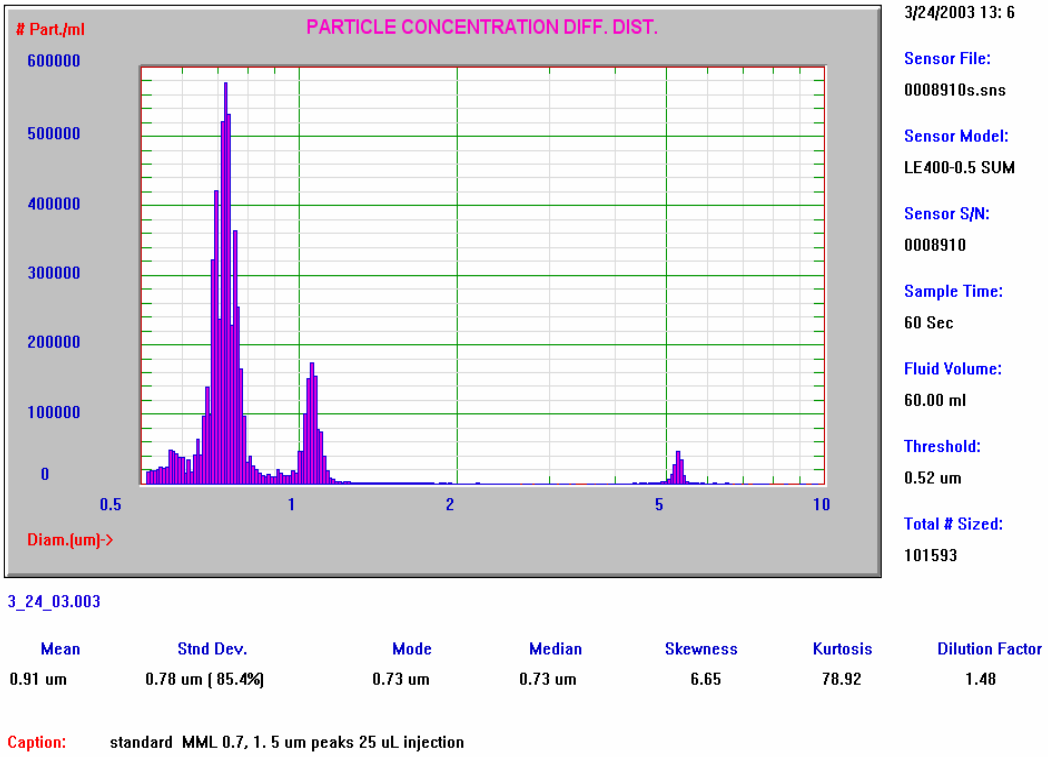

Figure A.1 Particle Size Distribution of Standards

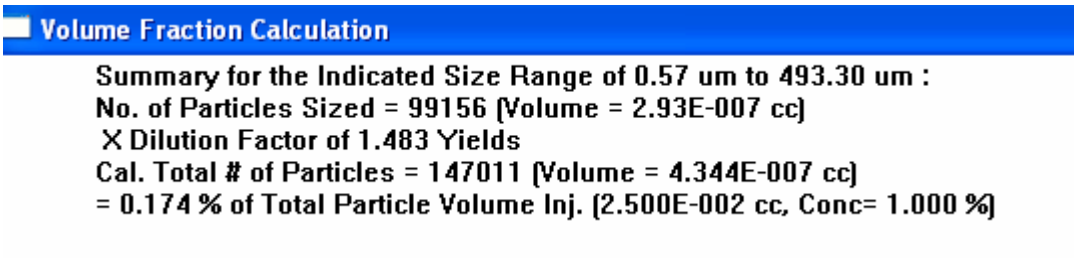

Figure A.2 Sample Number Calculation

:

Table A.1 Data Exported From PSD ASCII File

Particle Sizing Systems, Inc.
Santa Barbara, Calif.,
USA
Model 780 AccuSizer
Caption: standard MML 0.7, 1. 5 um peaks 25 uL injection
File Name = 3_24_03.003
Sensor Model: LE400-0.5 SUM S/N: 8910 Cal. File: 0008910s.sns
Elapsed Time of Data Collection = 60 Sec.
Background File = NONE
Total # Part. Sized (>=Thres. 0.52 um) = 101593
Calculated Total No. of Particles in Sample = 150625
Dilution Factor = 1.48
Fluid Volume Sampled = 60 ml No. of Channels = 512
NUM-WT Mean = 0.91 um Mode = 0.73 um Median = 0.73
VOL-WT Mean = 7.93 um Mode = 5.34 um Median = 5.32

Summary of Detailed Distribution, Weightings

Diameter (microns)	# Part. Sized	Cum Num >=Diam.	Num %	Vol %	Cum Num % >=Diam.	Vol Num % >=Diam.
0.52418	288	101593	0.283	0.007	100	100
0.5313	328	101305	0.323	0.009	99.717	99.993
0.53851	312	100977	0.307	0.009	99.394	99.984

Appendix A. (Continued)

0.55324	400	100313	0.394	0.012	98.74	99.965
0.56076	368	99913	0.362	0.012	98.346	99.953
0.56837	389	99545	0.383	0.013	97.984	99.941
0.57609	818	99156	0.805	0.028	97.601	99.928
0.58392	799	98338	0.786	0.028	96.796	99.901
0.59185	715	97539	0.704	0.026	96.01	99.872
0.59989	643	96824	0.633	0.025	95.306	99.846
0.60804	631	96181	0.621	0.025	94.673	99.821
0.6163	265	95550	0.261	0.011	94.052	99.796
0.62467	571	95285	0.562	0.025	93.791	99.784
0.63315	285	94714	0.281	0.013	93.229	99.76
0.64175	701	94429	0.69	0.033	92.948	99.747
0.65047	1084	93728	1.067	0.053	92.258	99.714
0.65931	709	92644	0.698	0.036	91.191	99.66
0.66826	1647	91935	1.621	0.088	90.493	99.624
0.67734	2336	90288	2.299	0.13	88.872	99.536
0.68654	1655	87952	1.629	0.096	86.573	99.407
0.69586	5436	86297	5.351	0.327	84.944	99.311
0.70532	7096	80861	6.985	0.445	79.593	98.984
0.7149	3987	73765	3.924	0.26	72.608	98.539
0.72461	8772	69778	8.634	0.596	68.684	98.279
0.73445	9730	61006	9.577	0.688	60.049	97.683
0.74443	8951	51276	8.811	0.659	50.472	96.995
0.75454	3857	42325	3.797	0.296	41.661	96.336
0.76479	6126	38468	6.03	0.489	37.865	96.04
0.77517	4295	32342	4.228	0.357	31.835	95.55
0.7857	2792	28047	2.748	0.242	27.607	95.193
0.79638	1624	25255	1.599	0.146	24.859	94.951
0.80719	509	23631	0.501	0.048	23.26	94.805
0.81816	680	23122	0.669	0.066	22.759	94.757
0.82927	447	22442	0.44	0.046	22.09	94.691
0.84054	331	21995	0.326	0.035	21.65	94.645
0.85195	250	21664	0.246	0.028	21.324	94.61
0.86352	202	21414	0.199	0.023	21.078	94.582
0.87525	181	21212	0.178	0.022	20.879	94.559
0.88714	225	21031	0.221	0.028	20.701	94.538
0.89919	180	20806	0.177	0.023	20.48	94.51
0.91141	181	20626	0.178	0.024	20.303	94.486
0.92379	354	20445	0.348	0.05	20.124	94.462
0.93633	267	20091	0.263	0.039	19.776	94.412
0.94905	197	19824	0.194	0.03	19.513	94.373
0.96194	190	19627	0.187	0.03	19.319	94.343
0.97501	196	19437	0.193	0.032	19.132	94.312
0.98825	313	19241	0.308	0.054	18.939	94.28
1.00168	254	18928	0.25	0.046	18.631	94.226
1.01528	794	18674	0.782	0.148	18.381	94.18
1.02907	784	17880	0.772	0.153	17.6	94.032
1.04305	1684	17096	1.658	0.341	16.828	93.88
1.05722	2565	15412	2.525	0.541	15.17	93.538
1.07158	2938	12847	2.892	0.646	12.646	92.997
1.08614	2610	9909	2.569	0.597	9.754	92.352
1.10089	1310	7299	1.289	0.312	7.185	91.754
1.11584	1259	5989	1.239	0.312	5.895	91.442

Appendix A. (Continued)

1.131	670	4730	0.659	0.173	4.656	91.13
1.14636	328	4060	0.323	0.088	3.996	90.957
1.16193	134	3732	0.132	0.038	3.673	90.869
1.17772	106	3598	0.104	0.031	3.542	90.831
1.19371	60	3492	0.059	0.018	3.437	90.8
1.20993	47	3432	0.046	0.015	3.378	90.782
1.22636	31	3385	0.031	0.01	3.332	90.767
1.24302	39	3354	0.038	0.013	3.301	90.757
1.2599	37	3315	0.036	0.013	3.263	90.744
1.27702	22	3278	0.022	0.008	3.227	90.73
1.29436	17	3256	0.017	0.007	3.205	90.722
1.31194	34	3239	0.033	0.014	3.188	90.716
1.32976	32	3205	0.031	0.013	3.155	90.702
1.34783	19	3173	0.019	0.008	3.123	90.688
1.36613	28	3154	0.028	0.013	3.105	90.68
1.38469	23	3126	0.023	0.011	3.077	90.667
1.4035	14	3103	0.014	0.007	3.054	90.656
1.42256	22	3089	0.022	0.011	3.041	90.65
1.44189	13	3067	0.013	0.007	3.019	90.638
1.46147	13	3054	0.013	0.007	3.006	90.631
1.48132	14	3041	0.014	0.008	2.993	90.624
1.50144	10	3027	0.01	0.006	2.98	90.616
1.52184	15	3017	0.015	0.009	2.97	90.61
1.54251	8	3002	0.008	0.005	2.955	90.6
1.56346	11	2994	0.011	0.008	2.947	90.595
1.5847	14	2983	0.014	0.01	2.936	90.588
1.60622	16	2969	0.016	0.012	2.922	90.578
1.62804	6	2953	0.006	0.005	2.907	90.566
1.65015	7	2947	0.007	0.006	2.901	90.561
1.67257	10	2940	0.01	0.008	2.894	90.556
1.69529	14	2930	0.014	0.012	2.884	90.547
1.71832	6	2916	0.006	0.005	2.87	90.535
1.74166	9	2910	0.009	0.008	2.864	90.53
1.76531	9	2901	0.009	0.009	2.855	90.521
1.78929	13	2892	0.013	0.013	2.847	90.512
1.81359	8	2879	0.008	0.009	2.834	90.499
1.83823	3	2871	0.003	0.003	2.826	90.491
1.8632	5	2868	0.005	0.006	2.823	90.487
1.88851	7	2863	0.007	0.008	2.818	90.481
1.91416	6	2856	0.006	0.008	2.811	90.473
1.94016	3	2850	0.003	0.004	2.805	90.465
1.96651	10	2847	0.01	0.014	2.802	90.462
1.99322	5	2837	0.005	0.007	2.793	90.448
2.0203	1	2832	0.001	0.001	2.788	90.441
2.04774	3	2831	0.003	0.005	2.787	90.439
2.07555	3	2828	0.003	0.005	2.784	90.435
2.10375	3	2825	0.003	0.005	2.781	90.43
2.13232	3	2822	0.003	0.005	2.778	90.425
2.16129	3	2819	0.003	0.005	2.775	90.42
2.19064	3	2816	0.003	0.006	2.772	90.414
2.2204	9	2813	0.009	0.018	2.769	90.409
2.25056	4	2804	0.004	0.008	2.76	90.391
2.28113	4	2800	0.004	0.008	2.756	90.383
2.31211	4	2796	0.004	0.009	2.752	90.375

Appendix A. (Continued)

2.34352	3	2792	0.003	0.007	2.748	90.366
2.37535	4	2789	0.004	0.01	2.745	90.359
2.40762	1	2785	0.001	0.002	2.741	90.349
2.44032	3	2784	0.003	0.008	2.74	90.347
2.47347	4	2781	0.004	0.011	2.737	90.339
2.50706	3	2777	0.003	0.008	2.733	90.328
2.54112	2	2774	0.002	0.006	2.73	90.32
2.57563	2	2772	0.002	0.006	2.729	90.314
2.61062	3	2770	0.003	0.01	2.727	90.308
2.64608	3	2767	0.003	0.01	2.724	90.298
2.68202	0	2764	0	0	2.721	90.288
2.71845	3	2764	0.003	0.011	2.721	90.288
2.75538	2	2761	0.002	0.007	2.718	90.278
2.7928	2	2759	0.002	0.008	2.716	90.27
2.83074	0	2757	0	0	2.714	90.262
2.86919	4	2757	0.004	0.017	2.714	90.262
2.90816	1	2753	0.001	0.004	2.71	90.245
2.94766	3	2752	0.003	0.014	2.709	90.241
2.9877	3	2749	0.003	0.014	2.706	90.227
3.02828	5	2746	0.005	0.025	2.703	90.213
3.06942	1	2741	0.001	0.005	2.698	90.188
3.11111	3	2740	0.003	0.016	2.697	90.183
3.15337	0	2737	0	0	2.694	90.167
3.1962	2	2737	0.002	0.012	2.694	90.167
3.23961	1	2735	0.001	0.006	2.692	90.155
3.28362	1	2734	0.001	0.006	2.691	90.149
3.32822	0	2733	0	0	2.69	90.143
3.37343	3	2733	0.003	0.021	2.69	90.143
3.41925	0	2730	0	0	2.687	90.122
3.46569	0	2730	0	0	2.687	90.122
3.51277	0	2730	0	0	2.687	90.122
3.56048	0	2730	0	0	2.687	90.122
3.60885	1	2730	0.001	0.008	2.687	90.122
3.65787	2	2729	0.002	0.017	2.686	90.114
3.70755	0	2727	0	0	2.684	90.097
3.75791	1	2727	0.001	0.009	2.684	90.097
3.80896	1	2726	0.001	0.01	2.683	90.087
3.86069	3	2725	0.003	0.031	2.682	90.077
3.91313	0	2722	0	0	2.679	90.046
3.96629	2	2722	0.002	0.022	2.679	90.046
4.02016	5	2720	0.005	0.058	2.677	90.024
4.07477	3	2715	0.003	0.036	2.672	89.966
4.13012	2	2712	0.002	0.025	2.669	89.93
4.18622	2	2710	0.002	0.026	2.667	89.905
4.24308	1	2708	0.001	0.014	2.666	89.878
4.30071	4	2707	0.004	0.057	2.665	89.865
4.35913	2	2703	0.002	0.03	2.661	89.808
4.41834	6	2701	0.006	0.092	2.659	89.778
4.47835	1	2695	0.001	0.016	2.653	89.686
4.53918	6	2694	0.006	0.1	2.652	89.67
4.60084	6	2688	0.006	0.104	2.646	89.57
4.66333	4	2682	0.004	0.072	2.64	89.465
4.72668	8	2678	0.008	0.151	2.636	89.393
4.79088	26	2670	0.026	0.511	2.628	89.242

Appendix A. (Continued)

4.85595	25	2644	0.025	0.511	2.603	88.732
4.92191	21	2619	0.021	0.447	2.578	88.22
4.98877	39	2598	0.038	0.865	2.557	87.773
5.05653	58	2559	0.057	1.339	2.519	86.909
5.12522	104	2501	0.102	2.5	2.462	85.57
5.19483	222	2397	0.219	5.557	2.359	83.07
5.26539	468	2175	0.461	12.199	2.141	77.512
5.33691	772	1707	0.76	20.955	1.68	65.313
5.40941	567	935	0.558	16.026	0.92	44.359
5.48288	206	368	0.203	6.063	0.362	28.333
5.55736	47	162	0.046	1.44	0.159	22.27
5.63284	19	115	0.019	0.606	0.113	20.83
5.70936	9	96	0.009	0.299	0.094	20.223
5.78691	8	87	0.008	0.277	0.086	19.924
5.86551	2	79	0.002	0.072	0.078	19.647
5.94518	7	77	0.007	0.263	0.076	19.575
6.02594	4	70	0.004	0.156	0.069	19.313
6.10779	3	66	0.003	0.122	0.065	19.156
6.19075	2	63	0.002	0.085	0.062	19.034
6.27484	8	61	0.008	0.353	0.06	18.95
6.36007	1	53	0.001	0.046	0.052	18.597
6.44646	2	52	0.002	0.096	0.051	18.551
6.53403	3	50	0.003	0.149	0.049	18.455
6.62278	6	47	0.006	0.311	0.046	18.306
6.71274	3	41	0.003	0.162	0.04	17.994
6.80392	0	38	0	0	0.037	17.832
6.89634	1	38	0.001	0.059	0.037	17.832
6.99001	1	37	0.001	0.061	0.036	17.774
7.08496	0	36	0	0	0.035	17.713
7.18119	1	36	0.001	0.066	0.035	17.713
7.27873	0	35	0	0	0.034	17.647
7.3776	0	35	0	0	0.034	17.647
7.47781	2	35	0.002	0.149	0.034	17.647
7.57939	3	33	0.003	0.233	0.032	17.497
7.68234	4	30	0.004	0.324	0.03	17.264
7.78669	2	26	0.002	0.169	0.026	16.94
7.89246	4	24	0.004	0.351	0.024	16.772
7.99966	0	20	0	0	0.02	16.42
8.10832	0	20	0	0	0.02	16.42
8.21846	0	20	0	0	0.02	16.42
8.33009	0	20	0	0	0.02	16.42
8.44324	0	20	0	0	0.02	16.42
8.55792	1	20	0.001	0.112	0.02	16.42
8.67417	0	19	0	0	0.019	16.309
8.79199	0	19	0	0	0.019	16.309
8.91141	0	19	0	0	0.019	16.309
9.03246	0	19	0	0	0.019	16.309
9.15515	2	19	0.002	0.274	0.019	16.309
9.2795	1	17	0.001	0.143	0.017	16.034
9.40555	0	16	0	0	0.016	15.892
9.5333	0	16	0	0	0.016	15.892
9.6628	1	16	0.001	0.161	0.016	15.892
9.79405	1	15	0.001	0.168	0.015	15.731

Appendix A. (Continued)

9.92708	0	14	0	0	0.014	15.563
10.06192	0	14	0	0	0.014	15.563
10.19859	0	14	0	0	0.014	15.563
10.33712	0	14	0	0	0.014	15.563
10.47753	1	14	0.001	0.205	0.014	15.563
10.61985	0	13	0	0	0.013	15.358
10.7641	0	13	0	0	0.013	15.358
10.91031	1	13	0.001	0.232	0.013	15.358
11.05851	0	12	0	0	0.012	15.126
11.20872	0	12	0	0	0.012	15.126
11.36097	1	12	0.001	0.262	0.012	15.126
11.51528	0	11	0	0	0.011	14.864
11.6717	0	11	0	0	0.011	14.864
11.83024	0	11	0	0	0.011	14.864
11.99093	0	11	0	0	0.011	14.864
12.1538	0	11	0	0	0.011	14.864
12.31889	1	11	0.001	0.334	0.011	14.864
12.48622	0	10	0	0	0.01	14.53
12.65582	0	10	0	0	0.01	14.53
12.82773	0	10	0	0	0.01	14.53
13.00197	0	10	0	0	0.01	14.53
13.17857	1	10	0.001	0.409	0.01	14.53
13.35758	1	9	0.001	0.426	0.009	14.121
13.53902	0	8	0	0	0.008	13.696
13.72292	0	8	0	0	0.008	13.696
13.90932	0	8	0	0	0.008	13.696
14.09825	0	8	0	0	0.008	13.696
14.28975	1	8	0.001	0.521	0.008	13.696
14.48385	0	7	0	0	0.007	13.175
14.68059	0	7	0	0	0.007	13.175
14.87999	0	7	0	0	0.007	13.175
15.08211	0	7	0	0	0.007	13.175
15.28697	0	7	0	0	0.007	13.175
15.49462	0	7	0	0	0.007	13.175
15.70508	0	7	0	0	0.007	13.175
15.91841	1	7	0.001	0.72	0.007	13.175
16.13463	1	6	0.001	0.75	0.006	12.454
16.35379	0	5	0	0	0.005	11.704
16.57593	0	5	0	0	0.005	11.704
16.80108	0	5	0	0	0.005	11.704
17.02929	0	5	0	0	0.005	11.704
17.2606	0	5	0	0	0.005	11.704
17.49505	0	5	0	0	0.005	11.704
17.73269	0	5	0	0	0.005	11.704
17.97356	1	5	0.001	1.037	0.005	11.704
18.21769	0	4	0	0	0.004	10.668
18.46515	1	4	0.001	1.124	0.004	10.668
18.71596	0	3	0	0	0.003	9.543
18.97018	1	3	0.001	1.219	0.003	9.543
19.22786	0	2	0	0	0.002	8.324
19.48903	0	2	0	0	0.002	8.324
19.75375	1	2	0.001	1.376	0.002	8.324
20.02207	0	1	0	0	0.001	6.948
20.29403	0	1	0	0	0.001	6.948

Appendix A. (Continued)

20.56969	0	1	0	0	0.001	6.948
20.84909	0	1	0	0	0.001	6.948
21.13229	0	1	0	0	0.001	6.948
21.41933	0	1	0	0	0.001	6.948
21.71027	0	1	0	0	0.001	6.948
22.00517	0	1	0	0	0.001	6.948
22.30407	0	1	0	0	0.001	6.948
22.60702	0	1	0	0	0.001	6.948
22.9141	0	1	0	0	0.001	6.948
23.22534	0	1	0	0	0.001	6.948
23.54082	0	1	0	0	0.001	6.948
23.86058	0	1	0	0	0.001	6.948
24.18468	0	1	0	0	0.001	6.948
24.51318	0	1	0	0	0.001	6.948
24.84615	0	1	0	0	0.001	6.948
25.18363	0	1	0	0	0.001	6.948
25.52571	0	1	0	0	0.001	6.948
25.87242	0	1	0	0	0.001	6.948
26.22385	0	1	0	0	0.001	6.948
26.58006	0	1	0	0	0.001	6.948
26.9411	0	1	0	0	0.001	6.948
27.30704	0	1	0	0	0.001	6.948
27.67796	0	1	0	0	0.001	6.948
28.05391	0	1	0	0	0.001	6.948
28.43497	0	1	0	0	0.001	6.948
28.82121	0	1	0	0	0.001	6.948
29.21269	0	1	0	0	0.001	6.948
29.60949	0	1	0	0	0.001	6.948
30.01168	0	1	0	0	0.001	6.948
30.41933	0	1	0	0	0.001	6.948
30.83252	0	1	0	0	0.001	6.948
31.25132	0	1	0	0	0.001	6.948
31.67581	0	1	0	0	0.001	6.948
32.10607	0	1	0	0	0.001	6.948
32.54217	0	1	0	0	0.001	6.948
32.9842	0	1	0	0	0.001	6.948
33.43222	0	1	0	0	0.001	6.948
33.88634	1	1	0.001	6.948	0.001	6.948
34.34662	0	0	0	0	0	0
34.81316	0	0	0	0	0	0
35.28603	0	0	0	0	0	0
35.76532	0	0	0	0	0	0
36.25113	0	0	0	0	0	0
36.74353	0	0	0	0	0	0

Appendix B. Akta Prime Chromatography Data Output

Generated reports for each sample run show user designated data, method, run and evaluation notes.

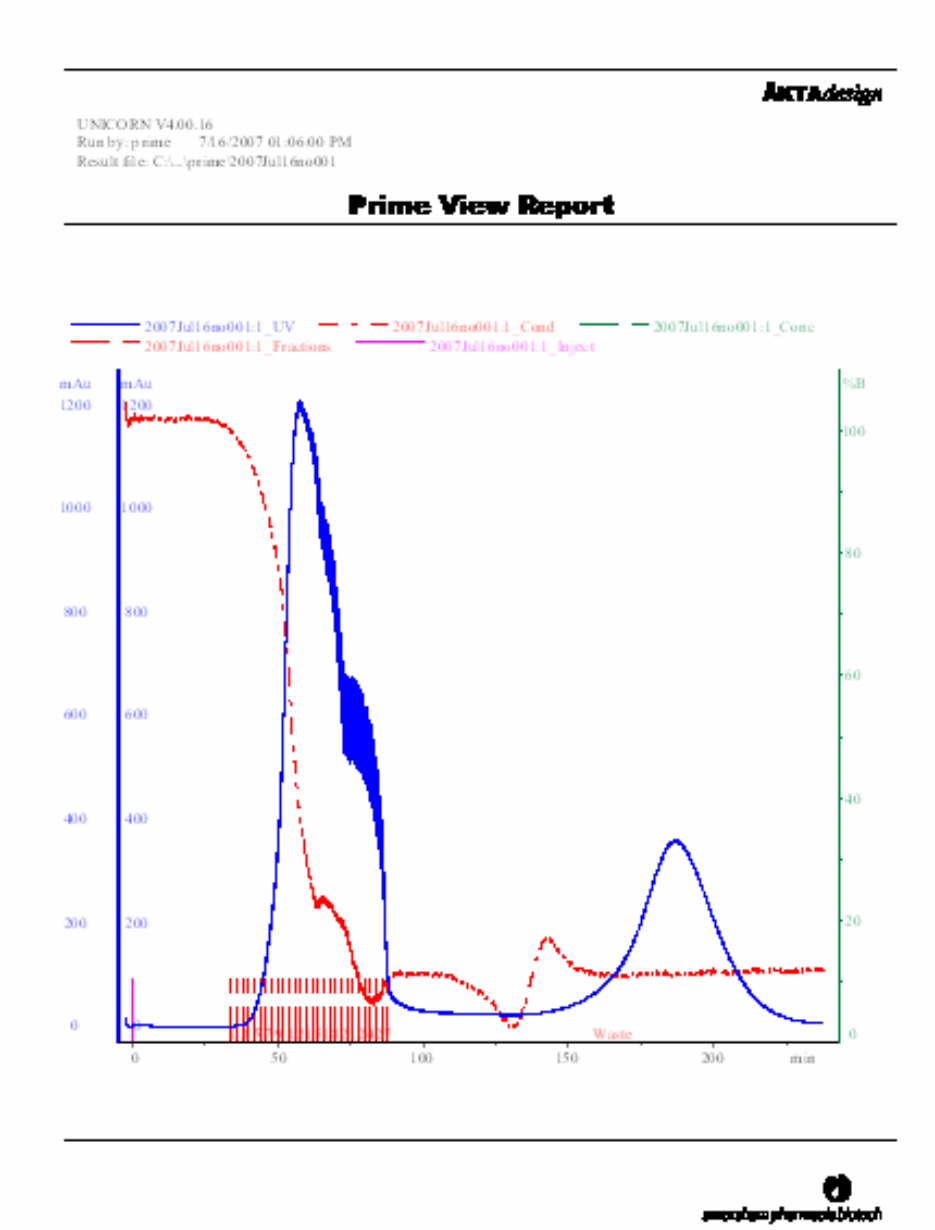

Figure B.1 Akta Prime Elution Chromatogram Showing UV Absorbance and Conductivity

Appendix B. (Continued)

UNICORN V4.00.16
Result file: C:\...\prime 2007Jul16no001

Method Notes

```
**********************************************************************
** Method Dump
**
** AKTAprime    Ver   , V2.02
**
** Dump Format Ver   , V1.00
**
**********************************************************************


*******************
** Method Settings
*******************
Method Type          ,PC Method
Method               ,9
Method base          ,ml
Frac base            ,ml
Max pressure (kPa)   ,400
Alarm (min/ml)       ,0.0

**********************
** Method Breakpoints
**********************

Brkp Volume    Conc Flow  Frac   Buff Inj     Peak    Autozero Eventmark
                                          (mAu/min)

,1   ,0.0      ,0   ,1.0  ,0.0   ,1   ,Load   ,0      ,N       ,N
,2   ,2.0      ,0   ,1.0  ,0.0   ,1   ,Inj    ,0      ,Y       ,N
,3   ,36.0     ,0   ,1.0  ,2.0   ,1   ,Inj    ,0      ,N       ,N
,4   ,90.0     ,0   ,1.0  ,0.0   ,1   ,Inj    ,0      ,N       ,N
,5   ,240.0    ,0   ,1.0  ,0.0   ,1   ,Inj    ,0      ,N       ,N
```

Run Notes

No information to print.

Evaluation Notes

No information to print.

Figure B.2 Akta Prime Method Notes

Appendix B. (Continued)

Each programmed method run created an overlay of all experimental curves generated. The data for each curve represented in the overlay can be individually exported as an ASCII file.

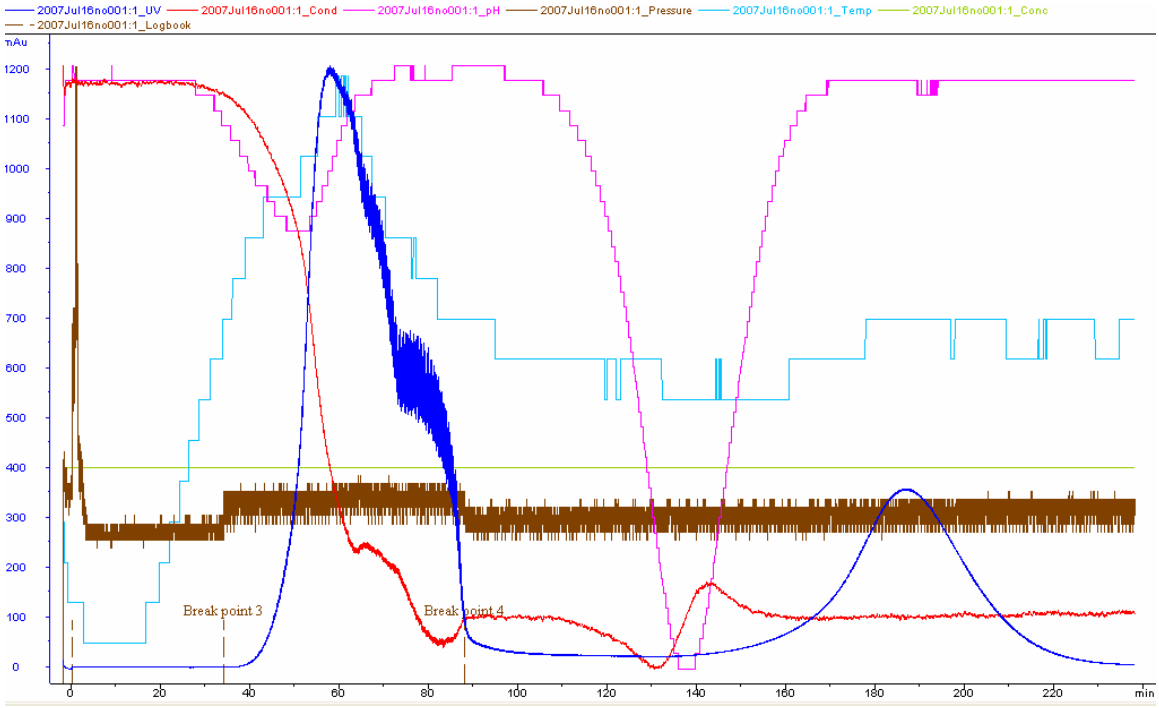

Figure B.3 Akta Prime Chromatogram Showing All Measures

Appendix C. Fluorescent Plate Reader

The BioTek Instruments fluorescent plate reader uses KC Junior software for creating an operating procedure and translating the intensity data into concentration data based on a designated calibration curve.

Below are the steps for setting up a 96 well plate and the resulting data available for export to Microsoft Excel.

C.1 Defined Protocol

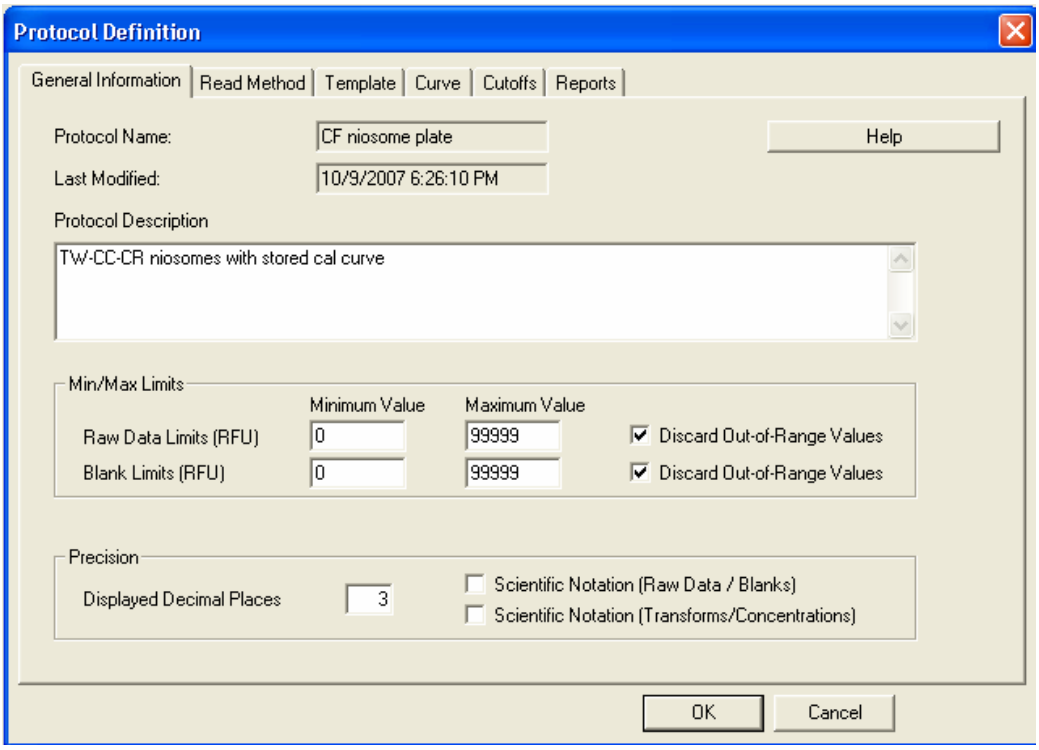

Figure C.1 Fluorescent Plate Reader: Protocol Definition

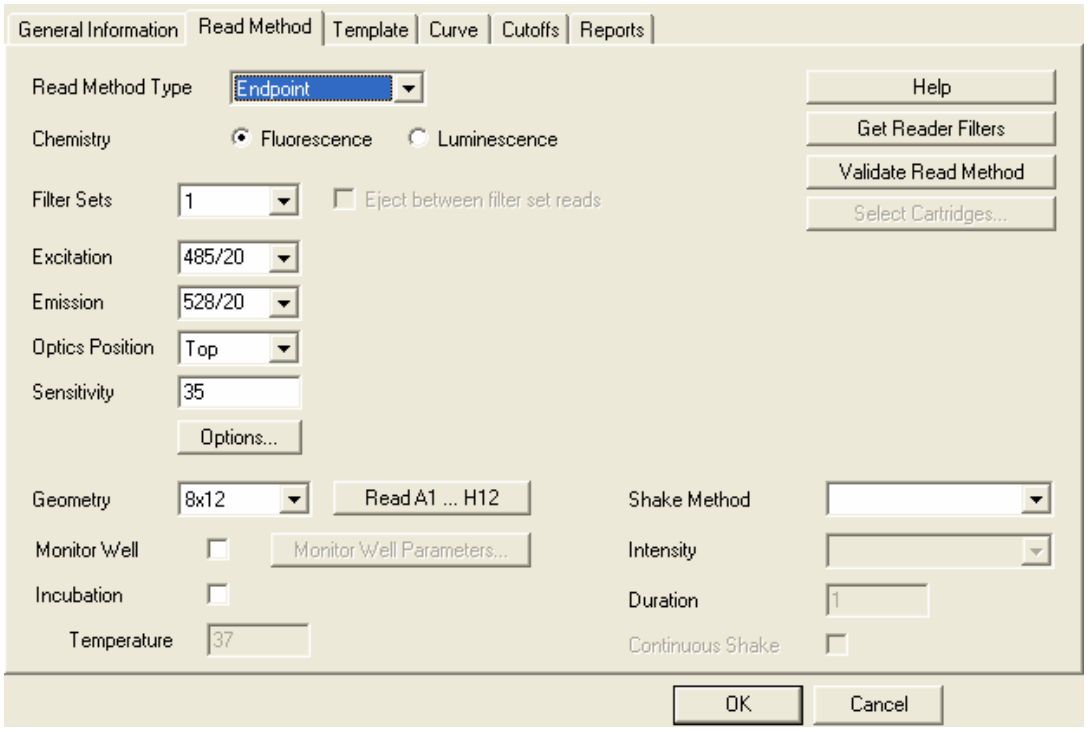

Figure C.2 Fluorescent Plate Reader: Defined Plate Reader Geometry

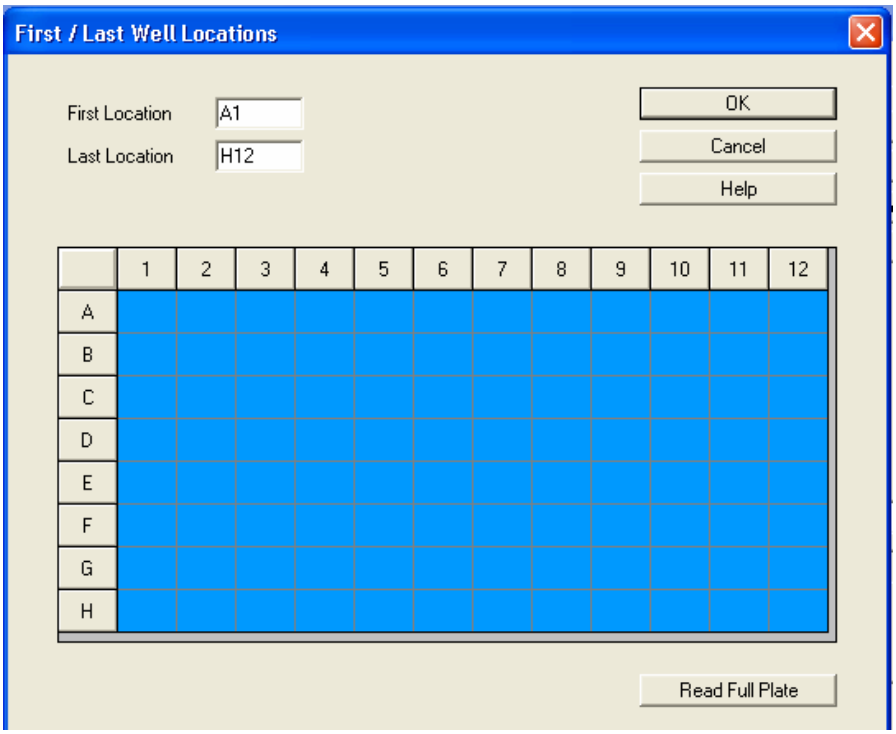

Figure C.3 Fluorescent Plate Reader: Define Individual Well Measurement Types

C.2 Stored Standard Curve Example

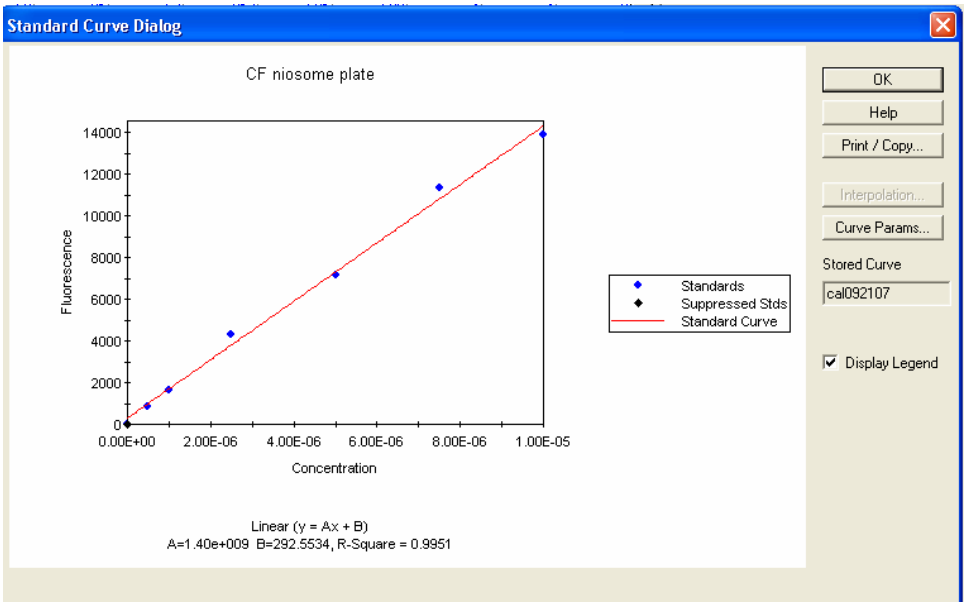

Figure C.4 Fluorescent Plate Reader: Stored Standard Curve

Measured Intensity

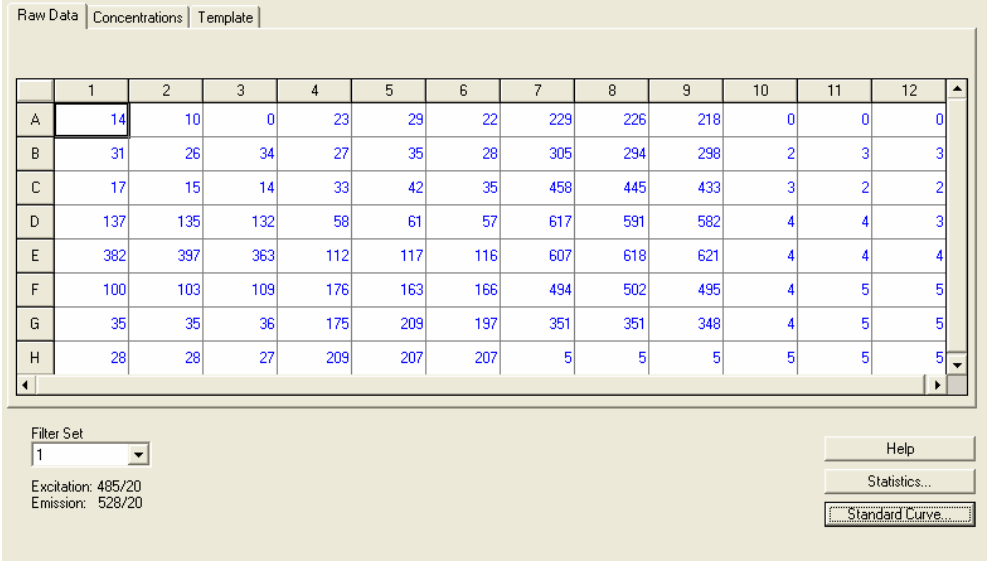

	1	2	3	4	5	6	7	8	9	10	11	12
A	14	10	0	23	29	22	229	226	218	0	0	0
B	31	26	34	27	35	28	305	294	298	2	3	3
C	17	15	14	33	42	35	458	445	433	3	2	2
D	137	135	132	58	61	57	617	591	582	4	4	3
E	382	397	363	112	117	116	607	618	621	4	4	4
F	100	103	109	176	163	166	494	502	495	4	5	5
G	35	35	36	175	209	197	351	351	348	4	5	5
H	28	28	27	209	207	207	5	5	5	5	5	5

Figure C.5 Fluorescent Plate Reader: Fluorescence Intensity by Wells

C.3 Data Exported to Excel

	A	B	C	D	E	F	G	H	I	J	K	L	M
1	Plate: break100807		Date Created: 10/8/2007 1:54:22 PM										
2													
3	Raw (1)												
4	14	10	0	23	29	22	229	226	218	0	0	0	
5	31	26	34	27	35	28	305	294	298	2	3	3	
6	17	15	14	33	42	35	458	445	433	3	2	2	
7	137	135	132	58	61	57	617	591	582	4	4	3	
8	382	397	363	112	117	116	607	618	621	4	4	4	
9	100	103	109	176	163	166	494	502	495	4	5	5	
10	35	35	36	175	209	197	351	351	348	4	5	5	
11	28	28	27	209	207	207	5	5	5	5	5	5	

Figure C.6 Fluorescent Plate Reader: Intensity Data Exported to Microsoft Excel

Appendix D. Matlab™ Image Analysis

The Matlab program which produced this example output was constructed by John Elliott, M.S. ChE while working in the Chemical Engineering Department at USF in 2006-2007. The overall process of the image analysis and the images produced was described in Section 5.2.4.3. Below is the data output from the Matlab Command Window.

These examples were run with 20x magnification images files from BAECs incubated with INs for 2 hours at 37˚C.

Command Window Output

```
caldata =

6x1 struct array with fields:
    Area
    Centroid
    BoundingBox


X_Cal =

    0.4669


handles =

          figure1: 153.0455
      pushbutton7: 7.0457
      pushbutton6: 6.0457
        listbox1: 5.0457
      pushbutton5: 4.0457
      pushbutton4: 3.0457
      pushbutton3: 2.0457
      pushbutton2: 1.0457
      pushbutton1: 0.0457
```

Appendix D. (Continued)

```
togglebutton1: 159.0455
          axes3: 154.0455
         output: 153.0455
       filename: 'W1_20x_D1.tif'
      root_file: 'C:\Program Files\MATLAB71\work\images\10-05-06\'
         banner: [1024x1360x3 uint8]
            Cal: 0.2180

h =

    1

h =

    2

celldata =

76x1 struct array with fields:
    Area
    Centroid
    BoundingBox

max_area =

       1243

cell_mean =

  104.2558

max_area2 =

   476

h =

    3

filename2 =

W1_20x_F1a.tif

root_file2 =
```

Appendix D. (Continued)

```
C:\Program Files\MATLAB71\work\images\10-05-06\

filename2 =

W1_20x_F1.tif

root_file2 =

C:\Program Files\MATLAB71\work\images\10-05-06\

h =

     4

celldata22 =

1699x1 struct array with fields:
    Area
    Centroid
    BoundingBox

handles =

          figure1: 153.0455
       pushbutton7: 7.0457
       pushbutton6: 6.0457
         listbox1: 5.0457
       pushbutton5: 4.0457
       pushbutton4: 3.0457
       pushbutton3: 2.0457
       pushbutton2: 1.0457
       pushbutton1: 0.0457
    togglebutton1: 159.0455
            axes3: 154.0455
           output: 153.0455
         filename: 'W1_20x_D1.tif'
        root_file: 'C:\Program Files\MATLAB71\work\images\10-05-06\'
           banner: [1024x1360x3 uint8]
              Cal: 0.2180
              myX: [1 1360]
              myY: [1 1024]
            sub_A: [571x571x3 uint8]
```

Appendix D. (Continued)

```
 rect_userD: [10.0968 248.8353 570.2515 570.2515]
          sub_B: [571x571 uint8]
         sub_BB: [571x571 uint8]
          sub_C: [571x571 logical]
        labeled: [571x571 double]
      numObjects: 76
       RGB_label: [571x571x3 uint8]
     numObjects2: 42
        red_set: [5 0 0 0 0 0 0 0 0 0 0 0 0 0 2 6 4 11 14]
        ful_set: [5 0 0 0 0 1 13 29 14 7 4 1 0 0 0 0 0 0 2]
        fatcell: [1 1 1 1 1 1 1 1 1 1 1 1 1 1 1 1 1 1 1 2 1 1 1 1 1 1 2 2 1 1 2]
             A2: [1024x1360x3 uint8]
         sub_A2: [571x571x3 uint8]
      RGB_label2: [571x571x3 uint8]
     nio_ful_set: [1630 41 13 6 2 1 0 0 2 1 0 0 1 0 0 0 0 1 0 1]
     nio_red_set: [1630 41 13 6 2 1 0 0 2 1 0 0 1 0 0 0 0 1 0 1]

handles =

          figure1: 153.0455
      pushbutton7: 7.0457
      pushbutton6: 6.0457
        listbox1: 5.0457
      pushbutton5: 4.0457
      pushbutton4: 3.0457
      pushbutton3: 2.0457
      pushbutton2: 1.0457
      pushbutton1: 0.0457
    togglebutton1: 159.0455
            axes3: 154.0455
           output: 153.0455
         filename: 'W1_20x_D1.tif'
        root_file: 'C:\Program Files\MATLAB71\work\images\10-05-06\'
           banner: [1024x1360x3 uint8]
              Cal: 0.2180
              myX: [1 1360]
              myY: [1 1024]
            sub_A: [571x571x3 uint8]
      rect_userD: [10.0968 248.8353 570.2515 570.2515]
           sub_B: [571x571 uint8]
          sub_BB: [571x571 uint8]
           sub_C: [571x571 logical]
         labeled: [571x571 double]
       numObjects: 76
```

Appendix D. (Continued)

```
 RGB_label: [571x571x3 uint8]
      numObjects2: 42
         red_set: [5 0 0 0 0 0 0 0 0 0 0 0 0 0 0 2 6 4 11 14]
         ful_set: [5 0 0 0 0 1 13 29 14 7 4 1 0 0 0 0 0 0 0 2]
         fatcell: [1 1 1 1 1 1 1 1 1 1 1 1 1 1 1 1 1 1 1 1 2 1 1 1 1 1 1 2 2 1 1 2]
             A2: [1024x1360x3 uint8]
          sub_A2: [571x571x3 uint8]
       RGB_label2: [571x571x3 uint8]
      nio_ful_set: [1630 41 13 6 2 1 0 0 2 1 0 0 1 0 0 0 0 1 0 1]
      nio_red_set: [1630 41 13 6 2 1 0 0 2 1 0 0 1 0 0 0 0 1 0 1]
        finalpic: [571x571x3 uint8]
   cellTotalCount: 80

handles =

          figure1: 153.0455
      pushbutton7: 7.0457
      pushbutton6: 6.0457
        listbox1: 5.0457
      pushbutton5: 4.0457
      pushbutton4: 3.0457
      pushbutton3: 2.0457
      pushbutton2: 1.0457
      pushbutton1: 0.0457
    togglebutton1: 159.0455
           axes3: 154.0455
          output: 153.0455
        filename: 'W1_20x_D1.tif'
       root_file: 'C:\Program Files\MATLAB71\work\images\10-05-06\'
          banner: [1024x1360x3 uint8]
             Cal: 0.2180
             myX: [1 1360]
             myY: [1 1024]
           sub_A: [571x571x3 uint8]
      rect_userD: [10.0968 248.8353 570.2515 570.2515]
           sub_B: [571x571 uint8]
          sub_BB: [571x571 uint8]
           sub_C: [571x571 logical]
         labeled: [571x571 double]
      numObjects: 76
       RGB_label: [571x571x3 uint8]
      numObjects2: 42
         red_set: [5 0 0 0 0 0 0 0 0 0 0 0 0 0 0 2 6 4 11 14]
         ful_set: [5 0 0 0 0 1 13 29 14 7 4 1 0 0 0 0 0 0 0 2]
```

Appendix D. (Continued)

```
 fatcell: [1 1 1 1 1 1 1 1 1 1 1 1 1 1 1 1 1 1 1 1 1 2 1 1 1 1 1 1 2 2 1 1 2]
              A2: [1024x1360x3 uint8]
           sub_A2: [571x571x3 uint8]
        RGB_label2: [571x571x3 uint8]
       nio_ful_set: [1630 41 13 6 2 1 0 0 2 1 0 0 1 0 0 0 0 1 0 1]
       nio_red_set: [1630 41 13 6 2 1 0 0 2 1 0 0 1 0 0 0 0 1 0 1]
          finalpic: [571x571x3 uint8]
    cellTotalCount: 80
         totalArea: 7.0877e+004

handles =

           figure1: 153.0455
       pushbutton7: 7.0457
       pushbutton6: 6.0457
         listbox1: 5.0457
       pushbutton5: 4.0457
       pushbutton4: 3.0457
       pushbutton3: 2.0457
       pushbutton2: 1.0457
       pushbutton1: 0.0457
     togglebutton1: 159.0455
           axes3: 154.0455
          output: 153.0455
        filename: 'W1_20x_D1.tif'
       root_file: 'C:\Program Files\MATLAB71\work\images\10-05-06\'
          banner: [1024x1360x3 uint8]
             Cal: 0.2180
             myX: [1 1360]
             myY: [1 1024]
           sub_A: [571x571x3 uint8]
      rect_userD: [10.0968 248.8353 570.2515 570.2515]
           sub_B: [571x571 uint8]
          sub_BB: [571x571 uint8]
           sub_C: [571x571 logical]
         labeled: [571x571 double]
      numObjects: 76
       RGB_label: [571x571x3 uint8]
     numObjects2: 42
         red_set: [5 0 0 0 0 0 0 0 0 0 0 0 0 0 2 6 4 11 14]
         ful_set: [5 0 0 0 0 1 13 29 14 7 4 1 0 0 0 0 0 0 2]
         fatcell: [1 1 1 1 1 1 1 1 1 1 1 1 1 1 1 1 1 1 1 1 1 2 1 1 1 1 1 1 2 2 1 1 2]
              A2: [1024x1360x3 uint8]
           sub_A2: [571x571x3 uint8]
```

Appendix D. (Continued)

```
   RGB_label2: [571x571x3 uint8]
      nio_ful_set: [1630 41 13 6 2 1 0 0 2 1 0 0 1 0 0 0 0 1 0 1]
      nio_red_set: [1630 41 13 6 2 1 0 0 2 1 0 0 1 0 0 0 0 1 0 1]
         finalpic: [571x571x3 uint8]
    cellTotalCount: 80
        totalArea: 7.0877e+004
     cell_density: 0.0011


handles =

           figure1: 153.0455
       pushbutton7: 7.0457
       pushbutton6: 6.0457
         listbox1: 5.0457
       pushbutton5: 4.0457
       pushbutton4: 3.0457
       pushbutton3: 2.0457
       pushbutton2: 1.0457
       pushbutton1: 0.0457
     togglebutton1: 159.0455
            axes3: 154.0455
           output: 153.0455
         filename: 'W1_20x_D1.tif'
        root_file: 'C:\Program Files\MATLAB71\work\images\10-05-06\'
           banner: [1024x1360x3 uint8]
              Cal: 0.2180
              myX: [1 1360]
              myY: [1 1024]
            sub_A: [571x571x3 uint8]
      rect_userD: [10.0968 248.8353 570.2515 570.2515]
            sub_B: [571x571 uint8]
           sub_BB: [571x571 uint8]
            sub_C: [571x571 logical]
          labeled: [571x571 double]
       numObjects: 76
        RGB_label: [571x571x3 uint8]
      numObjects2: 42
         red_set: [5 0 0 0 0 0 0 0 0 0 0 0 0 0 2 6 4 11 14]
         ful_set: [5 0 0 0 0 1 13 29 14 7 4 1 0 0 0 0 0 0 0 2]
         fatcell: [1 1 1 1 1 1 1 1 1 1 1 1 1 1 1 1 1 1 1 1 2 1 1 1 1 1 1 2 2 1 1 2]
              A2: [1024x1360x3 uint8]
           sub_A2: [571x571x3 uint8]
      RGB_label2: [571x571x3 uint8]
```

Appendix D. (Continued)

```
    nio_ful_set: [1630 41 13 6 2 1 0 0 2 1 0 0 1 0 0 0 0 1 0 1]
     nio_red_set: [1630 41 13 6 2 1 0 0 2 1 0 0 1 0 0 0 0 1 0 1]
        finalpic: [571x571x3 uint8]
   cellTotalCount: 80
       totalArea: 7.0877e+004
    cell_density: 0.0011
   nioTotalCount: 1699

handles =

          figure1: 153.0455
      pushbutton7: 7.0457
      pushbutton6: 6.0457
        listbox1: 5.0457
      pushbutton5: 4.0457
      pushbutton4: 3.0457
      pushbutton3: 2.0457
      pushbutton2: 1.0457
      pushbutton1: 0.0457
    togglebutton1: 159.0455
          axes3: 154.0455
         output: 153.0455
       filename: 'W1_20x_D1.tif'
      root_file: 'C:\Program Files\MATLAB71\work\images\10-05-06\'
         banner: [1024x1360x3 uint8]
            Cal: 0.2180
            myX: [1 1360]
            myY: [1 1024]
          sub_A: [571x571x3 uint8]
     rect_userD: [10.0968 248.8353 570.2515 570.2515]
          sub_B: [571x571 uint8]
         sub_BB: [571x571 uint8]
          sub_C: [571x571 logical]
        labeled: [571x571 double]
     numObjects: 76
      RGB_label: [571x571x3 uint8]
    numObjects2: 42
        red_set: [5 0 0 0 0 0 0 0 0 0 0 0 0 0 2 6 4 11 14]
        ful_set: [5 0 0 0 0 1 13 29 14 7 4 1 0 0 0 0 0 0 0 2]
        fatcell: [1 1 1 1 1 1 1 1 1 1 1 1 1 1 1 1 1 1 1 1 2 1 1 1 1 1 1 2 2 1 1 2]
             A2: [1024x1360x3 uint8]
         sub_A2: [571x571x3 uint8]
    RGB_label2: [571x571x3 uint8]
    nio_ful_set: [1630 41 13 6 2 1 0 0 2 1 0 0 1 0 0 0 0 1 0 1]
```

Appendix D. (Continued)

```
   nio_red_set: [1630 41 13 6 2 1 0 0 2 1 0 0 1 0 0 0 0 1 0 1]
         finalpic: [571x571x3 uint8]
    cellTotalCount: 80
        totalArea: 7.0877e+004
      cell_density: 0.0011
     nioTotalCount: 1699
```

Appendix E. Confocal Image Processing Data

The following is a text file generated by the Leica Confocal Software which details the operating parameters and the stacking instructions for combining the fluorescent images.

Leica Microsystems Heidelberg GmbH
This file is intended for read-only purposes changes here will not affect the images.
Date: Tuesday, June 19, 2007
Time: 16:05

File Version: 26000000

EXPERIMENT INFORMATION
Number of Images: 3
Type: Series with 'tif'-files

DIMENSION DESCRIPTION #0
Pixel Size in Byte: 1
Resolution in Bit: 8
Max Value: 255.0000000000
Min Value: 0.000000e+000
Label: I
Number of Dimensions: 4
Dimension_0: 120
Logical Size: 512
Physical Length: 1.365967e-004 m
Physical Origin: 0.000000e+000 m
Dimension_1: 121
Logical Size: 512
Physical Length: 1.365967e-004 m
Physical Origin: 0.000000e+000 m
Dimension_2: 6815843
Logical Size: 2
Physical Length: 0.000000e+000
Physical Origin: 0.000000e+000
Dimension_3: 122
Logical Size: 1
Physical Length: 0.000000e+000
Physical Origin: 0.000000e+000
Series Name: Series038

Appendix E. (Continued)

Description:

HARDWARE PARAMETER #0

AOTF (458)	49.328449	
AOTF (476)	0.000000	
AOTF (488)	50.671551	
AOTF (514)	0.000000	
AOTF (561)	50.012210	
AOTF (633)	0.000000	
AOTF (458)	0.000000	
AOTF (476)	0.000000	
AOTF (488)	0.000000	
AOTF (514)	0.000000	
AOTF (561)	0.000000	
AOTF (633)	0.000000	
PMT 1	Active	Active
PMT 1 (Offs.)	-21.600000	
PMT 1 (HV)	631.887456	
PMT 2	Active	Active
PMT 2 (Offs.)	-13.600000	
PMT 2 (HV)	616.060961	
PMT 3	Inactive	Inactive
PMT Trans	Inactive	Inactive
Beam Expander	Beam Exp 6	Beam Exp 6
Excitation Beam Splitter FW	DD 488/568	DD 488/568
External Detection FW	Mirror	Mirror
Hardware Type No.	2.000000	
Scan Field Rotation	-0.038943	
Rotation Direction	1	
X Scan Actuator	Active	Active
X Scan Actuator (Gain)	2.745308	
X Scan Actuator (Offs.)	0.000000	
Y Scan Actuator	Active	Active
Y Scan Actuator (Gain)	2.745308	
Y Scan Actuator (Offs.)	0.000000	
Z Scan Actuator	Inactive	Inactive
Z Scan Actuator (POS)	-0.000048	
Scan Speed	200.000000	
Phase	10.546875	
Y-Phase	0.122100	
SP Mirror 1 (left)	500.000000	
SP Mirror 1 (right)	550.000000	
SP Mirror 1 (stain)	FITC	FITC
SP Mirror 2 (left)	570.000000	

Appendix E. (Continued)

SP Mirror 2 (right) 700.000000
SP Mirror 2 (stain) TRITC TRITC
SP Mirror 3 (left) 750.000000
SP Mirror 3 (right) 850.000000
SP Mirror 3 (stain) None None
Objective HCX PL APO CS 40.0x1.25 OIL UV HCX PL APO CS 40.0x1.25 OIL UV
Order number (Obj.) 506179
Numerical aperture (Obj.) 1.250000

SCANNER INFORMATION #0
RoiScan 0
IsSequential 0
ChaserUVShutter 0
ChaserVisibleShutter 0
MPShutter 0
UVShutter 0
VisibleShutter 1
ScanMode xyz Active
Pinhole [m] 0.000081
Pinhole [airy] 0.998666
Size-Width [µm] 136.596680
Size-Height [µm] 136.596680
Size-Depth 0.000000
StepSize [µm] 0.040703
Voxel-Width [µm] 0.266790
Voxel-Height [µm] 0.266790
Voxel-Depth 0.000000
Zoom 2.745308
Scan-Direction 1
Y-Scan-Direction 1
SequentialMode 0
Frame-Accumulation 1
Frame-Average 1
Line-Average 1
Resolution 8
Channels 2
Format-Width 512
Format-Height 512
Sections 1

TIME INFORMATION #0
Stamped Dimension: 2
Stamp_0: 2007:06:19,15:38:12:546

Appendix E. (Continued)

Stamp_1: 2007:06:19,15:38:12:546

LUT DESCRIPTION #0
LUT_0
Name: Green
Inverted (1=yes / 0=no): 0
LUT_1
Name: Red
Inverted (1=yes / 0=no): 0

SEQUENTIAL INFORMATION #0
Sequence Count: 0

SERIES INFORMATION #0
Number of Series: 3

IMAGES INFORMATION #0
Number of Images: 2
Image Width: 512
Iamge Length: 512
Bits per Sample: 8
Samples per Pixel: 1

**********NEXT IMAGE**********
DIMENSION DESCRIPTION #1
Pixel Size in Byte: 1
Resolution in Bit: 8
Max Value: 255.0000000000
Min Value: 0.000000e+000
Label: I
Number of Dimensions: 4
Dimension_0: 120
Logical Size: 512
Physical Length: 1.365967e-004 m
Physical Origin: 0.000000e+000 m
Dimension_1: 121
Logical Size: 512
Physical Length: 1.365967e-004 m
Physical Origin: 0.000000e+000 m
Dimension_2: 6815843
Logical Size: 2
Physical Length: 0.000000e+000
Physical Origin: 0.000000e+000
Dimension_3: 122

Appendix E. (Continued)

Logical Size: 3
Physical Length: -3.256268e-007 m
Physical Origin: -3.661267e-005 m
Series Name: Series045
Description:

HARDWARE PARAMETER #1
AOTF (458) 49.328449
AOTF (476) 0.000000
AOTF (488) 50.671551
AOTF (514) 0.000000
AOTF (561) 50.012210
AOTF (633) 0.000000
AOTF (458) 0.000000
AOTF (476) 0.000000
AOTF (488) 0.000000
AOTF (514) 0.000000
AOTF (561) 0.000000
AOTF (633) 0.000000
PMT 1 Active Active
PMT 1 (Offs.) -21.600000
PMT 1 (HV) 631.887456
PMT 2 Active Active
PMT 2 (Offs.) -13.600000
PMT 2 (HV) 616.060961
PMT 3 Inactive Inactive
PMT Trans Inactive Inactive
Beam Expander Beam Exp 6 Beam Exp 6
Excitation Beam Splitter FW DD 488/568 DD 488/568
External Detection FW Mirror Mirror
Hardware Type No. 2.000000
Scan Field Rotation -0.038943
Rotation Direction 1
X Scan Actuator Active Active
X Scan Actuator (Gain) 2.745308
X Scan Actuator (Offs.) 0.000000
Y Scan Actuator Active Active
Y Scan Actuator (Gain) 2.745308
Y Scan Actuator (Offs.) 0.000000
Z Scan Actuator Inactive Inactive
Z Scan Actuator (POS) -0.000043
Scan Speed 200.000000
Phase 10.546875
Y-Phase 0.122100

Appendix E. (Continued)

SP Mirror 1 (left) 500.000000
SP Mirror 1 (right) 550.000000
SP Mirror 1 (stain) FITC FITC
SP Mirror 2 (left) 570.000000
SP Mirror 2 (right) 700.000000
SP Mirror 2 (stain) TRITC TRITC
SP Mirror 3 (left) 750.000000
SP Mirror 3 (right) 850.000000
SP Mirror 3 (stain) None None
Objective HCX PL APO CS 40.0x1.25 OIL UV HCX PL APO CS 40.0x1.25 OIL UV
Order number (Obj.) 506179
Numerical aperture (Obj.) 1.250000

SCANNER INFORMATION #1
RoiScan 0
IsSequential 0
ChaserUVShutter 0
ChaserVisibleShutter 0
MPShutter 0
UVShutter 0
VisibleShutter 1
ScanMode xyz Active
Pinhole [m] 0.000081
Pinhole [airy] 0.998666
Size-Width [µm] 136.596680
Size-Height [µm] 136.596680
Size-Depth [µm] 0.325627
StepSize [µm] 0.162813
Voxel-Width [µm] 0.266790
Voxel-Height [µm] 0.266790
Voxel-Depth [µm] 0.162813
Zoom 2.745308
Scan-Direction 1
Y-Scan-Direction 1
SequentialMode 0
Frame-Accumulation 1
Frame-Average 1
Line-Average 1
Resolution 8
Channels 2
Format-Width 512
Format-Height 512
Sections 84

Appendix E. (Continued)

TIME INFORMATION #1
Stamped Dimension: 2
Stamp_0: 2007:06:19,15:45:23:593
Stamp_1: 2007:06:19,15:45:23:593
Stamp_2: 2007:06:19,15:45:26:843
Stamp_3: 2007:06:19,15:45:26:843
Stamp_4: 2007:06:19,15:45:30:93
Stamp_5: 2007:06:19,15:45:30:93

LUT DESCRIPTION #1
LUT_0
Name: Green
Inverted (1=yes / 0=no): 0
LUT_1
Name: Red
Inverted (1=yes / 0=no): 0

SEQUENTIAL INFORMATION #1
Sequence Count: 0

IMAGES INFORMATION #1
Number of Images: 6
Image Width: 512
Iamge Length: 512
Bits per Sample: 8
Samples per Pixel: 1

************************************ NEXT IMAGE *********************************
DIMENSION DESCRIPTION #2
Pixel Size in Byte: 1
Resolution in Bit: 8
Max Value: 255.0000000000
Min Value: 0.000000e+000
Label: I
Number of Dimensions: 4
Dimension_0: 120
Logical Size: 512
Physical Length: 1.372375e-004 m
Physical Origin: 0.000000e+000 m
Dimension_1: 121
Logical Size: 512
Physical Length: 1.372375e-004 m
Physical Origin: 0.000000e+000 m
Dimension_2: 6815843

Appendix E. (Continued)

Logical Size: 2
Physical Length: 0.000000e+000
Physical Origin: 0.000000e+000
Dimension_3: 122
Logical Size: 125
Physical Length: -2.018886e-005 m
Physical Origin: -3.815939e-005 m
Series Name: Series049
Description:

HARDWARE PARAMETER #2
AOTF (458) 49.328449
AOTF (476) 0.000000
AOTF (488) 50.671551
AOTF (514) 0.000000
AOTF (561) 50.012210
AOTF (633) 0.000000
AOTF (458) 0.000000
AOTF (476) 0.000000
AOTF (488) 0.000000
AOTF (514) 0.000000
AOTF (561) 0.000000
AOTF (633) 0.000000
PMT 1 Active Active
PMT 1 (Offs.) -21.600000
PMT 1 (HV) 631.887456
PMT 2 Active Active
PMT 2 (Offs.) -13.600000
PMT 2 (HV) 616.060961
PMT 3 Inactive Inactive
PMT Trans Inactive Inactive
Beam Expander Beam Exp 6 Beam Exp 6
Excitation Beam Splitter FW DD 488/568 DD 488/568
External Detection FW Mirror Mirror
Hardware Type No. 2.000000
Scan Field Rotation -0.038943
Rotation Direction 1
X Scan Actuator Active Active
X Scan Actuator (Gain) 2.732488
X Scan Actuator (Offs.) 0.000000
Y Scan Actuator Active Active
Y Scan Actuator (Gain) 2.732488
Y Scan Actuator (Offs.) 0.000000
Z Scan Actuator Inactive Inactive

Appendix E. (Continued)

Z Scan Actuator (POS) -0.000048
Scan Speed 200.000000
Phase 10.546875
Y-Phase 0.122100
SP Mirror 1 (left) 500.000000
SP Mirror 1 (right) 550.000000
SP Mirror 1 (stain) FITC FITC
SP Mirror 2 (left) 570.000000
SP Mirror 2 (right) 700.000000
SP Mirror 2 (stain) TRITCTRITC
SP Mirror 3 (left) 750.000000
SP Mirror 3 (right) 850.000000
SP Mirror 3 (stain) None None
Objective HCX PL APO CS 40.0x1.25 OIL UV HCX PL APO CS 40.0x1.25 OIL UV
Order number (Obj.) 506179
Numerical aperture (Obj.) 1.250000

SCANNER INFORMATION #2
RoiScan 0
IsSequential 0
ChaserUVShutter 0
ChaserVisibleShutter 0
MPShutter 0
UVShutter 0
VisibleShutter 1
ScanMode xyz Active
Pinhole [m] 0.000081
Pinhole [airy] 0.998666
Size-Width [µm] 137.237549
Size-Height [µm] 137.237549
Size-Depth [µm] -20.188864
StepSize [µm] 0.162813
Voxel-Width [µm] 0.268042
Voxel-Height [µm] 0.268042
Voxel-Depth [µm] 0.162813
Zoom 2.732488
Scan-Direction 1
Y-Scan-Direction 1
SequentialMode 0
Frame-Accumulation 1
Frame-Average 1
Line-Average 1
Resolution 8

Appendix E. (Continued)

Channels 2
Format-Width 512
Format-Height 512
Sections 125

TIME INFORMATION #2
Stamped Dimension: 2
Stamp_0: 2007:06:19,15:54:21:453
Stamp_1: 2007:06:19,15:54:21:453
Stamp_2: 2007:06:19,15:54:24:703
Stamp_3: 2007:06:19,15:54:24:703
Stamp_4: 2007:06:19,15:54:27:953
Stamp_5: 2007:06:19,15:54:27:953
Stamp_6: 2007:06:19,15:54:31:203
Stamp_7: 2007:06:19,15:54:31:203
Stamp_8: 2007:06:19,15:54:34:437
Stamp_9: 2007:06:19,15:54:34:437
Stamp_10: 2007:06:19,15:54:37:687
Stamp_11: 2007:06:19,15:54:37:687
Stamp_12: 2007:06:19,15:54:40:937
Stamp_13: 2007:06:19,15:54:40:937
Stamp_14: 2007:06:19,15:54:44:187
Stamp_15: 2007:06:19,15:54:44:187
Stamp_16: 2007:06:19,15:54:47:437
Stamp_17: 2007:06:19,15:54:47:437
Stamp_18: 2007:06:19,15:54:50:687
Stamp_19: 2007:06:19,15:54:50:687
Stamp_20: 2007:06:19,15:54:53:937
Stamp_21: 2007:06:19,15:54:53:937
Stamp_22: 2007:06:19,15:54:57:187
Stamp_23: 2007:06:19,15:54:57:187
Stamp_24: 2007:06:19,15:55:00:437
Stamp_25: 2007:06:19,15:55:00:437
Stamp_26: 2007:06:19,15:55:03:687
Stamp_27: 2007:06:19,15:55:03:687
Stamp_28: 2007:06:19,15:55:06:937
Stamp_29: 2007:06:19,15:55:06:937
Stamp_30: 2007:06:19,15:55:10:187
Stamp_31: 2007:06:19,15:55:10:187
Stamp_32: 2007:06:19,15:55:13:437
Stamp_33: 2007:06:19,15:55:13:437
Stamp_34: 2007:06:19,15:55:16:687
Stamp_35: 2007:06:19,15:55:16:687
Stamp_36: 2007:06:19,15:55:19:937

Appendix E. (Continued)

Stamp_37: 2007:06:19,15:55:19:937
Stamp_38: 2007:06:19,15:55:23:187
Stamp_39: 2007:06:19,15:55:23:187
Stamp_40: 2007:06:19,15:55:26:437
Stamp_41: 2007:06:19,15:55:26:437
Stamp_42: 2007:06:19,15:55:29:687
Stamp_43: 2007:06:19,15:55:29:687
Stamp_44: 2007:06:19,15:55:32:937
Stamp_45: 2007:06:19,15:55:32:937
Stamp_46: 2007:06:19,15:55:36:187
Stamp_47: 2007:06:19,15:55:36:187
Stamp_48: 2007:06:19,15:55:39:437
Stamp_49: 2007:06:19,15:55:39:437
Stamp_50: 2007:06:19,15:55:42:687
Stamp_51: 2007:06:19,15:55:42:687
Stamp_52: 2007:06:19,15:55:45:937
Stamp_53: 2007:06:19,15:55:45:937
Stamp_54: 2007:06:19,15:55:49:187
Stamp_55: 2007:06:19,15:55:49:187
Stamp_56: 2007:06:19,15:55:52:437
Stamp_57: 2007:06:19,15:55:52:437
Stamp_58: 2007:06:19,15:55:55:687
Stamp_59: 2007:06:19,15:55:55:687
Stamp_60: 2007:06:19,15:55:58:937
Stamp_61: 2007:06:19,15:55:58:937
Stamp_62: 2007:06:19,15:56:02:187
Stamp_63: 2007:06:19,15:56:02:187
Stamp_64: 2007:06:19,15:56:05:437
Stamp_65: 2007:06:19,15:56:05:437
Stamp_66: 2007:06:19,15:56:08:687
Stamp_67: 2007:06:19,15:56:08:687
Stamp_68: 2007:06:19,15:56:11:937
Stamp_69: 2007:06:19,15:56:11:937
Stamp_70: 2007:06:19,15:56:15:187
Stamp_71: 2007:06:19,15:56:15:187
Stamp_72: 2007:06:19,15:56:18:437
Stamp_73: 2007:06:19,15:56:18:437
Stamp_74: 2007:06:19,15:56:21:687
Stamp_75: 2007:06:19,15:56:21:687
Stamp_76: 2007:06:19,15:56:24:937
Stamp_77: 2007:06:19,15:56:24:937
Stamp_78: 2007:06:19,15:56:28:187
Stamp_79: 2007:06:19,15:56:28:187
Stamp_80: 2007:06:19,15:56:31:437

Appendix E. (Continued)

Stamp_81: 2007:06:19,15:56:31:437
Stamp_82: 2007:06:19,15:56:34:687
Stamp_83: 2007:06:19,15:56:34:687
Stamp_84: 2007:06:19,15:56:37:937
Stamp_85: 2007:06:19,15:56:37:937
Stamp_86: 2007:06:19,15:56:41:187
Stamp_87: 2007:06:19,15:56:41:187
Stamp_88: 2007:06:19,15:56:44:437
Stamp_89: 2007:06:19,15:56:44:437
Stamp_90: 2007:06:19,15:56:47:687
Stamp_91: 2007:06:19,15:56:47:687
Stamp_92: 2007:06:19,15:56:50:937
Stamp_93: 2007:06:19,15:56:50:937
Stamp_94: 2007:06:19,15:56:54:187
Stamp_95: 2007:06:19,15:56:54:187
Stamp_96: 2007:06:19,15:56:57:437
Stamp_97: 2007:06:19,15:56:57:437
Stamp_98: 2007:06:19,15:57:00:687
Stamp_99: 2007:06:19,15:57:00:687
Stamp_100: 2007:06:19,15:57:03:937
Stamp_101: 2007:06:19,15:57:03:937
Stamp_102: 2007:06:19,15:57:07:187
Stamp_103: 2007:06:19,15:57:07:187
Stamp_104: 2007:06:19,15:57:10:437
Stamp_105: 2007:06:19,15:57:10:437
Stamp_106: 2007:06:19,15:57:13:687
Stamp_107: 2007:06:19,15:57:13:687
Stamp_108: 2007:06:19,15:57:16:937
Stamp_109: 2007:06:19,15:57:16:937
Stamp_110: 2007:06:19,15:57:20:187
Stamp_111: 2007:06:19,15:57:20:187
Stamp_112: 2007:06:19,15:57:23:437
Stamp_113: 2007:06:19,15:57:23:437
Stamp_114: 2007:06:19,15:57:26:687
Stamp_115: 2007:06:19,15:57:26:687
Stamp_116: 2007:06:19,15:57:29:937
Stamp_117: 2007:06:19,15:57:29:937
Stamp_118: 2007:06:19,15:57:33:187
Stamp_119: 2007:06:19,15:57:33:187
Stamp_120: 2007:06:19,15:57:36:437
Stamp_121: 2007:06:19,15:57:36:437
Stamp_122: 2007:06:19,15:57:39:687
Stamp_123: 2007:06:19,15:57:39:687
Stamp_124: 2007:06:19,15:57:42:937

Appendix E. (Continued)

Stamp_125: 2007:06:19,15:57:42:937
Stamp_126: 2007:06:19,15:57:46:187
Stamp_127: 2007:06:19,15:57:46:187
Stamp_128: 2007:06:19,15:57:49:437
Stamp_129: 2007:06:19,15:57:49:437
Stamp_130: 2007:06:19,15:57:52:687
Stamp_131: 2007:06:19,15:57:52:687
Stamp_132: 2007:06:19,15:57:55:921
Stamp_133: 2007:06:19,15:57:55:921
Stamp_134: 2007:06:19,15:57:59:171
Stamp_135: 2007:06:19,15:57:59:171
Stamp_136: 2007:06:19,15:58:02:421
Stamp_137: 2007:06:19,15:58:02:421
Stamp_138: 2007:06:19,15:58:05:671
Stamp_139: 2007:06:19,15:58:05:671
Stamp_140: 2007:06:19,15:58:08:921
Stamp_141: 2007:06:19,15:58:08:921
Stamp_142: 2007:06:19,15:58:12:171
Stamp_143: 2007:06:19,15:58:12:171
Stamp_144: 2007:06:19,15:58:15:421
Stamp_145: 2007:06:19,15:58:15:421
Stamp_146: 2007:06:19,15:58:18:671
Stamp_147: 2007:06:19,15:58:18:671
Stamp_148: 2007:06:19,15:58:21:921
Stamp_149: 2007:06:19,15:58:21:921
Stamp_150: 2007:06:19,15:58:25:171
Stamp_151: 2007:06:19,15:58:25:171
Stamp_152: 2007:06:19,15:58:28:421
Stamp_153: 2007:06:19,15:58:28:421
Stamp_154: 2007:06:19,15:58:31:671
Stamp_155: 2007:06:19,15:58:31:671
Stamp_156: 2007:06:19,15:58:34:921
Stamp_157: 2007:06:19,15:58:34:921
Stamp_158: 2007:06:19,15:58:38:171
Stamp_159: 2007:06:19,15:58:38:171
Stamp_160: 2007:06:19,15:58:41:421
Stamp_161: 2007:06:19,15:58:41:421
Stamp_162: 2007:06:19,15:58:44:671
Stamp_163: 2007:06:19,15:58:44:671
Stamp_164: 2007:06:19,15:58:47:921
Stamp_165: 2007:06:19,15:58:47:921
Stamp_166: 2007:06:19,15:58:51:171
Stamp_167: 2007:06:19,15:58:51:171
Stamp_168: 2007:06:19,15:58:54:421

Appendix E. (Continued)

Stamp_169:	2007:06:19,15:58:54:421
Stamp_170:	2007:06:19,15:58:57:671
Stamp_171:	2007:06:19,15:58:57:671
Stamp_172:	2007:06:19,15:59:00:921
Stamp_173:	2007:06:19,15:59:00:921
Stamp_174:	2007:06:19,15:59:04:171
Stamp_175:	2007:06:19,15:59:04:171
Stamp_176:	2007:06:19,15:59:07:421
Stamp_177:	2007:06:19,15:59:07:421
Stamp_178:	2007:06:19,15:59:10:671
Stamp_179:	2007:06:19,15:59:10:671
Stamp_180:	2007:06:19,15:59:13:921
Stamp_181:	2007:06:19,15:59:13:921
Stamp_182:	2007:06:19,15:59:17:171
Stamp_183:	2007:06:19,15:59:17:171
Stamp_184:	2007:06:19,15:59:20:421
Stamp_185:	2007:06:19,15:59:20:421
Stamp_186:	2007:06:19,15:59:23:671
Stamp_187:	2007:06:19,15:59:23:671
Stamp_188:	2007:06:19,15:59:26:921
Stamp_189:	2007:06:19,15:59:26:921
Stamp_190:	2007:06:19,15:59:30:171
Stamp_191:	2007:06:19,15:59:30:171
Stamp_192:	2007:06:19,15:59:33:421
Stamp_193:	2007:06:19,15:59:33:421
Stamp_194:	2007:06:19,15:59:36:671
Stamp_195:	2007:06:19,15:59:36:671
Stamp_196:	2007:06:19,15:59:39:921
Stamp_197:	2007:06:19,15:59:39:921
Stamp_198:	2007:06:19,15:59:43:171
Stamp_199:	2007:06:19,15:59:43:171
Stamp_200:	2007:06:19,15:59:46:421
Stamp_201:	2007:06:19,15:59:46:421
Stamp_202:	2007:06:19,15:59:49:671
Stamp_203:	2007:06:19,15:59:49:671
Stamp_204:	2007:06:19,15:59:52:921
Stamp_205:	2007:06:19,15:59:52:921
Stamp_206:	2007:06:19,15:59:56:171
Stamp_207:	2007:06:19,15:59:56:171
Stamp_208:	2007:06:19,15:59:59:421
Stamp_209:	2007:06:19,15:59:59:421
Stamp_210:	2007:06:19,16:00:02:671
Stamp_211:	2007:06:19,16:00:02:671
Stamp_212:	2007:06:19,16:00:05:921

Appendix E. (Continued)

Stamp_213: 2007:06:19,16:00:05:921
Stamp_214: 2007:06:19,16:00:09:171
Stamp_215: 2007:06:19,16:00:09:171
Stamp_216: 2007:06:19,16:00:12:421
Stamp_217: 2007:06:19,16:00:12:421
Stamp_218: 2007:06:19,16:00:15:671
Stamp_219: 2007:06:19,16:00:15:671
Stamp_220: 2007:06:19,16:00:18:921
Stamp_221: 2007:06:19,16:00:18:921
Stamp_222: 2007:06:19,16:00:22:171
Stamp_223: 2007:06:19,16:00:22:171
Stamp_224: 2007:06:19,16:00:25:421
Stamp_225: 2007:06:19,16:00:25:421
Stamp_226: 2007:06:19,16:00:28:671
Stamp_227: 2007:06:19,16:00:28:671
Stamp_228: 2007:06:19,16:00:31:921
Stamp_229: 2007:06:19,16:00:31:921
Stamp_230: 2007:06:19,16:00:35:171
Stamp_231: 2007:06:19,16:00:35:171
Stamp_232: 2007:06:19,16:00:38:421
Stamp_233: 2007:06:19,16:00:38:421
Stamp_234: 2007:06:19,16:00:41:671
Stamp_235: 2007:06:19,16:00:41:671
Stamp_236: 2007:06:19,16:00:44:921
Stamp_237: 2007:06:19,16:00:44:921
Stamp_238: 2007:06:19,16:00:48:171
Stamp_239: 2007:06:19,16:00:48:171
Stamp_240: 2007:06:19,16:00:51:421
Stamp_241: 2007:06:19,16:00:51:421
Stamp_242: 2007:06:19,16:00:54:671
Stamp_243: 2007:06:19,16:00:54:671
Stamp_244: 2007:06:19,16:00:57:921
Stamp_245: 2007:06:19,16:00:57:921
Stamp_246: 2007:06:19,16:01:01:171
Stamp_247: 2007:06:19,16:01:01:171
Stamp_248: 2007:06:19,16:01:04:421
Stamp_249: 2007:06:19,16:01:04:421

LUT DESCRIPTION #2
LUT_0
Name: Green
Inverted (1=yes / 0=no): 0
LUT_1
Name: Red

Appendix E. (Continued)

Inverted (1=yes / 0=no): 0

SEQUENTIAL INFORMATION #2
Sequence Count: 0

IMAGES INFORMATION #2
Number of Images: 250
Image Width: 512
Iamge Length: 512
Bits per Sample: 8
Samples per Pixel: 1

About the Author

Elizabeth Hood received a B.S. in Chemical Engineering, magna cum laude, from USF in 2000. In 2002 she returned to USF to pursue a PhD in Biomedical Engineering and has presented and published proceedings and abstracts at several national and international meetings including AIChE 2003 and 2006 Annual Meetings, American Society of Echocardiography's 15th Annual Scientific Sessions 2004, and the 26th Annual International Conference of the IEEE Engineering in Medicine and Biology Society 2004. Also, Drug Delivery and Translational Research Symposium in 2006 at the Polytechnic University in Brooklyn, NY, the prestigious American College of Cardiology Annual Scientific Session in New Orleans in 2007, and several USF symposia.

She is a contributor in three patent disclosure applications, and the primary inventor in one. Elizabeth received the Peter Brown Fellowship 2004-2005, the Central Florida Arthritis Fellowship Summer 2005, and a Southern Section-American Federation for Medical Research grants in both 2006 and 2007. Elizabeth received an award for recognition of excellence at the USF Health Research Day 2006. Her first peer-reviewed journal article entitled 'Immuno-targeting of Nonionic Surfactant Vesicles to Inflammation' was published in 2007 in the International Journal of Pharmaceutics.

After graduating as one of the first to receive a Ph.D. in Biomedical Engineering from USF Elizabeth will be pursuing a National Institute of Health National Research Service Award post doctoral fellowship at the University of Pennsylvania's Institute for Environmental Medicine.